npower

Juice Fund

UK Tidal Current Resource & Economics: Appendix C

|June 2011

CARBON TRUST

BLACK & VEATCH
Building a world of difference

Document issue details:

Contract Name:	**UK Tidal Current Resource & Economics – Appendix C**				
Project Number:	121394				
Date	Description	Rev.	Orig.	Checked	Approved
30/04/2010	Final Report	0	SC, MW, AB, CL, YL, TM	CL, AB	AB
23/06/2011	Final Report (minor additions)	1	AB	HB	AB
24/06/2011	Final Report (minor modifications)	2	AB	HB	AB

B&V acknowledges Npower's contribution to funding this work through the Juice Fund.

CONTENTS

FIGURES

TABLES

1 EXECUTIVE SUMMARY

In 2004/5, as part of the Marine Energy Challenge (MEC), B&V defined a 'Significant Impact Factor' (SIF) to estimate the UK's 'extractable tidal stream resource' (the equivalent parameter is called the 'technical tidal current resource' in this report), representing the percentage of the total tidal stream resource at a site that could be extracted without significant economic, environmental or ecological effects [1]. Since the initial investigation, limited research has been reported on the SIF, although B&V and the University of Edinburgh have undertaken some specific site assessments. Due to various studies published since 2005 (e.g. the ABPmer study funded by Juice [31]), further work on understanding how to quantify the SIF (or extractable resource) at individual sites, as was recommended in B&V's 2005 report, is important.

B&V therefore applied for Juice funding in February 2008 to update our work on the SIF. Due to budget constraints at Juice, the work reported here was also partly funded by Carbon Trust. This Appendix draws extensively on work carried out by Scott Couch at the University of Edinburgh (UoE), with additional input from Michael MacWilliams of River Modelling (USA); B&V mainly acted as 'project manager and client' to ensure the output of this work could be used to inform the main 'UK Tidal Current Resource & Economics' report, carried out by B&V for Carbon Trust.

The focus of the work presented in this report is the far-field response of the tidal system with regard to the economic and environmental implications of widespread, large-scale TEC (tidal [current] energy converter) deployment. For this study, hydrodynamic tidal models adapted to simulate the large-scale impact of various hypothetical levels of energy extraction are used to assess the response of idealised representations of generic tidal regimes. Additional modelling of several real tidal environments, as opposed to generic representation, has then been used to undertake a partial validation of the generic results.

The original energy extraction test cases developed by UoE in 2004 using TFD-2D [3] have been replicated by River Modeling using the UnTRIM standard industry model. The test cases demonstrated that the implementation of the energy extraction method within the UnTRIM model provided very similar results to the implementation within the TFD model. The validation provided confidence in the methodology and enabled its application to real world examples where the UnTRIM model (without energy extraction) has previously been very well validated.

For the purposes of examining the potential to develop a parametric model that can be applied across a range of sites in order to enable a national resource study, the approach adopted in this report is to consider ideal representations of each of the (three) relevant hydrodynamic mechanisms which give rise to the tidal current conditions necessary for TEC deployment:

- <u>Tidal streaming</u>: Tidal streaming is the physical response of the tidal system to maintenance of the continuity equation; when a current is forced through a constriction, the flow must accelerate (e.g. Portland Bill).
- <u>Hydraulic current</u>: If two adjoining bodies of water are out of phase, or have different tidal ranges, a hydraulic current is set-up in response to the pressure gradient created by the difference in water level between the two bodies (e.g. Pentland Firth).
- <u>Resonant system</u>: Resonant systems occur as a consequence of a standing wave being established. A standing wave arises when the incoming tidal wave and a reflected tidal wave constructively interfere (e.g. Severn Estuary).

This then enabled parameterisation of the response of each of the three representations to energy harvesting through TEC deployment. This is crucial because the three identified mechanisms potentially respond differently to various levels of energy extraction, which has not as yet been explicitly addressed in detail in existing research.

In all three tidal regimes, an upper *theoretical limit* was identified beyond which attempts to extract more energy from the system actually reduces the overall energy that is harvested. The demonstrable occurrence of P_{max} for each domain and localised driving mechanism is of great practical value, as it indicates the existence of a theoretical extraction limit in a particular location using the TEC technology approach. This is indicative of a key component of tidal current energy resource dynamics – the existence of a theoretical tipping point beyond which the addition of additional extraction devices will harvest less overall resource due to the impact of the combined harvesting effort on the underlying tidal hydrodynamics. This highlights that the outdated 'farm' resource assessment methodology is fundamentally flawed, as first indicated in the 2004/5 MEC reports [1]. In each of the individual tidal regimes, there was good agreement on the theoretical maximum energy removal limit – which can be quantified with reference to the flow discharge in the undisturbed (natural) simulation case (Q_{max}) and the available driving head difference (a_0). The flow discharge, flow velocities and tidal range were all reduced by energy harvesting, as expected, and these effects would at some point have impacts on the environment and the project economics that would be unacceptable, as outlined in the 2004/5 MEC reports [1].

Consideration of arbitrarily prescribed 'environmentally and economically acceptable' impacts of energy removal on the overall tidal hydrodynamics of the system enables assessment of an 'acceptable' energy removal limit. Again, a common metric for determination of the *technical energy removal limit* has been identified in each of the three cases, again related to Q_{max} and a_0.

As was previously hypothesised in the 2004/5 MEC reports [1], the present work demonstrates conclusively that the response of different generic regimes to energy harvesting, although demonstrating similar trends, is not consistent. This is summarised in the table below. The caveats raised in the discussion in the body of this report must be borne in mind when considering these results, as must the differing definitions of a_0.

	Expression of theoretical limit of tidal current energy harvesting.	Expression of technical limit of tidal current energy harvesting.	Hydrodynamic response limiting energy harvesting.
Hydraulic current	$P_{Theoretical} = 0.2\rho g Q_{\max} a_o$	$P_{Technical} = 0.086\rho g Q_{\max} a_o$	Velocity reduction
Resonant basin	$P_{Theoretical} = 0.2\rho g Q_{\max} a_o$	$P_{Technical} = 0.033\rho g Q_{\max} a_o$	Downstream tidal range
Tidal streaming	$P_{Theoretical} = 0.16\rho g Q_{\max} a_o$	$P_{Technical} = 0.020\rho g Q_{\max} a_o$	Downstream tidal range

Energy extraction was implemented in two real world models to provide confidence in the generic results obtained. The Strangford Lough case presents good to excellent agreement between detailed tidal hydrodynamic simulations and the simple parametric model derived from the generic cases. Despite the lack of extensive testing, the combined numerical modelling analyses provide confidence in applying the key metrics identified for quantifying the *theoretical resource* equations in the final proposed parametric approach. There is also good confidence in the basis for the *technical resource* calculations, although the actual difference between the theoretical and technical resource is determined by the prescription of currently arbitrary (but reasonably informed) limits to the impacts. In a national or regional resource assessment, sensitivity testing of these arbitrarily prescribed limits is recommended, and different regions may well need to prescribe different 'base-line' limits due to different local environments. Clearly, consideration of the practical resource should consider acceptable limits to the impacts on a site-by-site basis, in conjunction with all the other aspects that would limit practical resource extraction.

Certain caveats as to the accuracy of the parametric approach are still necessary. Most sites will obviously not be fully representative of the idealised representations of the three generic regimes, and many sites will be significantly different, for instance with all three regimes being present. In these cases, the parametric expressions will not be as accurate. The impact on power extraction levels if alternative flow pathways are available is one common example of a caveat that needs to be borne in mind. In such scenarios, which are not uncommon, the derivation of the theoretical (and technical, if ones assumes the imposed limits are representative) tidal current energy resource in the parametric methodology is an upper bound on the power available for extraction from the tidal current energy resource. Examples of such caveats include:

- Tidal systems where alternative flow channels are available [7]. Also see [10, 11].
- Channels where only a partial tidal fence (or array) is installed across the cross-section [6].
- The extreme case of a TEC device or small array in a theoretically (laterally) unbounded domain [6].

The other major issue requiring further consideration is the prescription of how much of the energy removal from the tidal hydrodynamic system can actually be ascribed to useful energy generation. Potential device coefficients of performance Cp and conversion efficiencies are of course fairly well understood, and best practice understanding of TEC device performance envelopes have been utilised in some of the key assumptions necessary in this analysis. However, the energy removal from the system that is due simply to the presence of the TEC device itself has not been considered in any detail in the analysis presented in this report. Future focus to reduce this wasteful use of the resource by improved support structure design and streamlining has the potential to significantly reduce this loss of useful energy that would otherwise be available for harvesting.

2 GLOSSARY

Total Resource (TWh/y) – Total energy that exists within a defined tidal system.

Theoretical Resource (TWh/y) – Maximum energy that can be harvested from tidal currents in the region of interest without consideration of technical, economic or environmental constraints.

Technical Resource (TWh/y) – The energy (which is a proportion of the theoretical resource) that can be harvested from tidal currents using envisaged technology options and restrictions (including project economics) without undue impact on the underlying tidal hydrodynamic environment.

Practical Resource (TWh/y) – The energy (which is a proportion of the technical resource) that can be harvested after consideration of external constraints (e.g. grid accessibility, competing uses such as MOD, shipping lanes, etc.). This level of assessment fundamentally requires detailed project design and investigation on a case-by-case basis.

The Farm Method – Extraction methodology developed in the 2004/5 MEC study [1] and based on developing an array of tidal stream devices that each extract an equal amount of energy from the incoming flux. The number of devices and hence the extracted energy is purely dependent on the size of the device, its efficiency, and the packing density within the plan area.

The Flux Method – Extraction methodology developed in the 2004/5 MEC study [1] and based on the use of only the incoming kinetic energy flux across the front cross-sectional area of a flow channel. This is independent of the device type, efficiency and packing density, taking only the kinetic energy flowing in the channel into account.

Significant Impact Factor (SIF) (%) - Developed in the 2004/5 MEC study [1] the SIF represented the percentage of the kinetic energy flux that could be extracted by the Flux Method without significant economic or environmental effect, to give the Technical Resource.

TEC – Tidal Energy Converter, a device which captures energy from tidal currents.

V_{mnp} (m/s) – Mean neap peak velocity as defined by the Admiralty charts for a particular site, 5 m below the surface.

V_{msp} (m/s) – Mean spring peak velocity as defined by the Admiralty charts for a particular site, 5 m below surface.

V_{rated} (m/s) – Rated velocity of tidal stream device. Rated velocity is the velocity at which the device reaches maximum (rated) output.

3 INTRODUCTION

3.1 Scope and background

In 2004/5, as part of the Marine Energy Challenge (MEC), B&V defined a 'Significant Impact Factor' (SIF) to estimate the UK's 'extractable tidal stream resource' (the equivalent parameter is called the 'technical tidal current resource' in this report), representing the percentage of the total tidal stream resource at a site that could be extracted without significant economic, environmental or ecological effects. B&V and Ian Bryden's team at RGU (now at University of Edinburgh) noted that the SIF value, representing the resource that may be extracted without undue effect, was dependent on the type of site. Whilst the MEC report stated that the SIF was site dependent, there was not sufficient time or resources available at that time to calculate the SIF for each type of site. Therefore, a series of estimates were made for the different types of site, based on work undertaken by RGU for the Pentland Firth (the largest site). The concept of the SIF has since been adopted by other bodies, such as the Electrical Power Research Institute (EPRI).

Since the initial investigation, limited research has been reported on the SIF, although B&V and the University of Edinburgh have undertaken some specific site assessments. Due to various studies published since 2005 (e.g. the ABPmer study funded by Juice), further work on understanding how to quantify the SIF (or extractable resource) at individual sites is important.

B&V therefore applied for Juice funding in February 2008 to update our work on the SIF. Due to budget constraints at Juice, the work reported here was also partly funded by Carbon Trust. This Appendix draws extensively on work carried out by Scott Couch at the University of Edinburgh (UoE), with additional input from Michael MacWilliams of River Modelling (USA); B&V mainly acted as 'project manager and client' to ensure the output of this work could be used to inform the main 'UK Tidal Current Resource & Economics' report, carried out by B&V for Carbon Trust.

3.2 Overall Approach

The focus of the work presented in this report is the far-field response of the tidal system with regard to the economic and environmental implications of widespread, large-scale TEC (tidal [current] energy converter) deployment. Hence, individual devices are not modelled in detail; instead they are treated as a 'black-box' system that is simply parameterised. The alternative approach is to consider the detailed interaction of elements of a TEC device with the immediate fluid flow, and in particular the generation of a downstream wake structure. Conflicting requirements (particularly both grid and temporal resolution) ensure that modelling approaches appropriate for simulating detailed fluid-device interaction are not yet suitable for investigating the far-field response of the system. The appropriate numerical modelling approach, and the appropriateness of existing numerical tools to analyse fluid-device interaction scale problems, remain the subject of significant academic research and debate. Hence for this study, a hydrodynamic tidal model adapted to simulate the large-scale impact of various hypothetical levels of energy extraction is used to assess the response of idealised representations of generic tidal regimes. Additional modelling of several real tidal environments, as opposed to generic representation, has then been used to undertake a partial validation of the generic results.

4 REVIEW OF PROGRESS SINCE THE MARINE ENERGY CHALLENGE (MEC)

4.1 Marine Energy Challenge approach

The resource assessment conducted for the MEC in 2004/5 presented a figure of 18 TWh/y as the technically extractable (=technical in this report) UK tidal current resource [1]. This assessment of the tidal current energy resource was arrived at by the following process:

1. Identifying locations appropriate TEC operation (e.g. with Vmsp > 2m/s);
2. Characterising these locations using simple identified metrics (e.g. Vmsp, other tidal characteristics, potential horizontal extent of the array, depth in the proposed area);
3. Mathematically manipulating the identified metrics to arrive at annual energy availability for each location.
   a. The kinetic energy flux across a cross-section of area A normal to the flow direction is typically considered as a measure of the energy available for extraction by the wind industry [2],

$$P_{KE} = \frac{1}{2}\rho A U^3$$

Equation 1

   Hence, [3] adopted the same approach to energy extraction formulation for numerical model application assessing tidal current energy resources. In practise, Equation 1 is summed over the period of interest with the input values of ρ, A and U in the formulation varying as prescribed by the available data.
4. The available energy was then multiplied by a 'Significant Impact Factor' (SIF) to derive the 'technically extractable resource' (now called technical resource).

This approach is termed the 'flux' method, and replaced the previous 'farm' method. The farm method follows the first two steps in the flux method, but then determines the extractable energy by developing an array of tidal stream devices that each extracts an equal amount of energy from the incoming flux. The number of devices and hence the extracted energy is purely dependent on the size of the device, its efficiency, and the packing density within the plan area.

The flux approach was considered a significant improvement over the farm approach because it attempted to consider the implications of the dynamic feedback response of the local tidal system to energy extraction. The energy extraction derived using the flux method is further constrained by the farm method if the required packing density of devices derived using the flux approach becomes physically unrealistic. Although offering an improvement over the farm approach, there remained significant uncertainty in the accuracy of the flux approach. Each stage of the analysis contributes to this uncertainty:

- The accuracy of the data available to characterise the individual identified locations;
- The selection of the appropriate metrics considered to be representative of the site;
- The method used to determine the annual energy availability;
- The applicability and accuracy of the SIF.

In the 2004/5 MEC analysis, an acceptable value of the SIF was prescribed based upon consideration of the reduction of mid-range tidal current velocities, derived from a quasi-steady state analysis at such mid-range velocity conditions. A reduction in mid-range velocity of 10-15% was deemed to be the upper limit of acceptable flow alteration due to energy extraction, although it was noted that this could be as high as 30% for certain sites. Given the lack of environmental data at the time, this was as much based on impacts on economics as impacts on the environment.

4.2 Garrett et al.

Analysis presented by Garrett *et al.* [4-9] has significantly progressed theoretical understanding of tidal current energy harvesting potential. As opposed to previous analysis (including the MEC output), instead of focussing on the resource potential from the point of view of the extraction technology, the focus is fully on the response of the resource to energy harvesting. Although the basis of the analysis presented is similar to the flux approach, thereby eschewing the farm type approach, [5] highlights the limitations of application of Equation 1 within this context when considering resource impact. Instead, analytical derivation produces an alternative formulation and set of assumptions for the maximum extractable power (*theoretical* power in the language of this report):

$$P_{\max} = \gamma \rho g a Q_{\max}$$

Equation 2

Where the coefficient $\gamma = 0.22 \pm 10\%$. For hydraulic current cases, a is prescribed as the amplitude of the sinusoidal sea level difference between the two ends of the channel [5]. In a closed basin, a is prescribed as the tidal elevation amplitude at the entrance to the basin [8]. Q_{max} is the maximum volume flux through the channel in the undisturbed case. Although the first proper application of Equation 2 form in tidal current energy harvesting application, this formulation bears obvious similarity to methods previously used successfully in the oceanographic community to quantify the net flux of barotropic tidal energy (e.g. at the entrance to a basin), and to quantify tidal energy dissipation (including historically by Garrett himself). This transfer and adaptation of knowledge from oceanography to tidal current energy engineering is crucial to continued development of understanding of tidal current energy resource potential. This of course has to be married with the appropriate engineering understanding of TEC device operation and project economics. As highlighted in the previous section, application of resource assessment formulations like Equation 2 must also be undertaken with an appreciation of the requirements of TEC technologies. Equation 1 is of an appropriate form for describing the resource acting on a TEC device; however, Equation 2 is more appropriate for characterising the resource potential of a particular channel. Appropriately utilised in tandem, the formulations provide significant insight.

Other relevant key outcomes highlighted by the work of Garrett and colleagues include:

- Identification of an upper limit to total tidal current energy harvesting in a particular region, as discussed in the 2004/5 MEC reports. Harvesting energy from tidal currents reduces the flow discharge through the channel. Velocity variation in a channel is closely linked to the flow discharge rate, and hence is also reduced due to energy extraction. Reduction of velocity reduces the kinetic resource available to each installed TEC device. Hence, as the number of TEC devices installed in a channel is increased, there comes a point at which introducing additional devices reduces the overall cumulative power generated [5].
- The limiting impact on power extraction levels if alternative flow pathways are available, as discussed in the 2004/5 MEC reports. In such scenarios, Equation 2 is an upper bound on the theoretical power available for extraction from the tidal current energy resource. Example cases include:
    - Tidal systems where alternative flow channels are available [7]. Also see [10, 11].
    - Channels where only a partial tidal fence is installed across the cross-section [6].
    - The extreme case of a TEC device or small array in a theoretically unbounded (laterally) domain [6].
- In the analytical solution for a hydraulic current system, maximum power extraction occurs when the head loss at the extraction location accounts for 2/3 of the head loss occurring across the channel length. Additionally, the flow discharge through the cross-section is reduced to 58% of that in the natural regime [5, 7].

- Considering potential environmental constraints, the analytical solution for a hydraulic current system suggests that up to 44% of Equation 2 with $\gamma = 0.22 \pm 10\%$ can be harvested without incurring more than a 10% reduction in flow velocity [7].
- The importance of TEC device support structure losses in reducing the power available for harvesting due to the presence of the device are flagged [9].

4.3 Northwest National Marine Renewable Energy Center (NNMREC)

Recent research conducted by Polagye *et al.* at NNMREC has further progressed and clarified understanding of the interaction of tidal power generation activity with the host tidal current energy system [11, 14]. Key relevant outcomes highlighted in this body of work include:

- Further independent corroboration of the response of the tidal physical system to harvesting of the tidal current energy resource. This can be summarised as follows [14]:

  > "The extraction of kinetic power from estuaries has been shown to reduce flow volume exchanged, tidal range, advected energy and kinetic power density, as well as altering the timing of the tides. The magnitude of these impacts is strongly dependent on the level of power extraction."

  These findings are in good agreement with existing hypotheses proposed by Garrett *et al.* [4-9] and Couch *et al.* [3, 10, 15-17].
- Further developing the above understanding, the importance of time-dependent analysis of energy harvesting is highlighted. The findings suggest that steady state analysis overestimates the impact of energy harvesting on the tidal system, This is due to 'restorative feedback' of the driving head – as energy is harvested the downstream depth is reduced, hence increasing the overall driving head along the channel length [14]. It is proposed that this effect will be of less significance in hydraulic current cases (such as the Pentland Firth), and is most applicable to basin domains (resonant or otherwise).
- As also related in Section 4.2, [11, 14] further highlight that statements of the kinetic power density (e.g. Equation 1) are an appropriate measure of the resource intensity, but are not well suited to prescribing energy harvesting potential.
- A case study example provides evidence of locations where the availability and appropriateness of sea-bed conditions for TEC device installation are likely to be a more significant constraint on energy harvesting than likely far-field environmental constraints [11].

4.4 ABPmer study

ABPmer was commissioned by Juice in July 2007 to quantify the exploitable tidal energy resources in UK waters. This ABPmer Juice-funded study [31] is one of the recent studies that have not understood the Significant Impact Factor as it was proposed during the MEC [1]. This section describes the method used by the ABPmer study, its main results, and the reasons why the results differed from those generated during the MEC [1].

The general method consisted of:

- Assessing technical device constraints (depths and rated velocities);
- Reviewing areas of interest physically suited to the different technology types (depths from 4 to 100m; Vmsp > 1.5m/s);
- Compiling marine spatial planning constraints (exclusion and co-existing);
- Calculating the annual energy yield based on the above.

Whilst the general approach above is sensible, the assessment of the annual energy yield applied the flux method [1] in a different fashion to how it was intended to be used.

According to its authors, the ABPmer study "calculated the potential exploitable tidal resource for individual data cells rather than specific locations of tidal resource. This has avoided the need for a Significant Impact Factor (SIF) as in earlier work (Black & Veatch, 2005) as the power outputs are determined by the size and power rating of technologies that are predicted to be deployed in an individual cell, based on the current speeds and available depth. Other research (Bahaj & Myers, 2004, Black and Veatch, 2005) states that tidal energy converters should not remove more than 10-20% of the tidal energy available in the system and the detailed methodology adapted for this study has ensured that this does not occur with the maximum percentage of energy extracted at for an individual cell predicted at just over 7%" [31].

The study therefore does not actually account for the limitation intended to be imposed by the flux method, which was essentially intended to ensure that deployment of TECs in multiple data cells did not result in over extraction of the available energy. In fact, the ABPmer study essentially simply used the historical farm method without the aggregation of the output data into farms as it only presented cell data. Indeed, if there are a large number of cells in line with the flow direction (as is the case in some locations), the methodology extracts significantly more energy than the application of the flux method as it was intended to be used.

As a consequence, the ABPmer study predicted approximately five times more extractable energy than the 2004/5MEC study [1], causing significant confusion in the industry. Given the above explanation of the methodology applied, it is not surprising that the ABPmer prediction is similar to the farm method calculation presented in the 2004/5 MEC work and previous similar studies.

The assessment did consider physical constraints very thoroughly and provides an excellent source of information on constraints for developers.

4.5 Salter's Pentland Firth Analysis

In response to widespread consultation towards the development of the DTI Energy Review [38], an alternative viewpoint querying the quantitative output of the MEC was highlighted by Salter [39]. He suggests that the tidal current energy resource available in the Pentland Firth should be an order of magnitude greater than identified in the MEC analysis. The basis of this statement was through analogy with the amount of energy being 'wasted' or lost to bed friction. The Pentland Firth is acknowledged as a key location of concentrated high tidal current energy, accounting for a significant fraction of both the UK and European tidal current energy resource. Further analysis [40] proposed that an average output of approximately 150 TWh/y could be harvested from the Pentland Firth. A further evolution of the analysis applied to the Pentland Firth again suggests that the MEC analysis approach is under-estimating the technically extractable resource by "at least one and possibly nearly two orders of magnitude" [41].

Although connected to plausible proposals for a third generation TEC device, the basis of the tidal current energy resource evaluation proposed in [39-41] is open to question. Much of the argument presented relates to discussion of the amount of tidal current energy being lost to bed friction and assumption that similar levels of energy extraction by TEC devices would have limited impact by effectively extracting the energy that was previously lost to bed friction. Estimates of peak friction loss for the Pentland Firth presented include 100GW [39], 53GW [40] 104.8GW [41] and 75GW [42]. Given that best estimates of the tidal energy dissipation across the whole European Continental Shelf are of the order 200GW [43], the figures presented for the Pentland Firth seem very large. Calculation of energy loss due to bed friction is of course highly sensitive to the selection of the bed friction coefficient C_D. Values of C_D used in [39-42] are typically around 0.02. This is not typical of values of C_D advocated in tidal hydrodynamic applications. More typical values of C_D for tidal application are generally an order of magnitude smaller [44, 45]. For a simple harmonically varying tidal current, the energy dissipation due to bed friction per unit area averaged over a tidal cycle is [44]:

$$\frac{4}{3\pi} C_D \rho U^3$$

Using similar values as presented in [39-42] for the Pentland Firth (U = 3m/s, ρ = 1025 kg/m3, channel length = 23 km, channel width = 10 km) in combination with a more appropriate bed friction coefficient (C_D = 0.0015[1]), energy dissipated due to bed friction averaged over a tidal cycle calculated is 4.05 GW. This value is, not surprisingly given the change in C_D, an order of magnitude lower than the values proposed in [39-42]. Another reason that the estimates differ is that Salter tends to quote peak power, whereas the power averaged over a tidal cycle is considerably lower. The average value for U for the entire Pentland Firth is also probably closer to 2.25m/s, which would additionally lower both estimates by over 50%.

Tidal hydrodynamic modelling of the UK's continental shelf (as proposed by the Energy Technology Institute) could assist in improving the current estimates of C_D.

4.6 MacKay

Analysis presented by MacKay [46, 47] correctly states that "the power encapsulated in a tidal wave is not equal to the kinetic energy flux across a plane". There is a common misconception that the 2004/5 MEC [1] analysis 'flux' method makes this assumption. The MEC analysis procedure utilises the kinetic energy flux across a plane as a metric for the energy available to a TEC device for harvesting. It is plainly stated in the 2005 MEC report [1] that the kinetic flux "is clearly only a percentage of the total (kinetic and potential) energy in a site". However, a site location with a large total energy flux dominated by potential energy with limited kinetic energy is clearly unsuitable for tidal current energy harvesting as the TEC devices would never reach typical cut-in velocities.

Further analysis in [46, 47] does add value in incorporating both potential and kinetic energy components in a formulation of the 'total incident power' potentially appropriate for application to a progressive tidal wave condition. However, such an application assumes that the tidal flows that we are concerned with follow progressive wave theory, which by combining equations G2 and G3 in [47] would give the velocity in the Pentland Firth as only 0.43 m/s. The flow in Pentland Firth, the most important site considered, is obviously not just the result of progressive wave propagation. If it were, then the 'total incident power' would be only 1.5GW.

The analysis in [46, 47] proceeds to evaluate the total (theoretical in the language of this report) instantaneous power available from the Atlantic in UK territorial waters. An overall average figure of 450GW [46] is proposed. Little attention is initially paid to the means of energy extraction. Of the 450GW resource potential proposed in [46], an arbitrary percentage is presumed to be extractable.

In [47], assessment of the UK territorial extractable resource is based upon a return to the 'farm' approach to resource characterisation, apparently as the author is unconcerned by the potential interaction between devices and cumulative effects of energy harvesting. This version of the discredited farm approach also takes in very large areas of low energy resource of limited economic value for tidal current energy development even in the long-term (e.g. V_{msp} values of c. 1.65 m/s), exacerbated by unrealistically extrapolating tidal current data over extensive areas.

[1] See Section 5.4 for a discussion of different options for modelling seabed friction. This value of C_D is equivalent to a Manning's coefficient of c. 0.025.

5 NUMERICAL MODELLING: VALIDATION AND INITIAL DISCUSSION

5.1 Basis of the tidal hydrodynamic modelling

5.1.1 Governing equations

The results presented in Section 6 have been obtained by the University of Edinburgh (UoE) team using the Tidal Flow Development-2d model (TFD-2d). The continuity Equation 3, x-directed momentum flux Equation 4 and y-directed momentum flux Equation 5 represent the Shallow Water Equation (SWE) model set adopted in TFD-2D. This SWE model approach is of a standard form adopted in many research and commercially operated numerical model codes used for examining tidal flows and relevant engineering interactions in the coastal environment.

$$\frac{\partial \eta}{\partial t} + \frac{\partial (Uh)}{\partial x} + \frac{\partial (Vh)}{\partial y} = 0$$

Equation 3

$$\frac{\partial (Uh)}{\partial t} + \frac{\partial (UUh)}{\partial x} + \frac{\partial (UVh)}{\partial y} - fVh + gh\frac{\partial \eta}{\partial x} + gn^2 \frac{U\sqrt{U^2+V^2}}{h^{\frac{1}{3}}} -$$

$$\frac{\rho_a C_w W_x \sqrt{W_x^{\,2} + W_y^{\,2}}}{\rho} - \left(\frac{\kappa \sqrt{g} n \sqrt{U^2+V^2}\, h^{\frac{5}{6}}}{6} \right) \left[2\frac{\partial^2 (Uh)}{\partial x^2} + \frac{\partial^2 (Uh)}{\partial y^2} + \frac{\partial^2 (Vh)}{\partial x \partial y} \right] = 0$$

Equation 4

$$\frac{\partial (Vh)}{\partial t} + \frac{\partial (UVh)}{\partial x} + \frac{\partial (VVh)}{\partial y} + fUh + gh\frac{\partial \eta}{\partial y} + gn^2 \frac{V\sqrt{U^2+V^2}}{h^{\frac{1}{3}}} -$$

$$\frac{\rho_a C_w W_y \sqrt{W_x^{\,2} + W_y^{\,2}}}{\rho} - \left(\frac{\kappa \sqrt{g} n \sqrt{U^2+V^2}\, h^{\frac{5}{6}}}{6} \right) \left[2\frac{\partial^2 (Vh)}{\partial y^2} + \frac{\partial^2 (Vh)}{\partial y^2} + \frac{\partial^2 (Uh)}{\partial x \partial y} \right] = 0$$

Equation 5

TFD-2d is a research-orientated tool as opposed to a commercial product. Model verification and validation has been well documented [e.g. 18]. A small but robust user community of UK based researchers operate the model as part of their daily research activities. The author of the majority of the TFD-2d code led the UoE involvement in this project.

The energy extraction methodology formulated by UoE has been validated as part of this project by River Modeling using the UnTRIM modelling tool (see section 5.2). The UnTRIM model solves the Navier-Stokes equations on an unstructured grid in the horizontal plane. The numerical method allows full wetting and drying of cells in the vertical and horizontal directions. The governing equations are discretized using a finite difference – finite volume algorithm. Discretization of the governing equations and model boundary conditions are presented in detail in [33] and is not reproduced here. All details and numerical properties of this state-of-the-art three-dimensional model are well-documented in peer reviewed literature [33, 34].

5.1.2 Energy extraction formulation

In order to simulate the influence of extracting energy from the system, the TFD model needs to consider extra physical processes beyond the original model equations (the standard Shallow Water Equations typically applied in two-dimensional tidal hydrodynamic models). The extraction of energy from the modelled system is a new application for tidal hydrodynamic models, only considered in recent years due to the recent development of TEC technologies. An additional term is proposed to provide the facility to simulate energy extraction from the system. This will be presented as an additional (friction-like) retarding force in the momentum equations based on the analytical solution of the kinetic energy flux across a nominal cross-section. Fundamentally, this is similar to the development of the kinetic energy flux approach presented in [3]. A benefit of the formulation presented over explicitly relating energy extraction by a direct increase in bed friction is that it would enable the approach to be applied both in 2d and 3d (e.g. sigma-layer) model operation.

Let P_x be the power extracted per unit volume (Wm^{-3}) and consider a control volume with dimensions Δx, Δy and Δz (i.e. a computational cell as typically prescribed in a numerical model). Then the power extracted from this control volume is $\Delta x\Delta y\Delta zP_x$. Assuming a tidal flow of velocity u in the x-direction, the equivalent horizontal retarding force acting in the negative x-direction on the control volume is:

$$\frac{\Delta x\Delta y\Delta zP_x}{u}$$

Equation 6

Applying (the x-component of) Newton's 2nd Law of Motion to the control volume leads to:

$$\rho\Delta x\Delta y\Delta z\frac{Du}{Dt}=.....\ \text{(various terms)}.....-\frac{\Delta x\Delta y\Delta zP_x}{u}$$

Equation 7

Dividing the above equation through by $\rho\Delta x\Delta y\Delta z$, assuming P_x is constant over the depth and integrating from $z=-d$ to $z=\eta$ yields the following depth-averaged momentum equation (and as traditional for the similarly derived advective momentum terms occurring on the right-hand side of the equation, ignoring the slight non-linearity introduced by depth-integration):

$$\frac{\partial hU}{\partial t}.....=..........-\frac{hP_x}{\rho U}$$

Equation 8

By explicitly prescribing a value for the power extracted per unit volume P_x in relation to a notional extraction device operating at a notional device efficiency, the right hand side term in Equation 8 can be used to determine the energy loss and redistribution in the system when incorporated into the x-directed momentum flux Equation 4. Simultaneously, this enables the response of the hydrodynamic system to the additional energy loss term to be analysed.

For the sensitivity analyses in the following sections of the report, rather than prescribe the amount of energy extracted explicitly (which would take no account of the actual amount of 'driving' kinetic energy available for operating a TEC device), or propose a notional TEC device performance curve, a percentage of the in-situ kinetic energy in the system is extracted. This does imply a simplification in the analysis, as a real TEC device would have additional operational parameters such as a cut-in and rated operational velocity. However, the approach is attempting to be technology neutral. Additionally, the focus of the analysis is on the tidal response of the system to various levels of energy extraction. It must be highlighted that the direct impact of a TEC device on the tidal system remains unclear in existing scientific understanding. As well as the energy directly harvested by an individual device (as measured by the amount of energy delivered to the electricity grid), the conversion efficiency of the device, and additional resistance to flow imparted by the structure of the TEC device also need to be taken into consideration regarding the response of the tidal system to TEC device deployment and operation. These additional aspects of fluid-device interaction are not well understood. It is therefore proposed to examine the effect of varying levels of energy 'extraction', without directly apportioning how much of the energy extracted from the system is actually harvested or converted to electricity. The model adopts the format of expressing the energy extracted as a percentage of the in-situ kinetic energy flux through the relevant computational cell at that particular time-step (i.e. applying a selected fraction of the right-hand-side term in Equation 8, by expressing the value of P_x based upon **Error! Reference source not found.**, where $P_{\%}$ is the fractional representation of the percentage of extraction).

$$P_x = \frac{P_{\%}\left(\frac{1}{2}\rho h \Delta y U^3\right)}{h \Delta x \Delta y} = \frac{P_{\%}\rho U^3}{2\Delta x}$$

Equation 9

Error! Reference source not found. relates to the component of energy acting directly on a TEC device. This therefore provides a simple analytical means of expressing the amount of power 'extracted' within the numerical model. This formulation confers additional operational advantages for the purposes of this analysis as it requires no pre-knowledge of the final solution, and provides an easy means of varying the amount of power to be extracted for the purposes of sensitivity analysis. In order to be able to relate the power extracted back to something more intuitive, the instantaneous and equivalent average power extracted across a flood-ebb (semi-diurnal, M2 tidal constituent) period of the tidal cycle as simulated by the model is recorded for each sensitivity test.

5.1.3 Expected flow alterations

With the present state of development of TEC technology, real world observation of both the near- and far-field effects of energy extraction has still yet to be robustly investigated or reported on in the literature. The monitoring required to examine these processes in detail is a serious and significant undertaking. Nonetheless, various assumptions regarding the impact on flow development of TEC device operation can be proposed, supported by appropriate analogy. In the extreme case of complete flow blockage (e.g. an island), the near field effect is well understood:

- Upstream of a blockage, a local adverse pressure gradient is established, reducing the flow velocity from that in the free-stream in the direction of the blockage element.
- This creates an increased compensatory flow adjacent to the adverse pressure gradient region.
- In the lee of the blockage, a sheltered reduced flow region persists encapsulated by a depression in the free surface. In the complete blockage (island) case, there is potential for the development of flow separation and various eddy structures in the downstream sheltered region. Flow separation would not generally be expected in a partial blockage (e.g. TEC device) case.
- The downstream sheltered flow region is bounded by the increased compensatory flow in the horizontal. In the case of most typical TEC devices, it is also appropriate to expect increased flow velocities above and below the position of the TEC device energy capture surface, as would be the case for the analogous porous disk situation (assuming that the TEC device

capture surface is operating in some fraction of the water column between the sea bed and free surface).

- The persistence of the downstream sheltered region is a function of mixing and pressure gradients between the sheltered flow and adjacent high flow region. Significant energy transfer into the wake due to these mechanisms will promote the return to a balanced free-stream flow condition further downstream. Mixing across the boundary region between sheltered and adjacent high flow would be expected to be higher than typically experienced in the free stream in both the horizontal and vertical plane due to the velocity gradient between the two regions. The favouring pressure gradient acting towards the centre of the sheltered flow region established by the depression of the free surface in the wake region will also promote energy transfer into the wake.

5.2 Model validation

The test cases developed by UoE using TFD-2D [3] have been replicated by River Modeling using the UnTRIM standard industry model. The test cases demonstrated that the implementation of the energy extraction method within the UnTRIM model provides very similar results to the implementation within the TFD model. The validation provided confidence in the methodology and enabled its application to real world examples where the UnTRIM model (without energy extraction) has previously been very well validated. These examples are presented in Section 7.

5.3 Generic tidal current regimes

Locations appropriate for tidal current energy development share certain key characteristics. The most significant characteristic in judging the economic potential of extracting tidal current energy at a site is the intensity and extent of the natural resource available. The intensity of the resource is crucial to project economics – a wide, deep channel with relatively slow velocities may encapsulate the same overall kinetic energy resource as a narrow shallow channel with relatively faster velocities; however, TEC device operation is only economically suited to the latter situation.

This is because the TEC operating or 'capture' surface is operated on by the kinetic energy in the local flow, by definition, and the kinetic energy is related to the cube of the flow velocity. Although there is typically significantly more potential energy stored in a tidal energy system, TEC technologies are not directly operated on by potential energy and other technologies more suitable for extraction from potential energy (such as barrages) should be considered for sites where the kinetic energy intensity is too low for economic TEC deployment.

Of course there are a whole hierarchy of other important criteria that also impact on site identification and selection. However, a first pass analysis would sensibly concentrate on assessing the local energy harvesting potential from simple consideration of the local tidal current flow velocity characteristics. Historically, and as in the 2004/5 MEC reports, this has generally used parameters such as minimum mean spring peak velocity to initially identify sites that have economic potential.

[15] proposes a means of characterising a particular location as being dominated by one of five key mechanisms that prescribe the likely velocity characteristics of the site. The first two mechanisms (which predominate in most coastal regions) do not generate the characteristics that are of interest for economic TEC deployment. The other three mechanisms (see below), although much more unusual in their relative occurrence, can in the right circumstances generate flow conditions of potential interest for further investigation of TEC deployment.

Tidal streaming: Is the physical response of the tidal system to maintenance of the continuity equation; when a current is forced through a constriction, the flow must accelerate.

Hydraulic current: If two adjoining bodies of water are out of phase, or have different tidal ranges, a hydraulic current is set up in response to the pressure gradient created by the difference in water level between the two bodies. The resulting hydraulic current generated between the adjoining regions can become very large.

Resonant system: Resonant systems occur as a consequence of a standing wave being established. A standing wave arises when the incoming tidal wave and a reflected tidal wave constructively interfere. The interaction of the waves can create very large tidal amplitudes and associated tidal currents from the enhanced local pressure gradient.

For the purposes of examining the potential to develop a parametric model that can be applied across a range of sites in order to enable a national resource study, the approach adopted in this report is to consider exemplar cases of each of the three relevant mechanisms. This then enables parameterisation of the response of each of the three systems to energy harvesting through TEC deployment. This is crucial because the three identified mechanisms potentially respond differently to various levels of energy extraction, which has not as yet been explicitly addressed in detail in existing research.

The drawback of developing a parametric approach to a complex non-linear system is of course the obvious simplification that is required in order to prescribe a simple set of generic parameters. The benefit is the potential ability to extrapolate the analysis across a large number of cases without requiring the extensive (time and economic) resources required to conduct detailed individual case-by-case assessments. In this particular case, it is important to highlight that although for the purposes of analysis the three mechanisms will be considered individually, a specific real world location will potentially be impacted by all five mechanisms. The analysis conducted for this piece of work makes the simplifying assumption that the tidal regime at any particular location will be dominated by one of the mechanisms. This limitation is necessary in order to ensure that the research problem is tractable within the constraints of the programme of work. Even although these qualifiers are necessary, the methodology used potentially adds significantly to existing understanding of tidal energy harvesting potential.

5.4 Key metrics for comparison of generic scenarios

A number of key parameters have been selected as the metrics for comparison of the various generic scenarios presented. Each parameter is evaluated to establish the instantaneous, maximum, minimum, average and summed value of each variable across a simulated flood-ebb cycle (semi-diurnal, M2 tidal constituent period). The parameters evaluated were:

- Power extracted (P);
- Discharge through the cross-sectional area (Q);
- Depth-averaged streamwise velocity amplitude (U);
- Head loss at the energy extraction site;
- Tidal range immediately upstream and downstream of the extraction location.[2]

After extensive evaluation of the various simulation results, an additional variable was added to the list of key metrics presented, the % of average energy flux extracted over a tidal cycle (β), which is derived during post-processing of each simulation modelled:

[2] Although there is some relationship between the head loss occurring at the extraction location and alterations to tidal range, the response is non-linear. What is important to recognise is that the head loss is not equivalent to a similar reduction in overall tidal range. In fact, although head loss can be large, the tidal range impact is generally significantly smaller. The head loss is to a large extent a consequence of a change of phase promoted by energy harvesting as opposed to an overall reduction of tidal range in the system.

$$\beta = \frac{\left(\sum_{t=0}^{t=T} P_{\%} \frac{1}{2} \rho \Delta y h U^3\right) \Big/ T}{\rho g a Q_{max}}$$

Equation 10

Note the similarity of the denominator in Equation 10 to Equation 2 without the coefficient γ (at this stage). In fact, calculation of β is equivalent to determining the local value of γ for the particular experimental case under consideration.

Certain potential variables or simulation characteristics were held constant in all the scenarios considered, and hence did not require individual analysis in each case. These included:

- All cases used a cold start initial condition (i.e. both velocities and surface elevation were set to zero throughout the domain on the initial time-step).
- The first M2 period of each simulation was used as a model 'spin up' period; hence results were only examined after 12.4 hours of simulated time (unless otherwise stated)..
- No wind stress was applied in any case.
- Manning's friction coefficient[3] (representative of generic sea-bed conditions) = 0.025 sm-1/3. (These unusual units are necessary to adhere to SI units, although Manning's friction coefficient is often considered as non-dimensional in practice).
- A uniform depth of 35 metres was applied in all the generic cases considered unless otherwise stated. This is deemed an appropriate depth for the installation and operation of the 'first-generation' of leading TEC device technologies currently at the stage of pre-commercialisation full-scale device demonstration and testing. Additional tests using depths appropriate for 2nd generation device operation (65 metres depth) are also presented.
- All driving tidal boundary conditions were specified as being represented by a single dominant (M2) semi-diurnal constituent (period = 12.4 hours).
- For all energy extraction cases, the energy extraction term acted across the full width of the model domain, mid-way between the upstream and downstream boundary conditions (i.e. the centre of the domain) unless otherwise stated.

Additional case specific details are highlighted in the description of the individual tests.

5.5 Theoretical, technical and practical resource considerations

Not all resource assessments are conducted utilising the same constraints. The intention of the methodology presented within this document is to arrive at appropriate means of assessing the theoretical and technical resource availability in the three generic regimes identified. Consideration of the practical resource is project specific, requiring investigation on a case-by case basis.

[3] Manning's friction coefficient is used as this is the standard term for describing seabed friction in tidal hydrodynamic modelling (the Chezy number is also sometimes used). Manning's friction coefficient (n) is defined by:

$$C_D = gn^2 H^{-1/3}$$

The Chezy number is defined by: $C_D = \dfrac{g}{C^2}$

A value of n of 0.025 implies values for C_D of c. 0.002 (depth dependent). Most literature relating to hydrodynamic modelling implies a value for C_D of c. 0.001-0.004.

Quantifying the theoretical tidal current energy resource is of limited practical end-user application. Likely limitations of acceptable impact on the physical environment potentially reduce the energy available for extraction below that of the theoretical harvestable limit. Potential limiting physical environmental impact factors that need to be minimised in the context of energy harvesting are far-field resource effects such as:

- change in the tidal range (e.g. impacting on key intertidal regions such as mudflats and saltmarshes);
- change in the velocity flow field (e.g. impacting on sediment erosion and deposition rates [17]);
- change in the volumetric flow rate (e.g. impacting on flushing of estuaries through altering the tidal prism);
- Change in the overall kinetic energy density due to variation of all of the above criteria (e.g. impacting on the economics of any potential tidal current energy development in the region).

Near field effects are more relevant to the operation of individual devices and interaction of devices in an array (e.g. the wake region generated by the fluid interaction with the TEC device limits the 'packing' density of devices in an array). The different scales of the key concerns ensure that different numerical modelling tools are appropriate for examining the various processes. As the focus of this analysis is on the wider response of the resource to energy harvesting, far field effects are considered to be of most generic relevance. To enable further discussion on potential limitation on the harvesting of the theoretical tidal current energy resource, arbitrary statements of acceptable resource response to energy harvesting will be examined.

For the purpose of this analysis, a 10% reduction in mean peak flow velocity or 0.1-metre reduction in tidal amplitude (0.2-metre reduction in tidal range) were considered as being the notional limits of environmental sensitivity. Ecological systems encountered at sites of high tidal current energy density are deemed to remain relatively unaffected by small changes in peak velocities of the order of 10%: these systems are inherently accustomed to high variability in local tidal stream velocity and sedimentation is unlikely to be an issue as most suitable sites feature a relatively rocky type of seabed[4]. Based on previous knowledge and experience, the notional limit of tidal range sensitivity was conservatively set to 0.1-metre reduction in tidal amplitude (0.2-metre reduction in tidal range) or 5% of the mean spring range value, whichever gives the minimum figure. For simplification, the 0.2m notional tidal range limit is used in every graph presented in Section 6.

It should be noted that these expressions of environmentally acceptable alterations have no legislative or regulatory basis; they are simply hypotheses. Understanding of environmental impacts and sensitivity of project development will likely have to be examined in great detail on a case-by-case basis once large-scale TEC deployment becomes a reality. In the near term where individual devices or small arrays of multiple (< 10) devices are likely, environmental impacts of the order of the 'acceptable' limits suggested here are unlikely to be a constraint.

[4] For further discussion of this aspect, see Section 4.3.5.2 of the 2005 MEC report.[1]

6 NUMERICAL MODELLING: SIMULATIONS, RESULTS AND ANALYSIS

6.1 Hydraulic current scenario analysis

A hydraulic current is representative of the flow conditions most often considered in early tidal energy resource assessments, as this incorporates a regime where the boundary conditions can be simply prescribed (accepting some basic assumptions), particularly when developing an analytical solution [e.g. 5, 19]. In a numerical model, these conditions are also simple to simulate, as a hydraulic current scenario is equivalent to explicitly specifying the upstream and downstream boundary conditions in order to generate an imposed varying pressure gradient across the domain. This also mimics the real world physical processes in action (under the assumption that the outer regions connected by the channel will be insensitive to flow alterations in the interior introduced in the simulation scenarios). From a coastal oceanographic perspective, classic cases of this type of flow regime include French Pass in New Zealand [20], the Strait of Messina, Italy [21] and the Naruto Strait, Japan [22]. In the UK, although other mechanisms also play a part, the Pentland Firth, Falls of Corryvrecken and Strangford Narrows can be considered as example regions where a hydraulic current is the dominant feature.

6.1.1 Experimental set-up

As hydraulic currents are typically generated in channels linking two larger bodies of water, simple rectangular cross-section channels with lateral topographic boundaries were considered. As earlier indicated, both upstream and downstream boundary conditions were explicitly prescribed. Simple M2-like sinusoidal elevation boundary conditions were imposed, with a phase shift between the two boundaries selected as necessary to generate the desired driving pressure gradient variation across the domain. As this is the regime type that has been the focus of most of the existing research, various cases were considered to test the various theories that have been proposed in the literature as detailed in Section 4. The various model domains simulated involved the additional change of one domain specific variable for each experiment to examine the sensitivity of the solution.

In each of the simulated cases listed in Table 1, the phase shift of the upstream and downstream boundary conditions (with reference to the flood tide), created a compensatory varying pressure gradient (head difference) across the domain length. As the two prescribed boundaries were sinusoidal, the variability of the head difference across the channel was also sinusoidal on the same period, with a phase shift dependent upon how different the imposed phase difference was from the naturally occurring difference due to propagation of the tidal wave. Figure 1 demonstrates how this is manifested in the case 1 experiment.

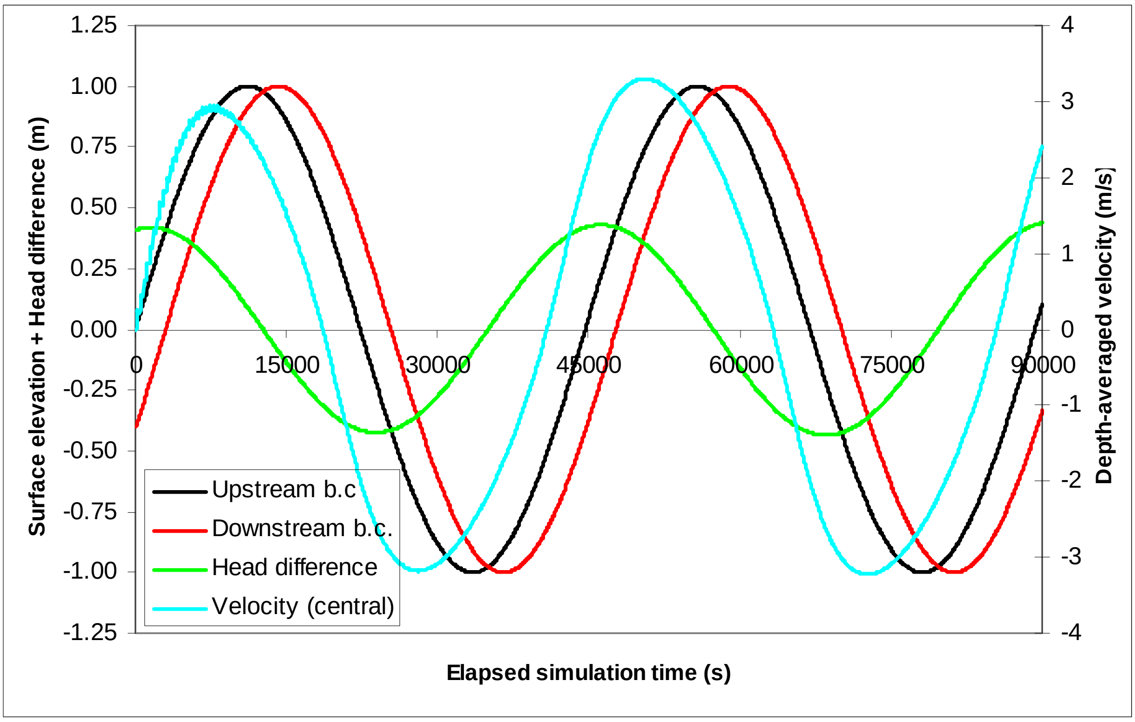

Figure 1 Upstream and downstream elevation driving boundary conditions, the subsequent pressure head variation established along the 6km domain length, and depth-averaged velocity variation in the centre of the domain (case 1).

Case number	Δx (m)	# cells in x-direction	Δy (m)	# cells in y-direction	Uniform depth (m)	Boundary elevation amplitude (m)	Phase shift (s)	Velocity generated (m/s)
1	43	140	43	71	35	1.0	3000	3.29
2	43	280	43	71	35	1.0	3000	2.05
3	43	280	43	71	35	1.0	6000	3.17
4	43	280	43	71	35	2.5	3000	3.65
5	43	140	43	71	65	1.0	3000	4.19

Table 1 Experimental set-up conditions for the hydraulic current scenarios.

Figure 2 demonstrates the simulated evolution of the free surface elevation and velocity in the centre of the domain for a flood-ebb cycle due to various levels of requested energy extraction in the case 1 experiment[5].

What is immediately obvious is that the depth-averaged velocity is much more sensitive to energy extraction than the free surface elevation. Both flow properties experience a small phase shift with increasing extraction, and additionally, their temporal variation evolves away from pure sinusoidal shapes. In terms of the free surface elevation, this variation in combination with the fixed upstream and downstream driving boundary conditions relates to the overall reduction in friction slope across the domain length. This is compensated by an increased head difference observed across the energy extraction model region (see **Figure 3**). This is in-line with the expected flow alterations discussed in Section 5.1.3, and the complimentary findings of the literature discussed in Section 4.

[5] The description in Section 5.1.1 explains the prescription of the % energy extraction applied in each model simulation. The actual percentage value is of no significance other than from a numerical model simulation operational perspective.

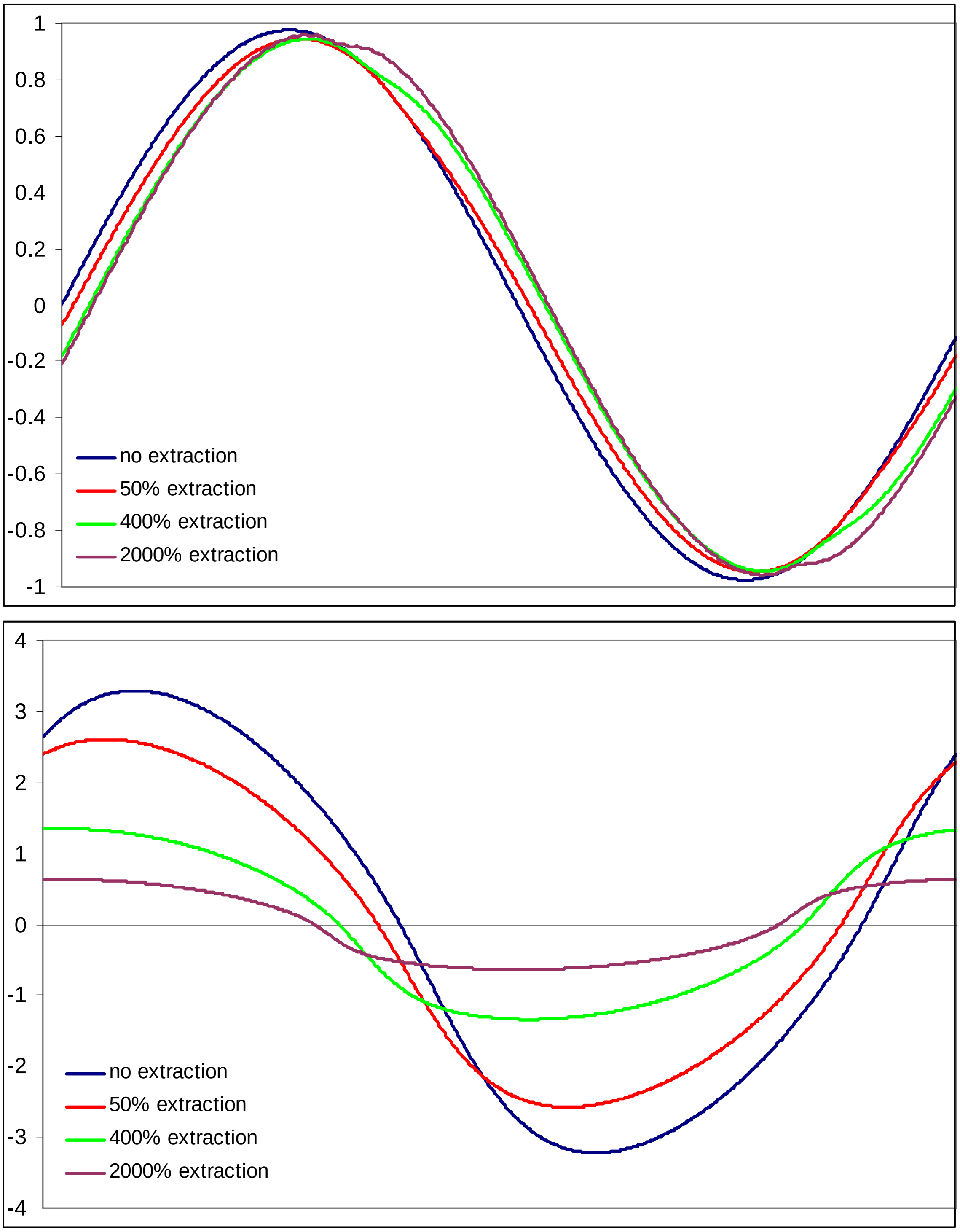

Figure 2 Evolution of (i) free surface elevation (m) and (ii) velocity (m/s) at the intended deployment location with varying levels of energy extraction for case 1. [6]

[6] The description in Section 5.1.1 explains the prescription of the % energy extraction applied in each model simulation. The actual percentage value is of no significance other than from a numerical model simulation operational perspective.

Considering the 'natural' (no energy extraction) flow regime established in each of the five experimental cases presented, the various alterations imposed on each simulation set-up can have a significant impact.

Case 1 is representative of the base case under consideration – a relatively short channel with appropriate depth and peak velocities of interest for energy harvesting consideration. The evolution of velocity in response to the sinusoidally varying head difference across the channel length is approximately 55 degrees out of phase with the free surface variation (≈ 1.9 hours). The velocity time history varies slightly from sinusoidal – the ebb tide is slightly shorter, and hence flood tide elongated (only by a few minutes). Peak flow velocities on the flood tide reach 3.29 m/s, 3.22 m/s on the ebb.

Case 2 exactly replicates case 1 apart from doubling the length of the channel (from 6 km to 12 km). As the prescribed head difference along the channel length is the same as for case 1, less forcing pressure gradient is developed. This is borne out in the simulation results, where a maximum peak velocity of 2.05 m/s is achieved.

Case 3 builds upon the previous case by doubling the phase difference used to prescribe the boundary conditions. In combination with the doubling of the length of the channel from case 1, at first pass, a similar result to case 1 would perhaps be expected. A similar general simulation is output from the model. However, the peak velocity is reduced to 3.17 m/s. This reduction in velocity in comparison with case 1 is easily explained. Two mechanisms are at work. First, the extended length of the channel ensures that more work is done overcoming friction than in case 1. Additionally, although the phase shift is doubled, as the channel length is also doubled, the propagation time for the tidal wave across the channel length is itself increased. Hence the natural head difference that would occur across the channel length due to progressive wave transmission is (slightly) closer to the imposed head difference than is the case in the shorter channel, partially off-setting the imposed hydraulic current.

Case 4 is a different extension of case 2, where the amplitude of the boundary condition sinusoids are both increased to 2.5 metres. The increased free-surface amplitude in combination with a phase difference generates significant head differences, and hence pressure gradients along the channel. This is reflected in the peak velocity occurring in the system (3.65 m/s).

Case 5 replicates the case 1 experiment, except the depth is increased to 65 metres in this case.

6.1.2 Sensitivity analysis

For each of the cases examined, a 4-diagram grid is provided to present in-depth data to enable consideration of generic resource responses. This summarises the overall analysis conducted to aid in the development of a parametric model that fits the available data. The presentation of these 4-diagram grids is representative of a substantial numerical modelling simulation and analysis effort to arrive at the findings regarding the response of the hydrodynamic system to energy harvesting, and to distil the findings into as user-friendly a format as possible.

For each domain, the response to various levels of energy extraction is presented. The base comparison scenario is the equivalent 'natural' state (no extraction). A series of levels of energy extraction in proportion with the dynamically varying available resource at the extraction location (as described in Section 5.1.1), are then examined. Interpretation of the first case 4-diagram grid is provided below. The 4-diagram grids for cases 1-5 are then presented. The outcome to be taken from the hydraulic current scenario cases is summarised in the 'Interpretation' section that follows.

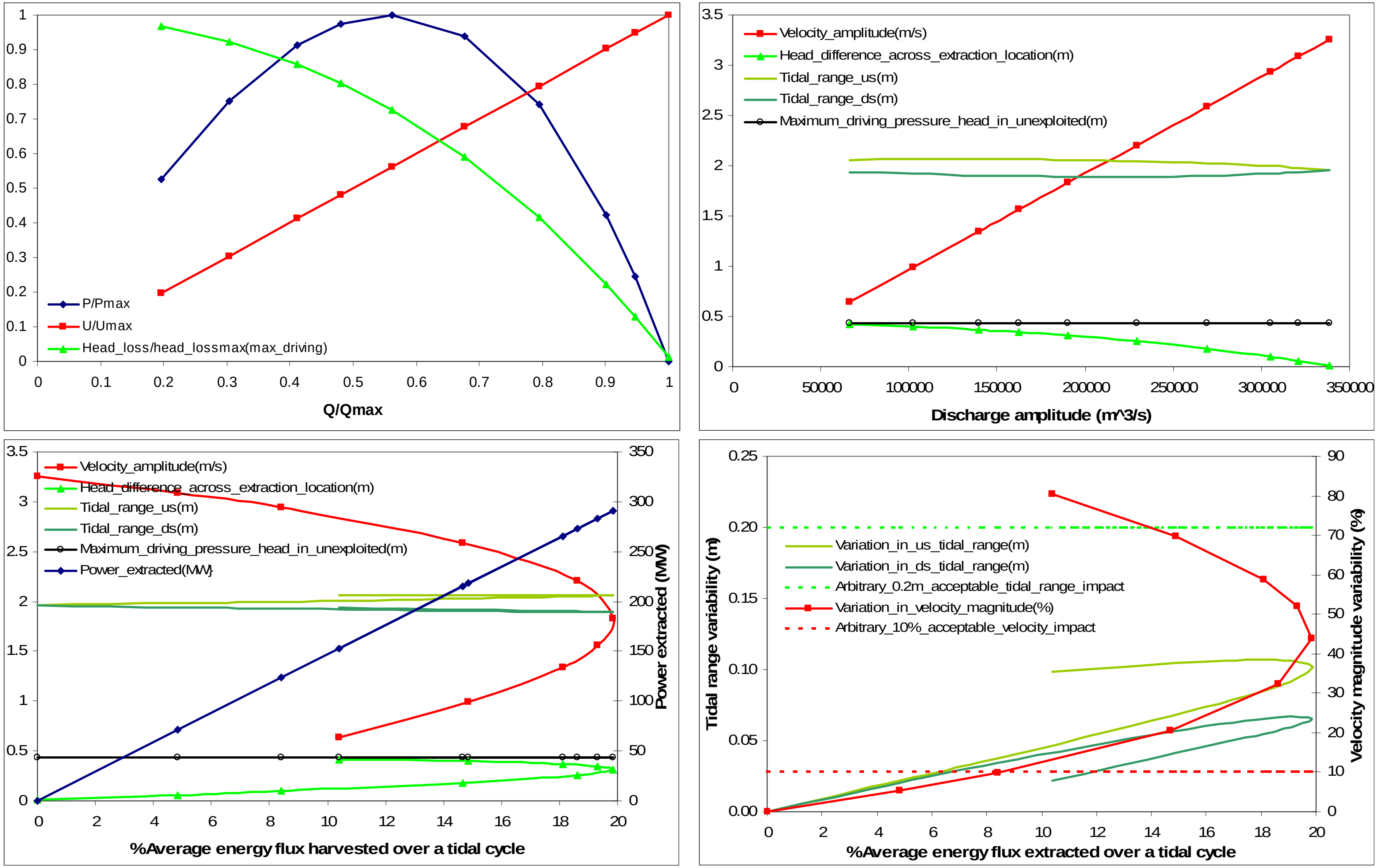

Figure 3 Impact of varying levels of energy extraction for hydraulic current case 1: (i) Non-dimensional analysis, (ii) Discharge amplitude dependence, (iii) % average energy flux extracted dependence, and (iv) Variation with % average energy flux extracted, and identification of constraint limits

Figure 3 encompasses four individual graphs that together describe the overall response of the case 1 experiment to various levels of energy harvesting.

- Graph 1: Following the general approach of [7], the response of various non-dimensionalised parameters across the range of energy extraction simulated is presented. Each non-dimensional variable on the y-axis is an expression of the fraction of the maximum value achieved in each set of simulations for that particular experimental 'case'. Each parameter is evaluated over a complete flood-ebb tidal cycle for inter-comparison between the cases. The x-axis represents the variation (reduction with increasing energy extraction) of peak flow discharge through the channel cross-section (the graph should be read right to left if starting from the no extraction case).
  - The red line describes the response of the peak velocity in each simulation. It is almost linearly related to the x-axis variability. This is not surprising given the relationship between the variables U and Q, and the relatively small variation of the overall flow depth h occurring in the simulations.
  - The green line describes the head loss response occurring across the extraction plane. The maximum value for comparison in this case is taken as the available maximum driving head along the channel prescribed by the maximum instantaneous difference in the upstream and downstream boundary conditions (see Figure 1). The head loss term with no energy extraction is equivalent to the friction slope occurring naturally in the simulated channel across the extraction plane (i.e. very small). With increasing energy extraction, more of the available head difference in the channel is transferred to the extraction plane. The reduction of available driving pressure gradient across the entire channel length that this represents is reflected in the corresponding reduction of both U and Q upstream and downstream. The variation of head loss is not linear. Although impossible to achieve in reality, in principle it is obvious from extrapolation on the graph that transfer of all of the head difference to the energy extraction plane would be equivalent to zero velocity and discharge through the channel.
  - The blue line describes the variation of the total mean power harvested across the flood-ebb cycle relative to the maximum achieved in each 'case' experiment. In the no extraction case (Q/Q_{max} = 1), obviously no power is harvested. The response of the P/P_{max} term is then observed for varying extraction scenarios. P/P_{max} peaks in this case at 0.56 of Q/Q_{max} (a reduction of 44%), although the exact value of peak power production was not heavily scrutinised due to time constraints that would be required for this iterative experimental process to completely refine the numerical simulations. At peak values of P/P_{max}, the peak velocity in the channel has also been reduced by 44%. The peak head loss occurring across the extraction plane in this case is 72% of the available maximum driving head difference. After reaching peak power harvesting, the overall amount of power harvested reduces with reduction in U and Q. However the amount of head loss occurring across the extraction plane continues to increase, even though less power is produced by energy extraction.

- Graph 2: As graph 1 demonstrates how significant the discharge through the cross-section is, graph 2 examines the variation of various parameters in each experiment in case 1 to the maximum discharge amplitude occurring (x-axis).
  - The red line describes the variation in velocity amplitude due to various levels of extraction from the system. This varies almost linearly with discharge amplitude as should be expected ($Q \rightarrow 0$ m^3/s, $U \rightarrow 0$ m/s).
  - The green 'head difference across the extraction plane' line is as in the previous graph. With reduction in discharge amplitude due to extraction, the head difference across the extraction plane tends towards the maximum driving head difference occurring along the channel due to the prescription of the boundary conditions (as portrayed by the blue line). The variation is not linear.

- The light green (tidal range upstream of the extraction plane) and dark green (tidal range downstream of the extraction plane) lines portray the variation of tidal range. Although the head difference across the extraction plane appears to play a key role in describing the amount of power extracted in each case, from an environmental impact perspective, alterations to tidal range are potentially of most interest. As extraction is altering both the magnitude and phase of various tidal characteristics, the alteration to tidal range is not just a function of head difference at the extraction plane. The upstream and downstream tidal ranges are identical in the no extraction case to all intents and purposes.
  - The downstream tidal range achieves a maximum value in the no extraction case. Hence the impact of energy harvesting is to reduce the tidal range downstream of the energy extraction plane. This reduction is limited by the controlling downstream boundary condition, which as set up for the hydraulic current channel experiment scenarios is insensitive to alterations occurring in the channel. The maximum reduction of downstream tidal range in this case is 0.066 metres (-3.3% of local no extraction case maximum tidal range). This maximum reduction in downstream tidal range is <u>not</u> directly related to the occurrence of peak power harvested.
  - The upstream tidal range achieves a minimum value in the no extraction case. Hence the impact of energy harvesting is to increase the tidal range upstream of the energy extraction plane. The increase is limited by the controlling upstream boundary condition, which as set up for the hydraulic current channel experiment scenarios is insensitive to alterations occurring in the channel. However, the tidal range immediately upstream of the extraction plane <u>exceeds</u> that of the input boundary condition – demonstration of the potential 'blocking' effect of energy harvesting. The maximum increase in upstream tidal range is 0.107 metres (+5.4% of local no extraction case maximum tidal range). This maximum increase in upstream tidal range is <u>not</u> directly related to the occurrence of peak power harvested, nor does it occur in the same experimental case as the minimum downstream tidal range.

  Alteration to tidal range in the domain is obviously a complex function of both (prescribed) upstream and downstream boundary conditions, energy harvested and local flow discharge. It is important to highlight that the change in tidal range observed in hydraulic current cases is not directly related to the head difference at the extraction plane.

- Graph 3: Compares the dependence of (i) maximum velocity magnitude, (ii) upstream tidal range, (iii) downstream tidal range, (iv) maximum head difference occurring across the extraction plane, and (v) the average power extracted across a simulated flood-ebb tidal cycle versus the % of average energy flux extracted over a tidal cycle shown on the x-axis (β – Equation 10). Basically, the x-axis is an assessment of the factor γ in Equation 2 for each particular extraction case scenario. What is immediately apparent is that each of the properties examined on the y-axis previously listed peaks at β (= γ) = 19.83%. This is indicative of the maximum *theoretical* power that can be extracted from this combination of domain and tidal regime.
  - The blue line indicates the average power harvested from the system over the simulated tidal cycle. This varies linearly with the x-axis property (as would be expected given the meaning of β. It is important to recognise that the maximum value of the average power extracted over the simulated cycle is equivalent to the *theoretical* power that can be extracted from this combination of domain and tidal regime (290.86 MW average throughout the simulated flood-ebb tidal cycle (as plotted), with an instantaneous peak value across the flood-ebb cycle of 597.1 MW). It is also important to recognise that the blue line encompasses values both increasing towards the maximum value achieved, and values decreasing after the peak value has been achieved (i.e. there is a data point lying on the blue line relating to each data point on the other plotted lines).

- The red line indicates the maximum velocity amplitude occurring in each extraction simulation.
- The variation of the three green lines representing the maximum head difference, upstream and downstream tidal range are fairly self-explanatory. However the variation of the tidal range values is not entirely obvious due to the small variation of these quantities. Hence graph 4 reports the *variation* in tidal range between the various extraction scenarios as opposed to the total value of these properties.

- Graph 4: Compares the variation in (i) maximum velocity magnitude, (ii) upstream tidal range and (iii) downstream tidal range versus the % of average energy flux extracted over a tidal cycle shown on the x-axis (β – Equation 10). This enables consideration of the environmental limitations proposed in Section 5.5 (indicated by the broken lines). Neither the variation in upstream or downstream tidal range exceeds the proposed acceptable limit even at the maximum *theoretical* power limit in this regime. However, the variation in velocity magnitude (indicated by the solid red line) intercepts the proposed acceptable limit for velocity variation (indicated by the broken red line) at around 8.5% of β. This is indicative of the maximum *technical* power that can be extracted from this combination of domain and tidal regime. In this case, the ratio of technical to theoretical power is 42.8%.

Figure 4-Figure 7 present the same format of results as just described for cases 2-5 listed in Table 1.

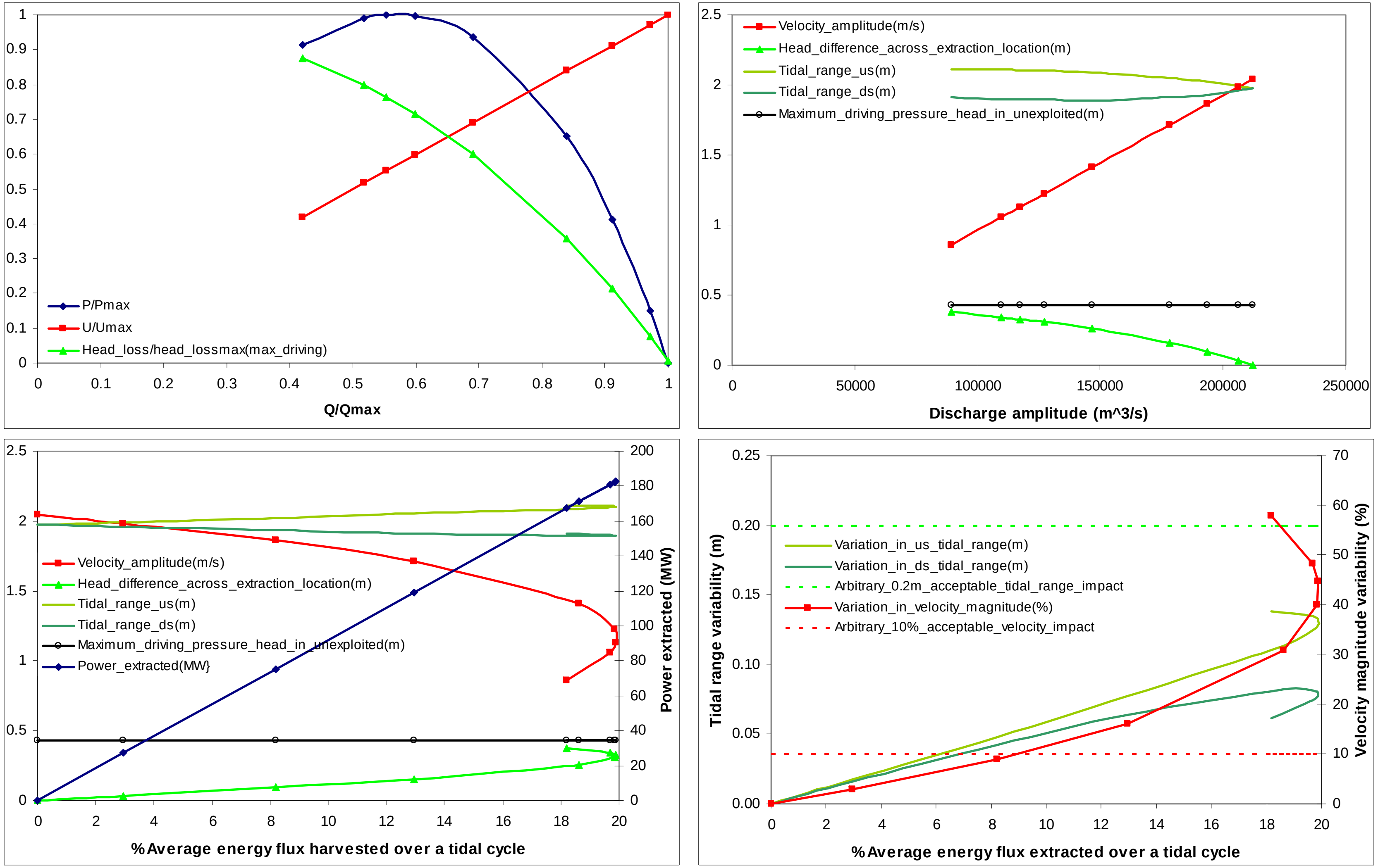

Figure 4 Impact of varying levels of energy extraction for hydraulic current case 2: (i) Non-dimensional analysis, (ii) Discharge amplitude dependence, (iii) % average energy flux extracted dependence, and (iv) Variation with % average energy flux extracted, and identification of constraint limits

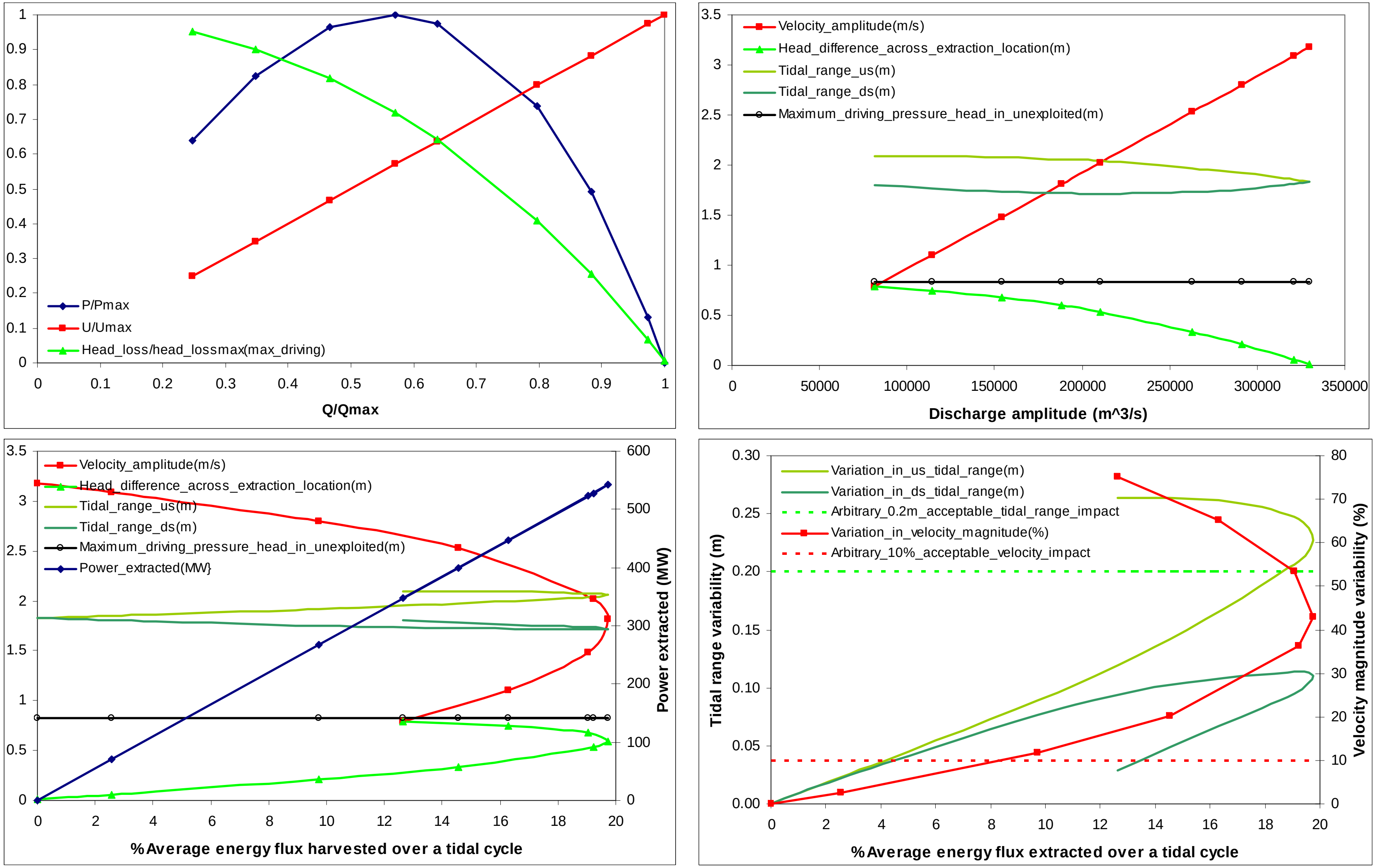

Figure 5 Impact of varying levels of energy extraction for hydraulic current case 3: (i) Non-dimensional analysis, (ii) Discharge amplitude dependence, (iii) % average energy flux extracted dependence, and (iv) Variation with % average energy flux extracted, and identification of constraint limits

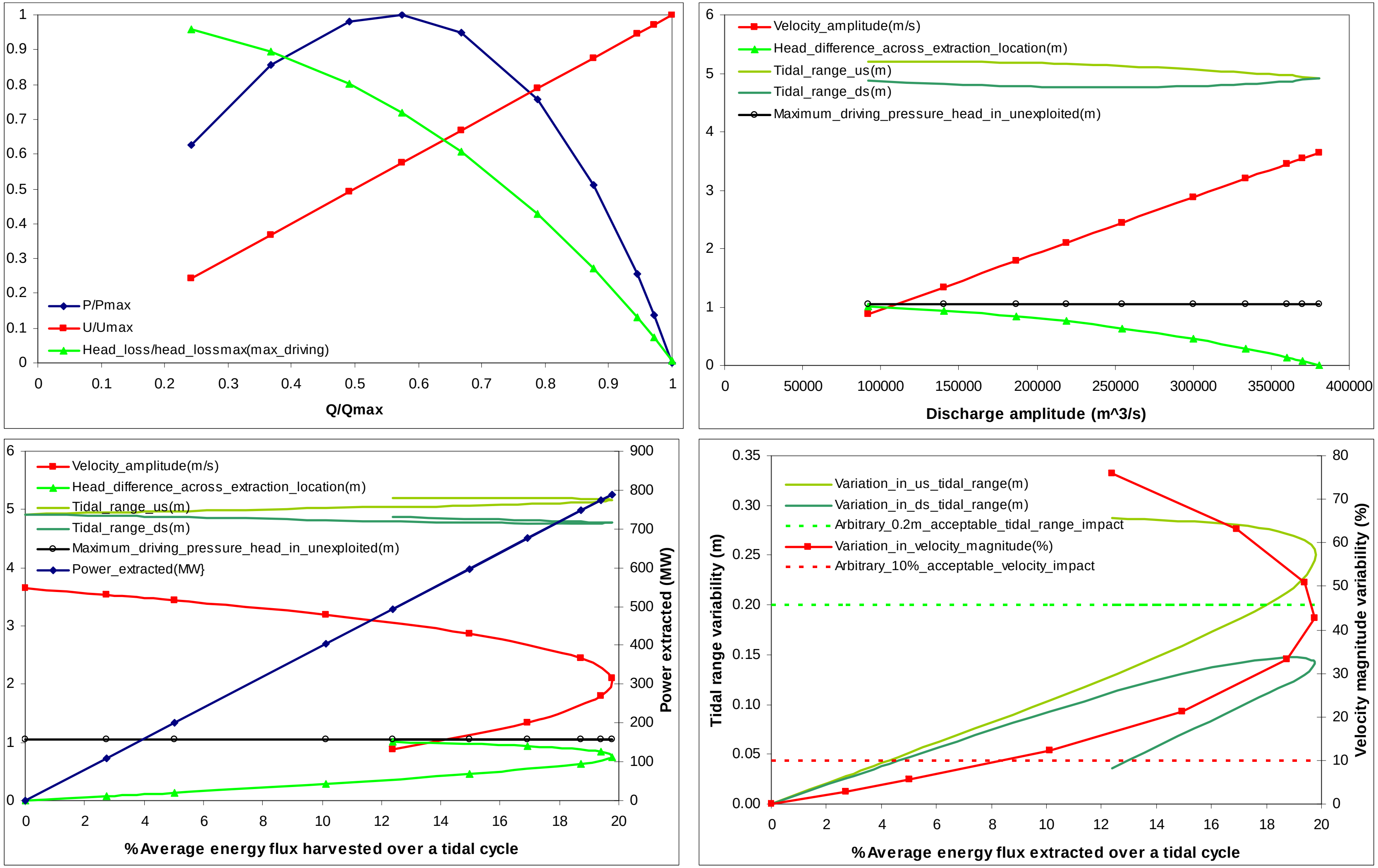

Figure 6 Impact of varying levels of energy extraction for hydraulic current case 4: (i) Non-dimensional analysis, (ii) Discharge amplitude dependence, (iii) % average energy flux extracted dependence, and (iv) Variation with % average energy flux extracted, and identification of constraint limits

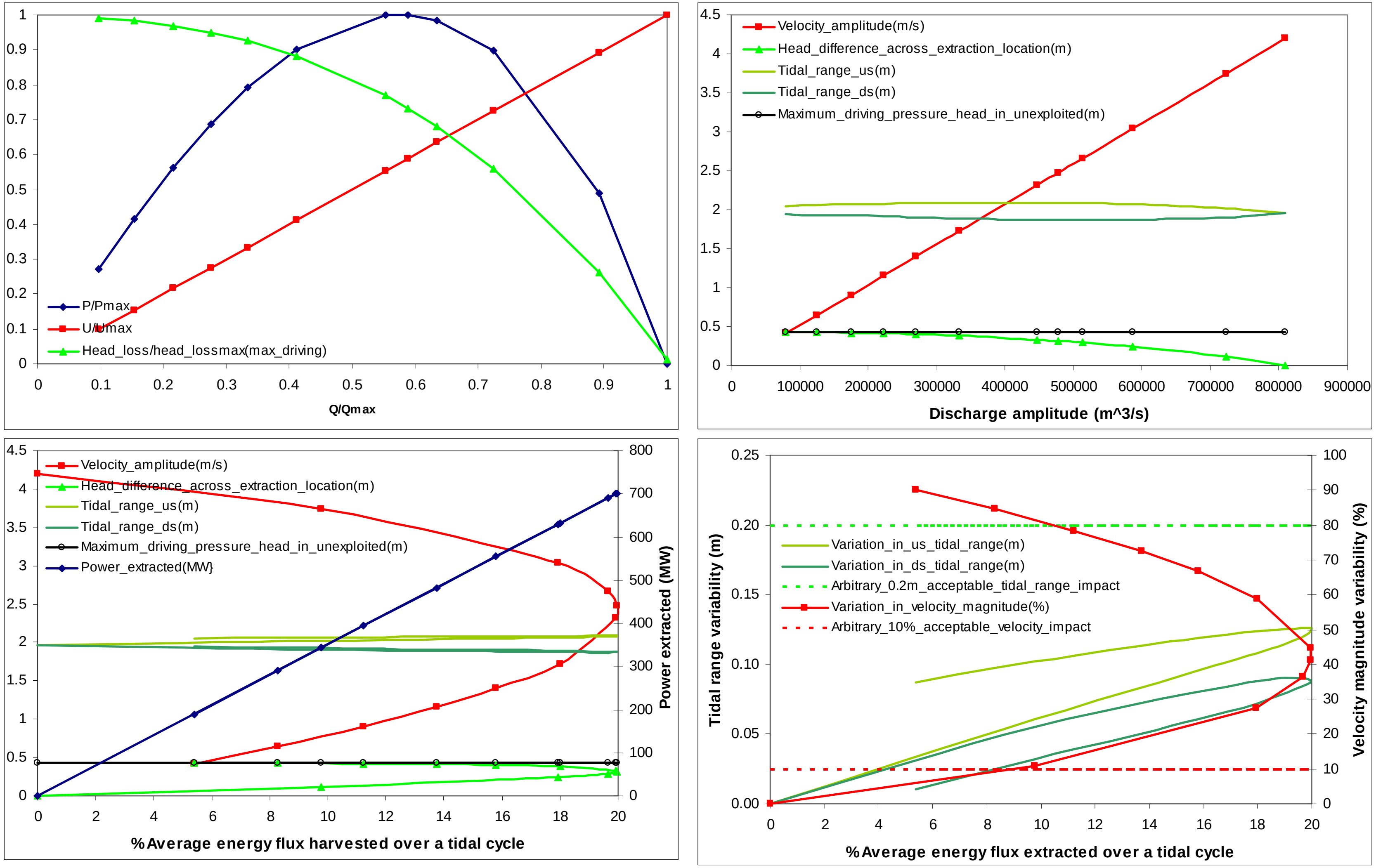

Figure 7 Impact of varying levels of energy extraction for hydraulic current case 5: (i) Non-dimensional analysis, (ii) Discharge amplitude dependence, (iii) % average energy flux extracted dependence, and (iv) Variation with % average energy flux extracted, and identification of constraint limits

Table 2 summarises the results encapsulated in Figure 3-Figure 7 for each of the hydraulic current case scenarios presented in the preceding sections, as listed in table 1. Many important parameters such as the velocity amplitude, maximum discharge and alteration in tidal range vary across the cases considered as would be expected. This is reflective of the different domains and boundary conditions imposed. What is significant is that a number of consistent themes arise across the cases for certain of the key characteristic properties identified as discussed in more detail in the next section.

	Case 1	Case 2	Case 3	Case 4	Case 5
Channel length (m)	5977	11954	11954	11954	5977
Velocity amplitude (U_o, m/s)	3.257	2.042	3.172	3.646	4.197
Driving head difference (a_o, m)	0.4312	0.4312	0.8287	1.048	0.4312
Cross-sectional area (A, m^2)	103845	103845	103845	103845	192855
Maximum discharge (Q_{max}, m^3/s)	338568	212242	329744	380855	809584
Maximum increase in u/s range (m)	0.107	0.138	0.264	0.281	0.126
Maximum decrease in d/s range (m)	0.066	0.082	0.114	0.130	0.090
Occurrence of P/P_{max} as a % of Q/Q_{max}	56	55.4	57.1	57.4	58.9
Average energy flux through the channel (MW)	1466.7	919.6	2745.2	3989.2	3509.6
% average tidal flux harvested ($B_{theoretical}$)	19.83	19.88	19.74	19.76	19.96
Ratio $B_{technical} / Bt_{heoretical}$ (%)	42.8	43.2	41.5	41.0	45.0
Average theoretical power harvested (MW)	290.86	182.82	541.98	768.54	700.42
Density of theoretical power harvested (kW/m^2)	2.80	1.76	5.22	7.59	3.63
Average technical power harvested (MW)	124.67	79.09	225.11	323.13	315.86
Density of technical power harvested (kW/m^2)	1.20	0.76	2.16	3.11	1.64

Table 2 Key metrics derived from each hydraulic current case experimental set-up.

6.1.3 Interpretation

The demonstrable occurrence of P_{max} for each domain and localised driving mechanism is of great practical value, as it confirms the existence of a *theoretical* extraction limit in a particular location using the TEC technology approach. This is indicative of a key component of tidal current energy resource dynamics – the existence of a theoretical tipping point beyond which the addition of additional extraction devices will harvest less overall resource due to the impact of the combined harvesting effort on the underlying tidal hydrodynamics. The response of each of the test cases as presented in the first diagram of each of the individual 4-diagram graph presentations are plotted together in Figure 8 to demonstrate the repeatability of findings across the various hydraulic current cases (case 6 introduced in Appendix A is also included). The relationship between the occurrences of P_{max} as a % of Q/Q_{max} is consistent across the hydraulic current test case experiments, occurring at around 57% of Q/Q_{max}. Given the relationship between U and Q, this also confirms that for this domain type, maximum energy harvesting occurs when the average flow velocity has been reduced by around 43%. This is a similar response as reported in the analytical findings of [5-7]. The variation of head loss occurring across the extraction plane also has good although not exact agreement between the cases. The theoretical extraction limit P_{max} coincides with the concentration of around 71% of the available driving head to the extraction location. This does differ slightly from the analytical response reported in [5-7] where 2/3rds of the available driving head was expected to occur across the extraction plane. There is a little more variability of this property than observed with the occurrence of P_{max} in relation to reduction in overall flow discharge and velocity. For case 6, part of this variability may be explained by the alteration in cell size in the simulation – as the distance across the extraction plane is fixed at one cell width. Potentially for this reason, case 6 is the most significant outlier for the head loss term in Figure 8.

However, the reasoning for the added variability (although still very good consistency of overall response) is as yet unclear in the other cases. It must also be made clear that the small amount of variability observed in the parameters that appear to be fairly consistent in Figure 8, as reported in Table 2, is likely to be over-stated as the cases were not specifically optimised on finding the absolute peak value. Instead, a series of cases representing the variability every 5-10% across the range of Q/Q_{max} values was desired. The effort required to run numerous simulation cases in an attempt to iteratively determine the exact peak value for each experiment was beyond the scope of this investigation given the restrictions of time and budget.

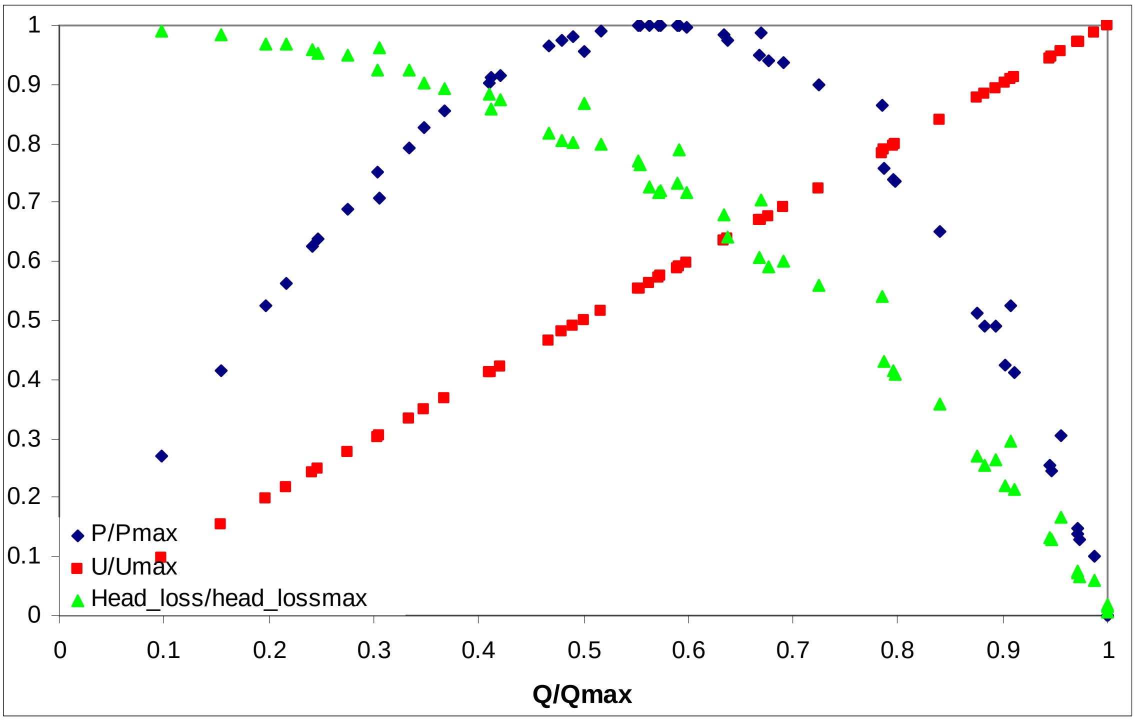

Figure 8 Compendium of variation of key non-dimensionalised parameters for hydraulic current cases 1-6.

Also of significance in Table 2 is the consistency of occurrence of the average energy flux through the channel, $\beta_{theoretical}$ (≈0.2). This consistency across the range of cases considered is crucial, as it provides a means of determining the *theoretical* tidal current energy resource for any other hydraulic current location using Equation 11 (where the very slight variability of β is appropriately rounded off):

$$P_{Theoretical} = 0.2 \rho g Q_{\max} a_o$$

Equation 11

This fits exactly within the bounds of the analytical solution proposed in [5] as discussed in Section 4.2, which provides additional reassurance in the numerical modelling conducted, beyond the rigorous development and validation of the model itself. This is important given the lack of availability of real world data from tidal current energy device operation and tidal hydrodynamic response to enable real world validation of the model with the energy extraction term.

The environmentally acceptable limitation on $\beta_{theoretical}$ at which point the impact of extraction on the tidal system has reduced mean peak tidal velocities by 10% (≈ 43%) also enables consideration of a reduction of $P_{theoretical}$ to account for generic environmental sensitivity:

$$P_{technical} = 0.086 \rho g Q_{\max} a_o$$

Equation 12

Again, this fits well with an analytical solution proposed in the literature [7].

The hydraulic current case has been considered first as analytical solutions have been presented in the literature that enable comparison with the tidal hydrodynamic modelling presented here. The good fit of the simulation results presented with available analytical solutions gives confidence in applying the numerical model to other cases not as fully considered (resonant system), or not yet approached (tidal streaming) in the literature.

6.2 Resonant basin scenario analysis

When a long period tidal wave encounters a coastal boundary, the wave is reflected. The incoming and reflected waves combine to produce the total observed condition. In the coastal ocean, these combined wave patterns, often including multiple reflected components from various changes in depth and reflections from local topographic features are already well established. Resonance occurs when the incident and reflected wave interference combine to produce a local increase in the overall amplitude of the incoming wave. In the extreme tidal case where the length of an estuary is close to the natural resonance period of the incoming wave, very large tidal amplifications and hence amplitudes occur. With very large tidal amplitudes, strong tidal currents can be generated by the locally increased pressure gradient occurring due to the passage of a wave of large amplitude. The Bay of Fundy/Gulf of Maine system in North America, Bristol Channel/Severn Estuary system in the United Kingdom and Yellow Sea in East Asia are textbook examples of resonant tidal basins.

6.2.1 Experimental set-up

The simplest method of simulating a resonant system is to establish a domain of length ¼ that of the wavelength of the input perturbation. The Severn Estuary/Bristol Channel system is an example of quarter wavelength resonance in action (although tidal streaming also plays an additional significant role in this case). The simple ¼ wavelength model incorporates certain simplifying assumptions that it is intended to avoid in order to provide a more realistic simulation. For instance, the ¼ wavelength rule for perfect resonance does not account for extra physical processes observed in real world tidal situations (e.g. friction, turbulent viscosities). While it is possible within the numerical model being operated to disable the model representations of these physical processes, that would create an overly simplified physical representation. Hence, sensitivity analysis was necessary to determine a suitable domain length/input condition relationship. An idealised M2 elevation boundary condition was again applied using a uniform depth of 35 metres throughout the domain.

With a uniform depth of 35 metres, the wave celerity (speed of wave propagation) is 18.5297m/s. The wavelength of one 12.4-hour wave period in an idealised fictitious domain of 35 metres constant depth is 827.2 km. In a 1D frictionless system with perfect reflection, optimum resonant amplitudes at the head of the estuary are achieved with a channel of extent ¼ wavelengths. An optimal basin length of approximately 207 km is therefore desirable. However, the Shallow Water Equations system incorporates various energy dissipating terms such as representations of bed stress and horizontal mixing processes, such that the appropriate basin length to optimise resonance will be less than the simplified ¼ wavelength model. Without conducting an exhaustive sensitivity analysis, a basin length of 194 km was settled upon from consideration of only a small number of cases (i.e. it is not suggested that this is *the* optimal condition, but this was effective in generating resonance given that the system was not as ideal as the linear theory would suggest).

The domain utilised was again 3km wide as for the previous cases. A cell size of 1000 metres wais imposed such that the domain was prescribed by 194x3 cells, with closed boundaries to the north, south and east of the domain. The input condition at the west of the domain was a 3-metre amplitude variation in the free surface. In the unexploited case, this domain length generated an increase in tidal range from 6 metres at the inlet to just over 11 metres at the closed boundary at the opposite end of the channel. This domain set-up is not unlike a (highly) simplified representation of the Bristol Channel system, where similar levels of amplification are observed. In the numerical simulations, it was necessary to spin-up from a 'cold-start' condition for 2 complete semi-diurnal periods to enable transmission of the incoming and reflected waves to occur and respond before the 3rd semi-diurnal tide was used for model output representative of the intended generic Spring tide condition. When energy extraction was imposed, it was conducted close to the entrance to the channel. In a ¼ wavelength resonant system, peak velocities occur at the entrance to the channel, and reduce the further into the channel considered. Obviously no horizontal flow can occur across the 'closed' downstream boundary. Hence the most interesting velocities from a tidal current energy extraction perspective are near the entrance of the idealised simulated channel. When extraction was included in the resonant case, it was imposed 10 km (10 cells) from the entrance of the channel.

6.2.2 Sensitivity analysis

Only one resonant basin case was considered as an approximately ¼ wavelength resonant regime is the general standard observed in the real world. Figure 9 summarises the response of the simulations to various energy harvesting scenarios. The first graph is in very good agreement with the hydraulic current cases presented in Section 6.1. The system has a similar response regarding the occurrence of a definite P_{max} for this particular experimental case. The variation of U and the head loss across the extraction plane are also very similar to the hydraulic current experience. The first major difference in comparison with the hydraulic current cases is exposed in the second graph in Figure 9, where the downstream reduction in tidal range is significantly greater than observed in previous cases. In the hydraulic current case, tidal range variation was less than the equivalent head loss occurring at the extraction site. However, in this resonant basin simulation, the reduction in downstream tidal range was larger than the head loss occurring at the extraction location. Once more, the third graph again demonstrates similar tendencies to the hydraulic current cases apart from the significant downstream range reduction in the resonant case. The actual values achieved are of course very different as the input tidal range in this resonant case is 6-metres in comparison with 2-metres in the majority of hydraulic current cases. Hence, for instance, the peak mean power harvested from the resonant system is substantially larger than in the equivalent hydraulic current case (in terms of channel width and depth) (1719MW vs. 597MW). However, the trends observed in terms of the variation of the parameters are in good agreement. Hence, in terms of the % of average energy flux harvested over a tidal cycle, the two regimes experience very similar upper (*theoretical*) limits (19.69% for the resonant basin scenario). The final graph in Figure 9 indicates that both the velocity and tidal range environmental constraints are breeched in the resonant basin case before reaching the *theoretical* extraction limit.

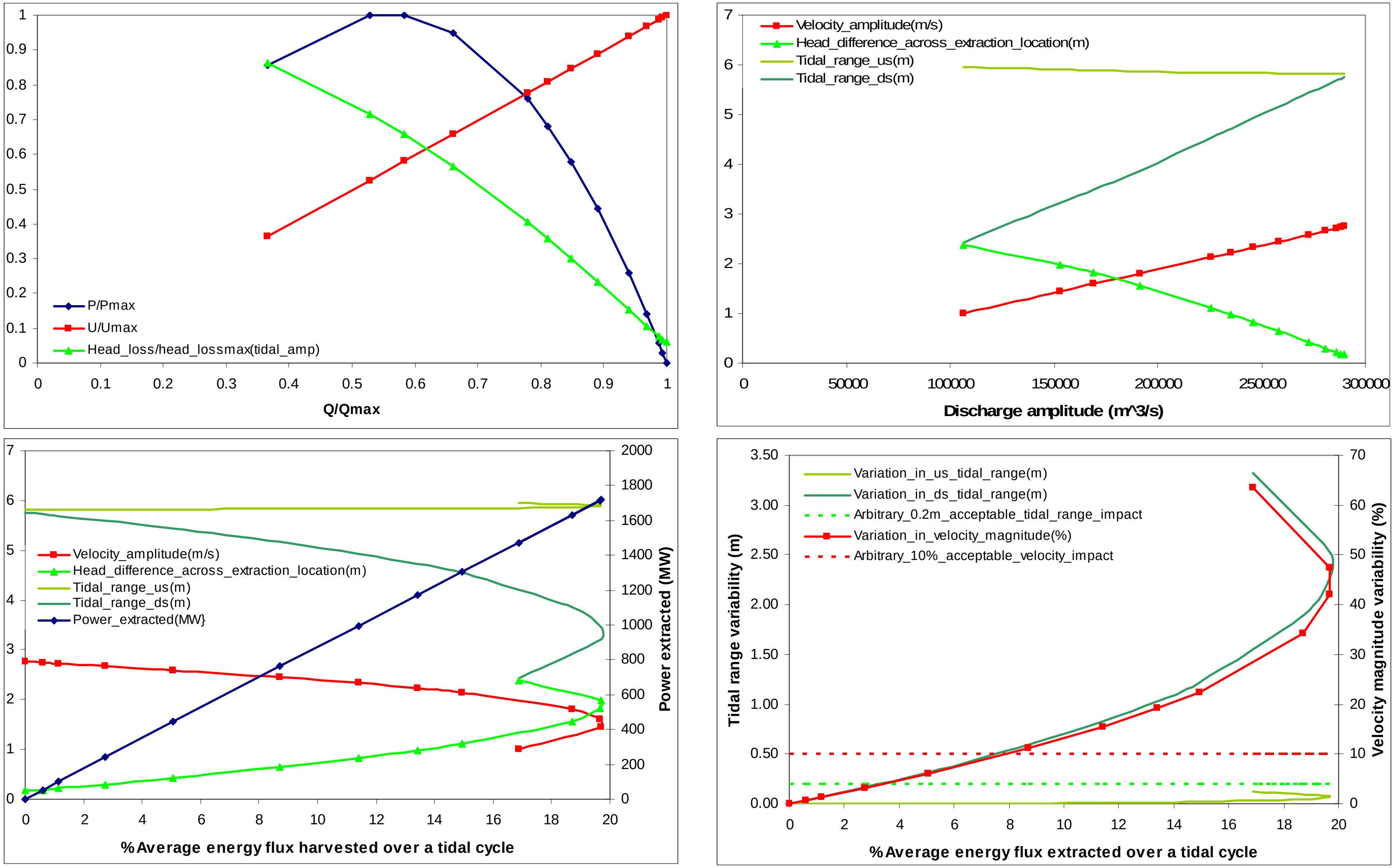

Figure 9 Impact of varying levels of energy extraction for hydraulic the resonant basin case: (i) Non-dimensional analysis, (ii) Discharge amplitude dependence, (iii) % average energy flux extracted dependence, and (iv) Variation with % average energy flux extracted and identification of constraints

6.2.3 Interpretation

The tendencies and trends observed in both the resonant basin and hydraulic current experimental cases are very similar as indicated in Figure 10. Hence, Equation 11 would appear to be appropriate for application to resonant basin systems to determine the *theoretical* tidal current energy resource, $P_{Theoretical}$. It is important however to highlight the slight difference in calculation of Equation 11 in the resonant basin case from the hydraulic current scenarios. In the resonant basin case, the value of a_o is the tidal amplitude occurring at the extraction location in the no extraction ('natural') case. This differs from the hydraulic current case where a_o is taken as the maximum driving amplitude imposed by the variation of the two imposed boundary conditions (as portrayed in Figure 1).

The significantly increased reduction in downstream tidal range observed in the resonant basin case is a consequence of the energy extraction scenarios altering the fine balance necessary to achieve significant resonance. The propagation phase in the downstream direction is retarded, and hence the interaction between the incoming wave propagating towards the head of the basin and the wave reflected from the head of the basin (which would also obviously be impacted) is altered. This impact on tidal resonance with high levels of energy extraction is likely to be unacceptable for real world development because of environmental concerns relating to the alteration of tidal range (e.g. impact on intertidal regions). However, although the restrictions imposed by the arbitrary selection of 'acceptable' variations of velocity and tidal range severely reduce the harvestable resource in comparison with the *theoretical* resource, the mean power extracted from the system within the 'acceptable' environmental constraints is still significant in terms of energy production (≈ 290MW). This 'environmentally constrained' harvestable resource is more or less identical to the identified $P_{technical}$ resource available for harvesting in the hydraulic current scenario in case 1. Given that the *theoretical* limit identified in the resonant system is significantly larger than in the equivalent hydraulic current case (1719MW vs. 597MW), this demonstrates that the resonant system is more constrained by the imposed environmental limitations (in this case the alteration to tidal range is the restriction, whereas the velocity condition was always the leading constraint in the hydraulic current cases considered). Hence the technical power constrained by the tidal range limitation can be prescribed as:

$$P_{technical} = 0.033 \rho g Q_{\max} a_o$$

Equation 13

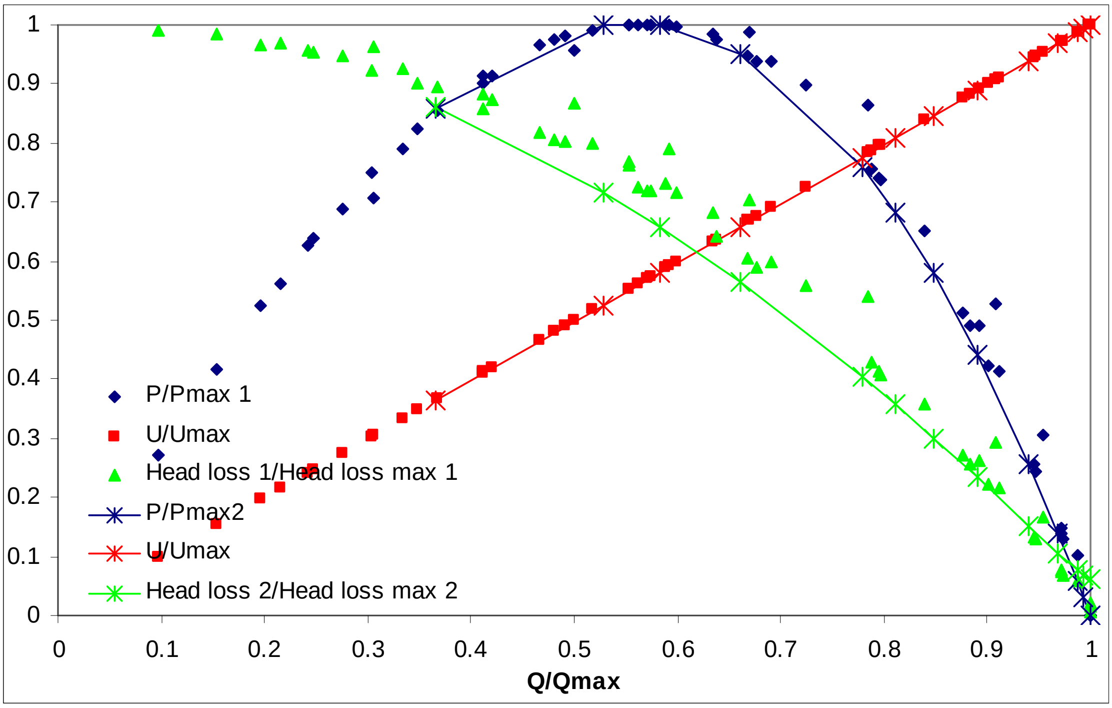

Figure 10 Comparison of variation of key non-dimensionalised parameters for hydraulic current cases 1-6 and the resonant basin case (indicated by the markers joined by lines).

6.3 Tidal streaming scenario analysis

A flow constriction is necessary to promote tidal streaming – the flow must accelerate to maintain flow continuity. An obvious occurrence of tidal streaming is as tides propagate from offshore to onshore. In the deep ocean, tidal flow velocities are very low. As the tide propagates onshore, the reduction in depth constrains the flow and therefore tidally induced flow velocities increase with reducing depth (the real world is a little more complex in that some of the incoming long period wave is reflected by the depth change, etc. but the overarching rationale is fundamentally sound). Assuming linear wave theory, in the shallow water limit, the depth-averaged velocity is given by Equation 14, which reaches maximum flow velocity at the extremes of tidal range.

$$U = \eta\sqrt{\frac{g}{d}}$$

Equation 14

Of course, not all tidal flows propagate locally as progressive waves, so Equation 14 is not universally applicable, and contains simplifying assumptions such as the lack of frictional effects, hence the requirement for more complex flow models such as the Shallow Water Equations used in the numerical model simulations in this work. In the horizontal, similar constraints such as headlands, islands and narrowing channels provide further flow constrictions that can act to accelerate flow velocities.

6.3.1 Experimental set-up

The approach adopted was to constrict the flow using topography (land) as opposed to bathymetry (sea bed) or a combination of both as is more often the case in real world application. Using only topographic constraints enabled the adoption of a uniform depth throughout the domain. A uniform depth of 35 metres was selected as being representative of an appropriate depth for installation and operation of ‘first generation’ TEC devices. Adopting a uniform depth significantly simplified the comparison and analysis of the data produced. The 'driving' boundary was prescribed using an idealised M2 sinusoidal elevation input condition. The other open boundary was prescribed using a radiating velocity condition.

The physical dimensions of the domain considered are depicted in Figure 11. The domain can be considered in three sections, two wider joined by one narrower section in the middle. The width of the narrow section is chosen to be similar to the preceding hydraulic current case considered in the previous section (order 3 km). The wider regions are mirror images where the channel expands to three times the width of the narrow region.

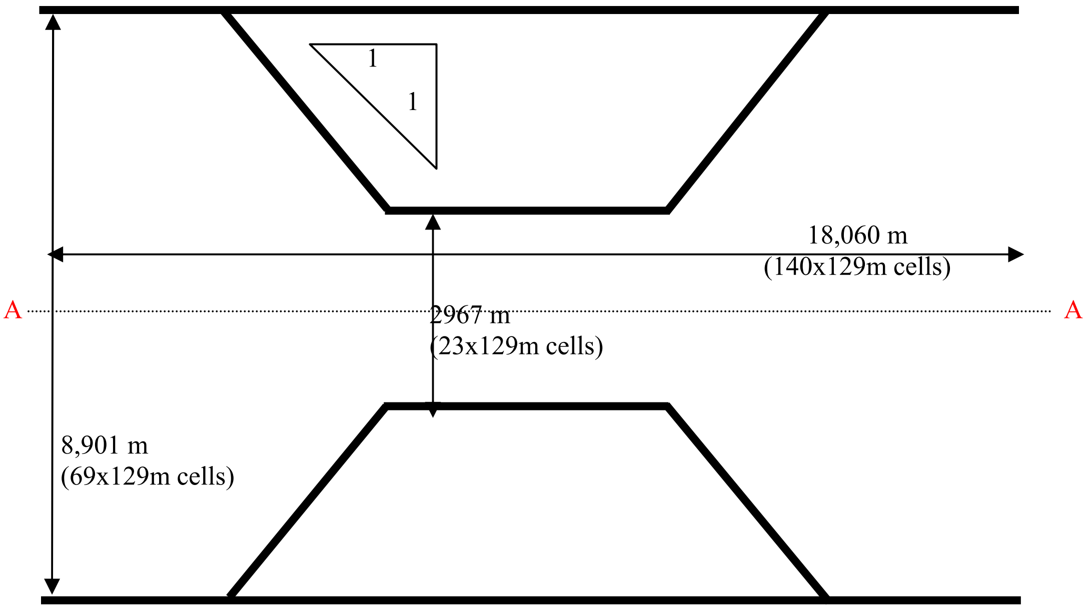

Figure 11 Tidal streaming numerical simulation domain.

In order to avoid computational expense in this larger (physical) domain, the cell size was tripled (129x129 metres) maintaining an overall domain of 140x71 cells. The time step imposed by the CFL condition was therefore able to be relaxed. In order to create an extreme tidal current of relevance for tidal energy extraction it was necessary to impose a suitably large tidal amplitude to generate the necessary forcing (3-metres in this case at the driving (west) boundary). A radiating boundary condition was imposed on the eastern boundary that enabled appropriate long wave propagation out of the domain in response to the local flow condition generated in the domain interior. In combination with the streaming effect of the narrow channel region, peak velocities of over 3 m/s were generated in the constriction. More representative no-slip closed boundary conditions were applied for these simulations. Free-slip conditions were used in the previous solution to ensure a 1D flow response. Simulations were allowed to spin-up for 1 semi-diurnal period. The 2nd semi-diurnal period was assumed to be representative of a Spring tide condition (in this more complex non-linear response domain the original case was run for a number of additional periods to confirm that there was minimal variation between outputs across the 2nd and later repeated semi-diurnal periods). Given the more complicated domain, the simulations generated are more involved than the pseudo-1D simulations generated in the previous case. Figure 12 is a simple representation of the flow conditions generated at various stages of the tidal cycle. At peak flow (on both the flood and ebb cycles), the tidal streaming effect of the flow constriction generated enhanced flow velocities. In the wider upstream portion of the channel, the flow achieved only moderate tidal velocities with strongest flow (of the order 1m/s) towards the centre of the channel and weaker flow towards the lateral boundaries. This was as expected given different effects such as partial wave reflection from the topographic boundary and the pressure gradient set-up in response to the downstream constriction. Downstream of the constriction, the flow separated from the boundary, producing a core jet-like flow dominating the centre of the cross-section. Additionally, an eddy formed in the lee of each of the headlands in response to flow separation and the ensuing locally established pressure gradients and vorticity roll-up.

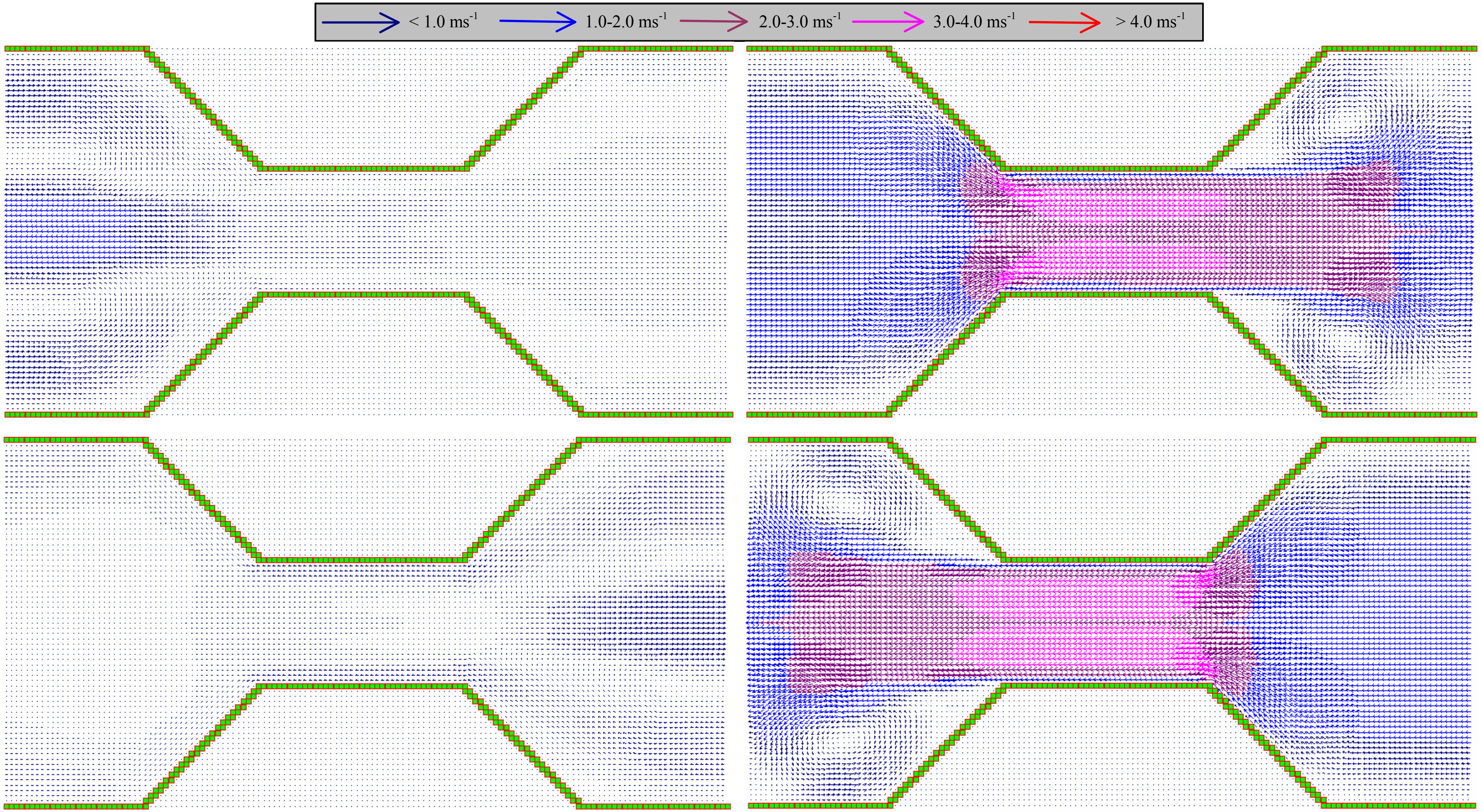

Figure 12 Velocity plots at (i) ebb tide slacks, (ii) peak flood tide, (iii) flood tide slacks, (iv) peak ebb tide.

Figure 13 provides an indication of the variation of free surface elevation and streamwise velocity through a cross-section along the central axis of the domain at peak flood tide conditions. The substantial increase in flow velocity through the mouth of the narrowing channel is supported by a significant decrease in surface elevation as would be expected.

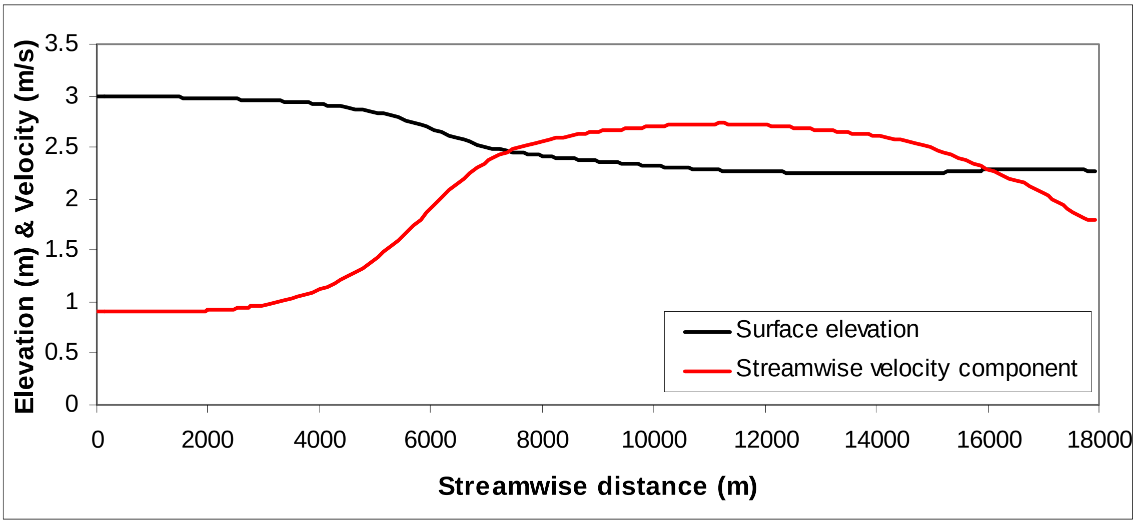

Figure 13 Variation of elevation and streamwise velocity through central cross-section A-A in Figure 11.

A second tidal streaming case was examined where the domain was extended by 40 cells (5.16 km). This extra length was inserted in the narrow channel region, thereby extending the narrow region without altering the 'inlet' and 'outlet' regions. Otherwise the second test case was an exact replica of the first case.

6.3.2 Sensitivity analysis

The output 4-diagram figures from the two tidal streaming cases are presented in Figure 14 and Figure 15 in what is now the usual manner with one key necessary variation. The tidal streaming case described in the experimental set-up is by its very nature not uniform in the y-direction. This initially provided some difficulty in terms of processing in comparison with the previous pseudo-1D simulations. However, with slight alterations to the TFD-2d numerical model code, an additional set of simulation outputs were produced that describe the variation of the key metrics of interest as averaged quantities across the cross-section of the extraction plane. Care was taken when conducting averaging to appropriately account for manipulation of the data generated (e.g. calculating power generated in each cell before averaging across the cross-section, rather than utilising the averaged cross-sectional velocity).

Although the detailed flow development in the two cases was obviously different due to the extension of the second domain, the characteristic parameters considered in the 4-diagram figures present very similar results.

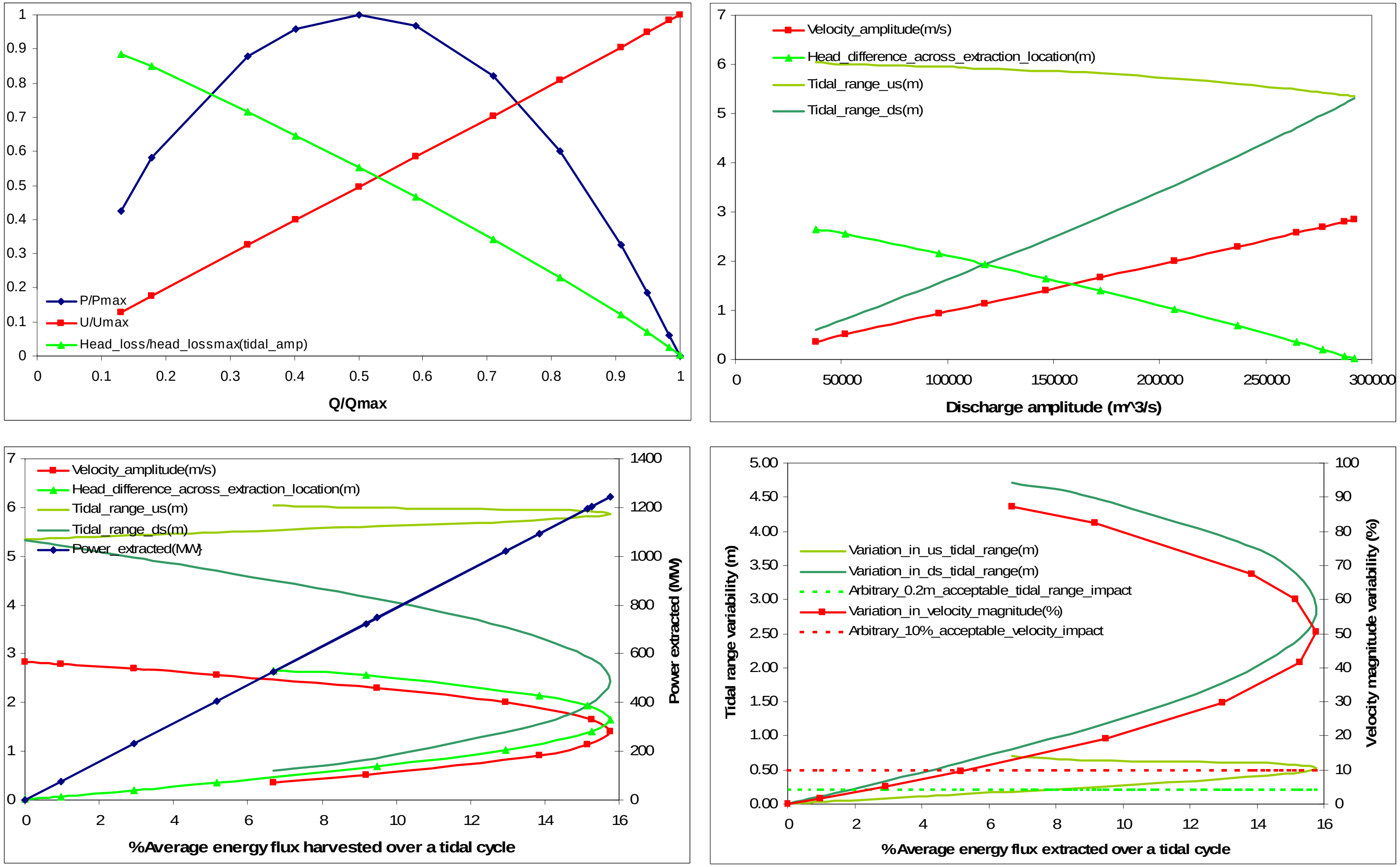

Figure 14 Impact of varying levels of energy extraction for tidal streaming case 1: (i) Non-dimensional analysis, (ii) Discharge amplitude dependence, (iii) % average energy flux extracted dependence, and (iv) Variation with % average energy flux extracted, and identification of constraint limits

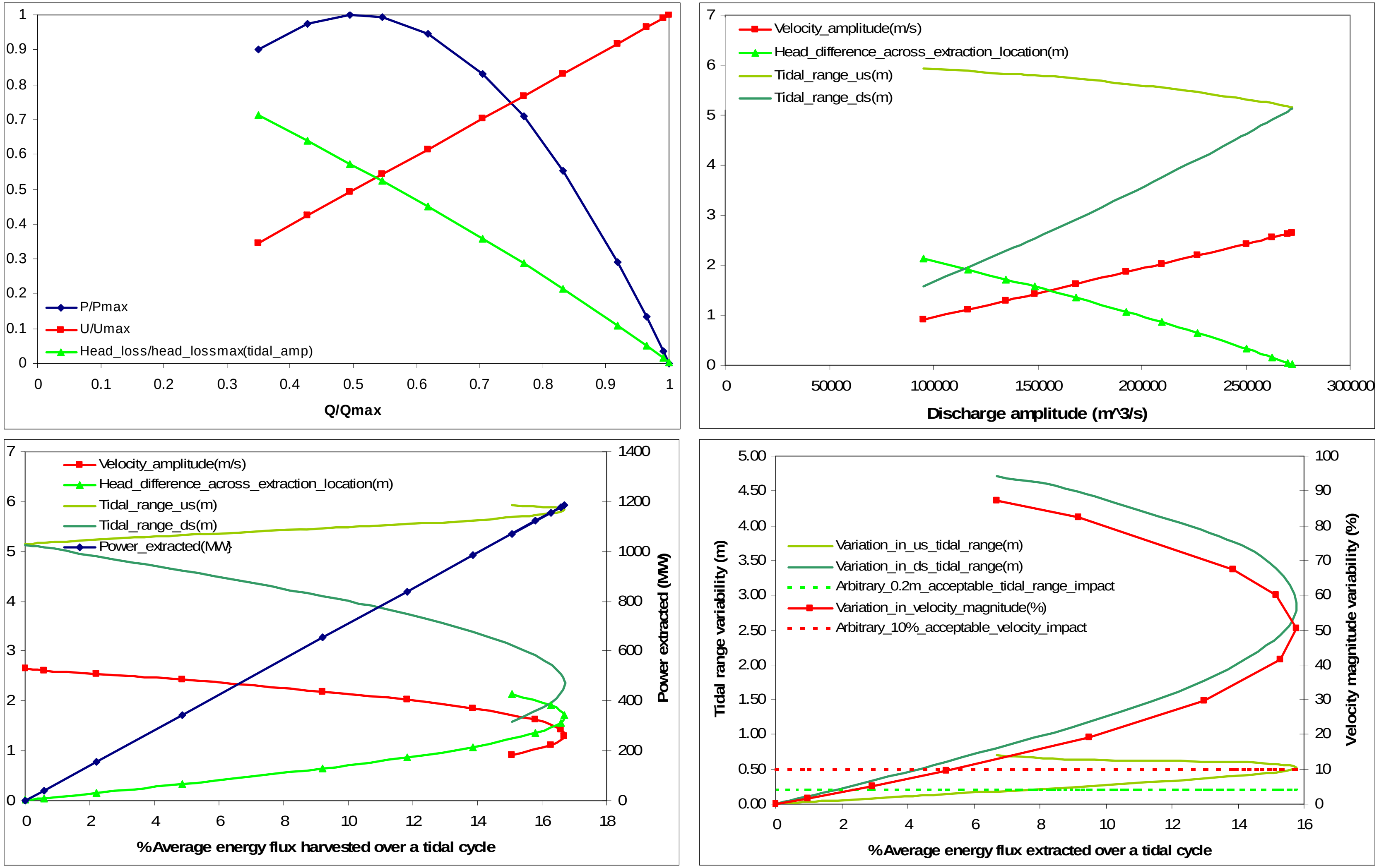

Figure 15 : Impact of varying levels of energy extraction for tidal streaming case 2: (i) Non-dimensional analysis, (ii) Discharge amplitude dependence, (iii) % average energy flux extracted dependence, and (iv) Variation with % average energy flux extracted, and identification of constraint limits

6.3.3 Interpretation

The tidal streaming cases examined demonstrate consistent responses with respect to the impact of energy extraction. Figure 16 indicates the consistency of response in terms of the non-dimensionalised variables. Although the two cases are consistent, and share common trends with the preceding cases examined, Figure 16 does indicate a small but significant difference from the hydraulic current and resonant basin cases; P_{max} corresponds exactly with 50% of Q_{max} (and hence U_{max}). In the previous two scenarios, P_{max} occurred at 57% of Q_{max}. The corresponding head loss in comparison with the maximum driving head (the input tidal amplitude in this case) is approximately 56% of maximum head loss. However, taking a step back, the general response of the system is still quite similar, and the *theoretical* tidal current energy resource limit from a tidal streaming channel can still be accurately described using the same formulation as previously, with a different multiplier:

$$P_{Theoretical} = 0.16 \rho g Q_{\max} a_o$$

Equation 15

As in the resonant basin scenario, a_o in Equation 15 refers to the maximum tidal amplitude in the extraction location observed in the no extraction case.

Considering the third graph in both sets of diagrams in Figure 14 and Figure 15 (and with the benefit of assessing the detailed simulation outputs), both tidal streaming domains produce a very similar overall *theoretical* tidal current energy resource, of the order 1200 MW averaged across the simulated Spring-like flood-ebb tidal cycle.

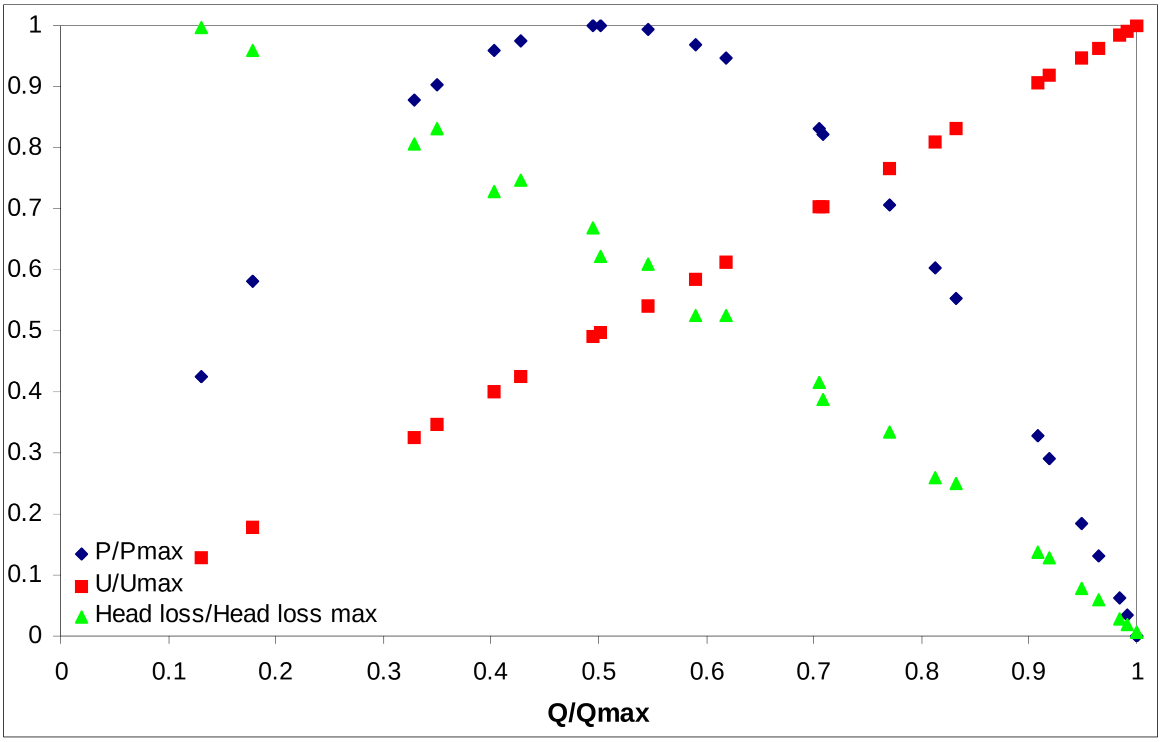

Figure 16 Compendium of variation of key non-dimensionalised parameters for both tidal streaming cases.

Examining the fourth graph in both sets of tidal streaming figures, both the velocity and tidal range environmental constraint limit are breeched. The downstream tidal range variability constraint is by far the most severe in both cases, limiting the harvestable tidal current energy potential to around 150 MW averaged across the simulated Spring-like flood-ebb tidal cycle. Once more the variability does appear to consistently be related to the flow discharge and free surface amplitude variation. Hence the arbitrarily imposed technical power in tidal streaming cases can be quantified as:

$$P_{technical} = 0.020 \rho g Q_{\max} a_o$$

Equation 16

6.4 Conclusions from generic scenarios

The responses of three generic representations of tidal systems exhibiting characteristics appropriate for potential exploitation through tidal current energy harvesting have been investigated. The *theoretical* potential for power extraction is significant in each case, and likely exceeds any credible attempt to actually harvest energy in each simulated domain due to consequent environmental responses and economic considerations. The response in each case shares common characteristics:

- The demonstrable occurrence of P_{max} for each domain and localised driving mechanism is of great practical value, as it indicates the existence of a *theoretical* extraction limit in a particular location using the TEC technology approach. This is indicative of a key component of tidal current energy resource dynamics – the existence of a theoretical tipping point beyond which the addition of additional extraction devices will harvest less overall resource due to the impact of the combined harvesting effort on the underlying tidal hydrodynamics. <u>This highlights that the outdated 'farm' resource assessment methodology is fundamentally flawed, as initially indicated in the 2004/5 MEC reports.</u>
- The response of each of the systems to extraction is head loss across the extraction location.
- Related to the head loss is a reduction in flow velocity <u>extending across each of the domains considered</u>. This is because the effect of head loss at the extraction site reduces the driving head between the fixed driving boundary condition (taken to be insensitive to flow development in the interior as it is connected to a much larger tidal system not significantly influenced by these local effects) and the extraction location. Obviously if the flow velocity is reduced significantly, the discharge through the channel is similarly reduced; hence the overall downstream flow potential is also reduced. When applying a tidal fence type of extraction, there is a measurable increase in flow velocity downstream of the extraction plane, compared to that upstream. This increased downstream flow does not compensate for the overall reduction in flow velocity in comparison with the natural (no extraction) case, as the impact of reduction in overall flow discharge is of much greater overall significance.
- At lower levels of extraction an increase (say doubling) in extraction generates a fairly linear response in terms of the variables considered (e.g. velocity retardation, tidal range, head loss). At higher levels of extraction, a more non-linear response is observed. This non-linear response grows with increasing extraction as the *theoretical* maximum extraction level is approached.
- A more non-linear response can be expected in the real world due to added complexity such as the inherent spatial variability of tidal currents, variable bathymetry, more varied topography, additional tidal harmonic constituents and addition of other spatially and temporally varying flow drivers such as wind, wave-current interaction and density driven flow processes.

- As was previously hypothesised in the 2004/5 MEC reports, this work demonstrates conclusively that the response of different generic regimes to energy harvesting, although demonstrating similar trends, is not consistent. This is summarised in Table 3. The caveats raised in the discussion in the preceding sections must be borne in mind when considering these results, as must the differing definitions of a_0.

	Expression of theoretical limit of tidal current energy harvesting.	Expression of technical limit of tidal current energy harvesting.	Hydrodynamic response limiting energy harvesting.
Hydraulic current	$P_{Theoretical} = 0.2\rho g Q_{\max} a_o$	$P_{Technical} = 0.086\rho g Q_{\max} a_o$	Velocity reduction
Resonant basin	$P_{Theoretical} = 0.2\rho g Q_{\max} a_o$	$P_{Technical} = 0.033\rho g Q_{\max} a_o$	Downstream tidal range
Tidal streaming	$P_{Theoretical} = 0.16\rho g Q_{\max} a_o$	$P_{Technical} = 0.020\rho g Q_{\max} a_o$	Downstream tidal range

Table 3 Summary of harvesting limits for the three identified energetic tidal flow driving mechanisms.

Other conclusions that arise from or are confirmed by the analysis include:

- The most effective orientation of devices is in one tightly packed row across the channel creating a ‘tidal fence’ like orientation. This is of course only the case in a highly idealised location as proposed in these simplified case studies – a channel of uniform cross-section and width in the extraction region. The tidal streaming domain immediately highlights that variation in the cross-sectional width creates regions of heightened and reduced flows due to the interaction of the incoming tidal wave with topography. Similar effects would be observed in the case of varying bathymetry. Even if a tidal fence was to be considered from the perspective of optimising the available resource, the need to design and build devices of different physical dimensions and power rating to fit the variable bathymetry would be a significant economic disincentive. It is highly unlikely in real world application that a ‘tidal fence’ like orientation will be the optimised economic solution for a given location. Hence, real world sites will benefit from detailed analysis and optimisation of device location both for individual devices and arrays of multiple devices.

- In some regions, ecological factors will for legitimate reasons curtail or exclude the harvesting of tidal energy in order to protect critical ecological systems identified as being susceptible to the impacts of project development, operation and related alterations to the physical system. However, this analysis suggests that in many cases, device spacing issues, spatial extent of economically harvestable resource, and fundamental economic considerations (e.g. diminishing returns from each additional device installed due to the cumulative impact of devices on the available resource, and the selection of the optimal locations for the earlier installed devices in a development) will be the driving force for limiting the extent of arrays.

- The effect of one TEC device or a small array of devices will have limited if any (measurable) impact on the wider flow characteristics, unless a very narrow channel where the device performance surface is a significant proportion of the channel cross-sectional area is the intended deployment location. The only significant effects on the tidal hydrodynamic system that can be envisaged from very small developments are highly localised, and relate to the impacts of the wake formed by the interaction of turbine blades and the incoming flow.

6.5 Limitations, assumptions and unknowns

A number of limitations in the analysis must be highlighted to provide the proper context in which to consider the results obtained. The first is that only a limited number of representations of each of the three key identified mechanisms are considered. In the real world, although a particular region may be dominated by one of the three mechanisms, there will be some contribution to the local flow development that relates to two or more of the mechanisms. The value of applying a numerical model in this analysis is in order to be able to specifically isolate different characteristics of tidal systems in order to understand their individual responses.

The area of greatest concern for application of the results is the tidal streaming cases, as the test cases considered are not fully representative of all commonly encountered cases. In particular, tidal streaming can also occur in areas which are not strictly channels, such as around headlands, where the opposite boundary is at the very least far distant. Portland Bill in the English Channel is a typical example of this kind of tidal streaming regime. However, the vast number of tidal streaming topographic geometries precludes consideration of all possible domains within this analysis. Nonetheless, it is worth considering the potential flow response in less constrained cases than the tidal streaming channel presented in Section 6.3. This tidal streaming domain was selected as it is representative of the most extreme case, and therefore provides an upper bound on the potential response of a tidal streaming case scenario. When the overall tidal hydrodynamic system is less constrained, such as a tidal streaming scenario around a headland, is likely have a similar response to energy harvesting but be more prone to having a localised flow ‘blockage’ effect. Flow ‘blockage’ indicates that some of the naturally occurring tidal resource will respond to the presence of energy harvesting by following the ‘path of least resistance’, hence reducing the discharge, flow velocity and kinetic energy density and energy extraction through the TEC array.

A similar concern in all the simulated cases considered is that the driving boundary conditions have been considered to be invariant in response to various alterations to the tidal flow development within the domain. At lower levels of energy harvesting as prescribed by the *technical* limits, examination of the far-field response contained within the simulated domain suggests that this assumption is reasonable. However, at higher levels of energy extraction approaching the *theoretical* limit, the flow perturbations within the channel are likely to have at least some impact beyond the boundaries of the regions simulated.

Related to the previous two discussion points is the availability of alternative flow paths. Obviously in the resonant basin case this is not a particular concern. However, in the hydraulic current and tidal streaming cases, the existence of alternative flow paths for tidal propagation other than being forced through the extraction plane would potentially alter the overall response. This flow ‘blockage’ phenomenon has been considered to some degree in the literature [7]. Again, this suggests that the formulations presented in the preceding sections would be an upper limit on the actual resource harvested for each of the three generic regime types. Once more, concerns that this aspect raises are alleviated to some extent by consideration of the extent of likely harvesting rates being limited by *technical* concerns to levels significantly below the *theoretical* limit.

Another major assumption is that although the parameterisation of energy extraction from the system is representative of the real world physical processes, the additional flow response of fluid-device interaction in generating a downstream wake structure is not encapsulated in this methodology. The reasoning for this is two-fold, first the resolution of the analysis is inappropriate to consider accurate modelling of fluid-device interaction and, more fundamentally, wakes of tidal turbines have yet to be successfully numerically modelled. There are various stakeholder groups attempting to conduct such analyses, but no rigorous science has yet emerged from this effort. When this scientific progress is made, the method applied herein to study the larger scale response could be enhanced with additional parameterisations describing the impact of wake characteristics.

Related to the lack of wake modelling is the fundamental lack of observations of the wake generation and structure downstream of a real full-scale operational device. Images such as Figure 17 indicate that the relatively unexpected persistence of fluid-device interaction wakes in the wind industry is of significance, having obvious impacts on device spacing and structural fatigue design for instance. How similar wake evolution in the tidal environment will be to the wind example presented remains unclear given the significance of the free surface in most aspects of tidal flow dynamics – an aspect that can largely be ignored in the wind case. Without proper understanding of wake effects in the tidal case, there remains no robust basis for establishing device spacing guidelines to maximise energy production and TEC device design life while minimising overall project cost.

Figure 17 Horns Rev offshore wind farm wake image [35]

Finally, it is noted that the equations at the core of the TFD-2d numerical model utilised for this analysis are derived from the fully 3-dimensional Navier-Stokes equations on the basis of certain assumptions about the flow situation to be considered (e.g. ratios of depth to wavelength, hydrostatic approximation). Given the domains and boundary conditions considered in the analysis presented, the use of TFD-2d or similar Shallow Water Equation models is deemed entirely appropriate.

Taken together, all of the limitations, assumptions and unknowns presented indicate that for detailed project development, detailed examination of a particular development location on a case-by-case basis is clearly required. The amalgamation of a large number of sites when considering a national scale resource assessment (which this work is intended to inform) assists in averaging out any errors that may occur when considering individual locations. The parametric model methodology developed herein is deemed appropriate to determine national scale tidal current energy resources given the current state-of-the-art.

Given the above, it was deemed appropriate to test the methodologies in a more complex representative domain. Assessment of known real world energetic tidal regimes is therefore considered in the next section.

7 REAL WORLD TEST CASES

7.1 Strangford Narrows

Strangford Narrows in Northern Ireland is a key location in the development of tidal current energy technologies, acting as the demonstration and testing location of the world's first commercial scale TEC device, SeaGen (Marine Current Turbines Ltd.). The extreme tidal flow in the Narrows (reported as averaging 7-8 knots [24]) is generated by a larger-scale hydraulic current like feature acting along the channel length [25]. The Narrows is approximately 8 kilometres long and varies in width down to around 500 metres at the narrowest point. This region has previously been the subject of a published numerical modelling simulation [24]. The modelling was conducted as part of a wider study examining the potential for generating tidal current power in Northern Ireland using TEC technologies [24].

Before outlining the Strangford Narrows case study developed in TFD-2d for the purposes of this report, findings from the previous modelling exercise [24] are summarised. The numerical modelling in [24] was conducted by an engineering consultancy using the industry standard MIKE-21 hydrodynamic software (Danish Hydraulics Institute). MIKE-21 and TFD-2d operate similarly as they are based upon the same underlying equation-set used to describe tidal hydrodynamics. Figure 18 reproduced from [24] indicates the peak tidal flow velocities generated in the simulation. Widespread areas of flow velocities above 3.0 m/s are indicated around the centre-line of the channel for much of the (shortened) channel length presented. Figure 18 also provides an indication of the complex topography and bathymetry encountered in the Narrows. The flooding and drying of shallow intertidal regions in the domain provides a stringent test of the numerical model operation. Three locations of potential interest for deployment of the SeaGen full-scale prototype were identified by the original investigators as indicated in the image. Point B is in fairly close proximity to the ultimate final location of the SeaGen prototype. Output from the MIKE-21 based numerical modelling presented in [24] at Point B is reproduced in Figure 19. Interpreting this data indicates that the flood tide is slightly shorter than the ebb, and that the flood tide has a slightly higher peak magnitude than the ebb (3.0 m/s vs. 2.7 m/s). The flow direction is very consistent on both the flood and ebb tide and is representative of a bi-directional flow. Tidal range at Point B in this simulation is indicated as approximately 3.5 metres.

7.1.1 Experimental set-up

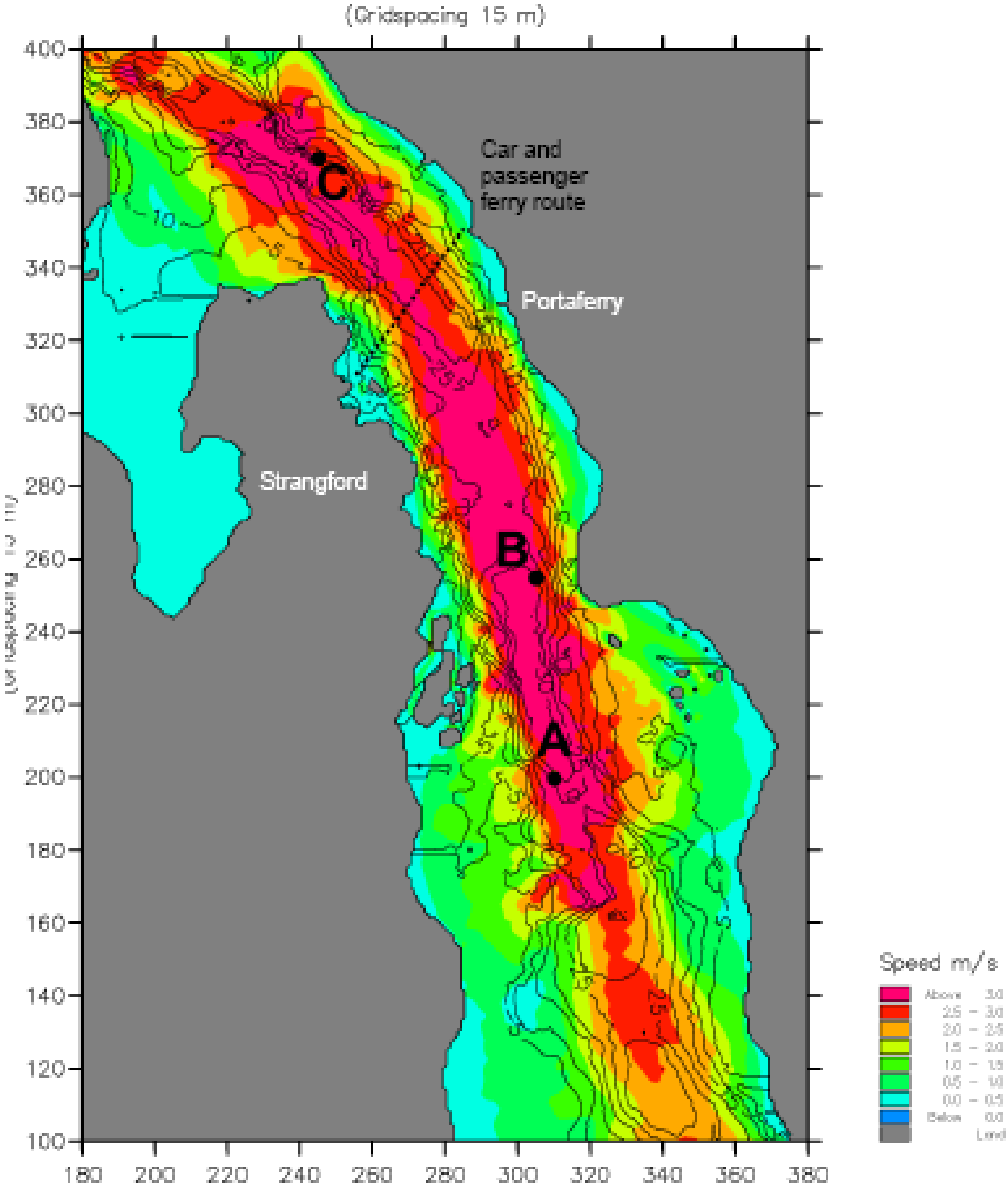

Figure 18 Peak Spring tidal speeds with bed contours to mean sea level (Source: Figure 12 in [24]).

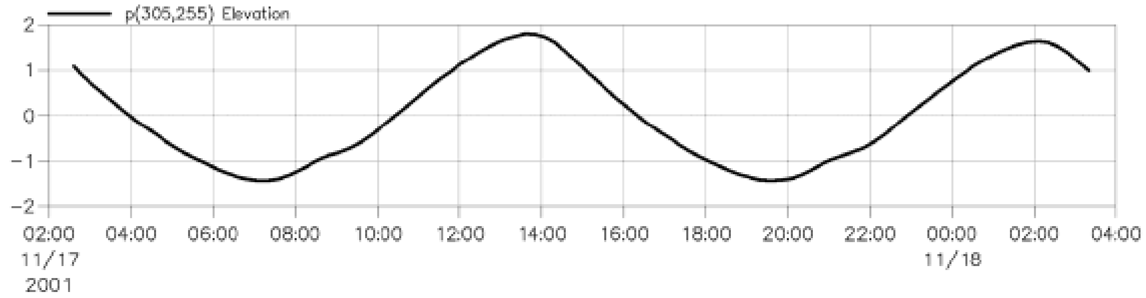

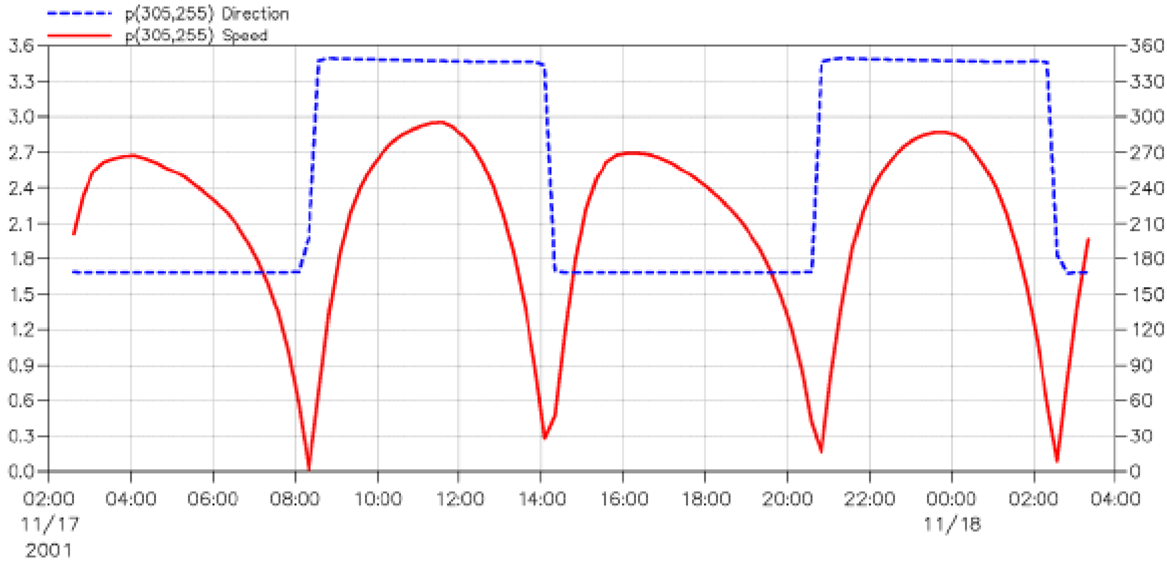

Figure 19 Spring tide elevation and velocity at Point B in Strangford Narrows (as indicated in Figure 18) (Source: Figure 14 in [24])

The bathymetric data for the Strangford Narrows TFD-2d simulation was obtained from Admiralty Chart 2159 "Strangford Narrows". The numerical grid uses a cell size of 50 x 50 metres, and is rotated so that the principal current direction at the southern boundary (near Killard Point) is perpendicular to the flow boundary. The northern end of the simulated region is curtailed as the Narrows region expands into Strangford Lough. The Lough is not of specific interest in these simulations, and would prove a stern challenge of any numerical model given the very large extent of intertidal regions in the Lough. In order to avoid generating unrealistic currents in the domain due to the prescription of the northern boundary condition, a falsified short extension is included in the numerical model. This is not an unusual numerical modelling approach. Similarly, some simplification of the southern boundary is also required immediately adjacent to the boundary in order to enable the driving boundary conditions to operate effectively (e.g. removal of intertidal and other very shallow regions on the domain boundary). In combination with a competent representation of the bathymetry and topography, the driving boundary conditions are key to the successful modelling of any tidal regime. The availability of reliable data for boundary conditions can severely limit robust application of numerical models. Detail regarding the southern boundary condition is provided at Killard Point in Admiralty publications (Charts and TotalTide) very close to the domain location, and hence is directly applied. In the interior of the Lough, further data is also provided in these sources. Data within the domain close to the port of Strangford, and further into the Lough at Killyleagh is also available. There is very little difference between the Admiralty data available for these two regions other than a phase lag of approximately 10 minutes (not unreasonable given the distance between the two locations). The consistency of these two data sources (one inside the domain region, the other outside the domain region) gave confidence in applying similar data at the northern boundary. The key aspects are a phase difference between

Killard Point and the northern boundary of 90 minutes, and a reduction of tidal range and shift of mean sea level at the northern boundary in comparison with the southern boundary. Discussion of the flow development in the Narrows region with local experts based at the Queen's University Marine Laboratory, Portaferry also proved insightful [G. Savidge and C. Boake, personal. communication]. Finally the following in [25] summarises the larger scale development of the tidal regime through the Narrows with relevance for prescription of boundary conditions:

> "Because of the construction of the Narrows, it takes some time for each rising tide to flow in Strangford Lough, and so high tides within the Lough lag behind those in the open sea. Even within the Narrows there is almost ninety minutes delay between Killard Point at the entrance and Audley's Point at the northern end. Within the Lough there is a further delay of thirty minutes. Another difference between the Lough and the Irish Sea is that the tidal range is less than four metres compared with above five on much of the open coast. Again, it is the Narrows creating this effect by hindering the tide levels in the Lough from reaching their potential maximum, and equally preventing them from completely ebbing before the next tide outside the Lough catches up again."

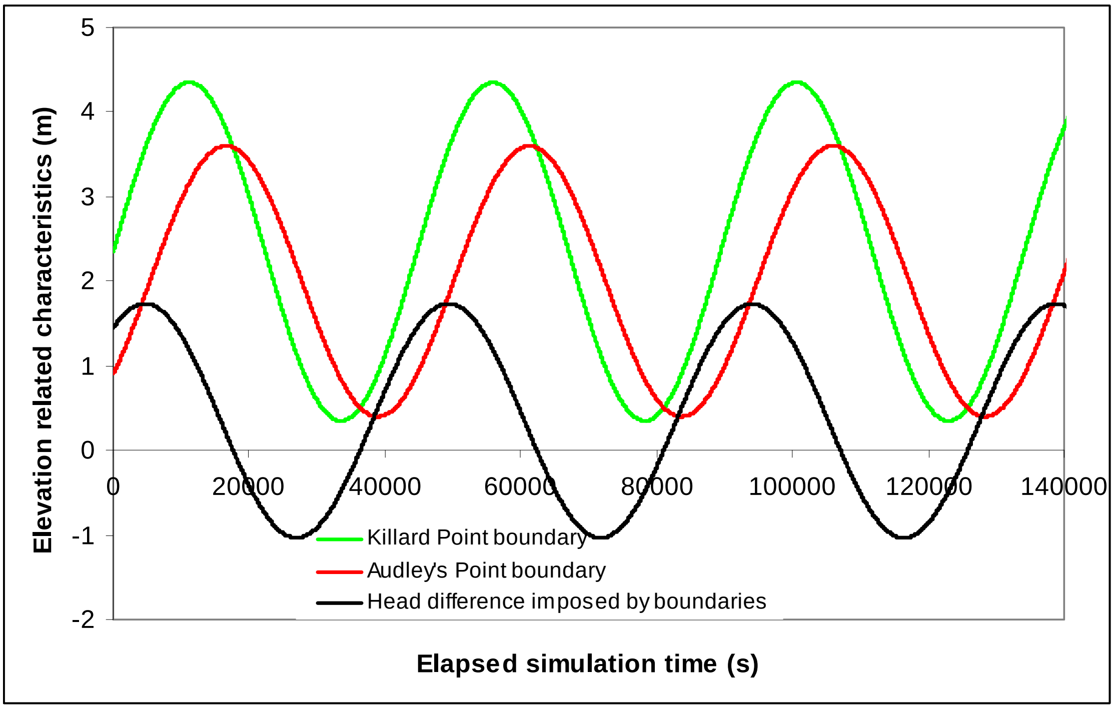

Figure 20 Upstream and downstream elevation driving boundary conditions and the subsequent pressure head variation acting across the channel length in the Strangford Narrows numerical model set-up

Taken in combination, each of these data sources was utilised to develop the boundary conditions prescribed for the numerical model operation as presented in Figure 20 (note that mean sea level in this region is not 0.0 metres). As is generally the case in Admiralty Chart publications, the charted bathymetry is set to a local 'Chart Datum', which is generally considered to be indicative of depths at the lowest astronomical tide. The overall head difference imposed by these boundary conditions is skewed towards flood-tide dominance.

The tidal flow development through the region of interest as generated by the numerical model simulation of the 'natural' (no energy extraction) case is presented in Figure 21 and Figure 22. The development of significant tidal flow velocities above 3.0 m/s across much of the central channel region through the constricted Narrows region is obvious. Peak flow velocities over 4.0 m/s are also observed on the flood tide in the narrowest sections of the channel. These narrow regions will present the largest concentration of kinetic energy within the Narrows system, hence it is unsurprising that the SeaGen device installation is adjacent to the narrow 'neck' region in the centre of the sub-domain presented in Figure 21 and Figure 22. The shallow and intertidal regions, especially in sections when the channel expands slightly create very complex localised flow features. The effects of flooding and drying are apparent in these regions, impacting the solution quite significantly. The numerical operation of flooding and drying is well known as potentially generating spurious shocks to the numerical simulation unless treated very carefully [41]. Small shocks are observed in the simulations of Strangford Narrows; not unexpected given the relatively large are of intertidal region in the domain. Although these shocks could be reduced or eliminated with judicious development of the flooding and drying algorithm, this was beyond the scope of the present investigation. The simulations generated provide a strong basis for development of engineering solutions as opposed to striving for purely scientific levels of accuracy.

7.1.2 Sensitivity analysis

As for the idealised generic flow regimes presented earlier, the hydrodynamic flow development within the domain was simulated with no energy extraction imposed, and then subsequently increased levels of energy extraction were imposed. No consideration is taken of TEC device cut-in or rated power, a fixed percentage of the instantaneously available resource is extracted as in the majority of the previous cases. Energy extraction is still simply prescribed across a cross-section of the channel. The cross-section selected is close to the location of the SeaGen installation, in the narrow 'neck' region of the domain where intense levels of kinetic energy density would be expected (as indirectly observed in Figure 21 and Figure 22).

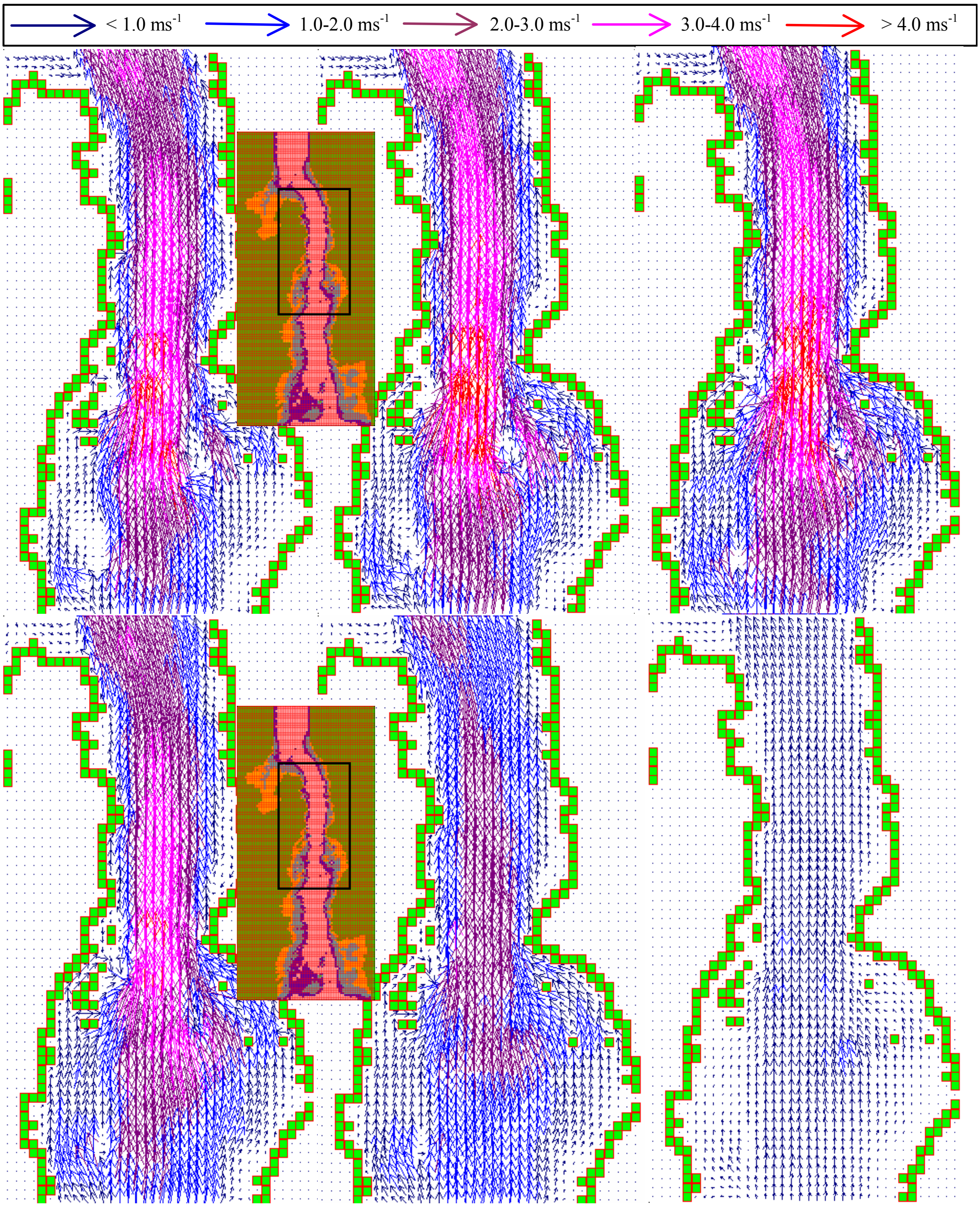

Figure 21 Instantaneous (hourly) snapshots of the flow development through the region of interest in Strangford Narrows (part 1). Inset indicates the zoomed area presented within the overall modelled region

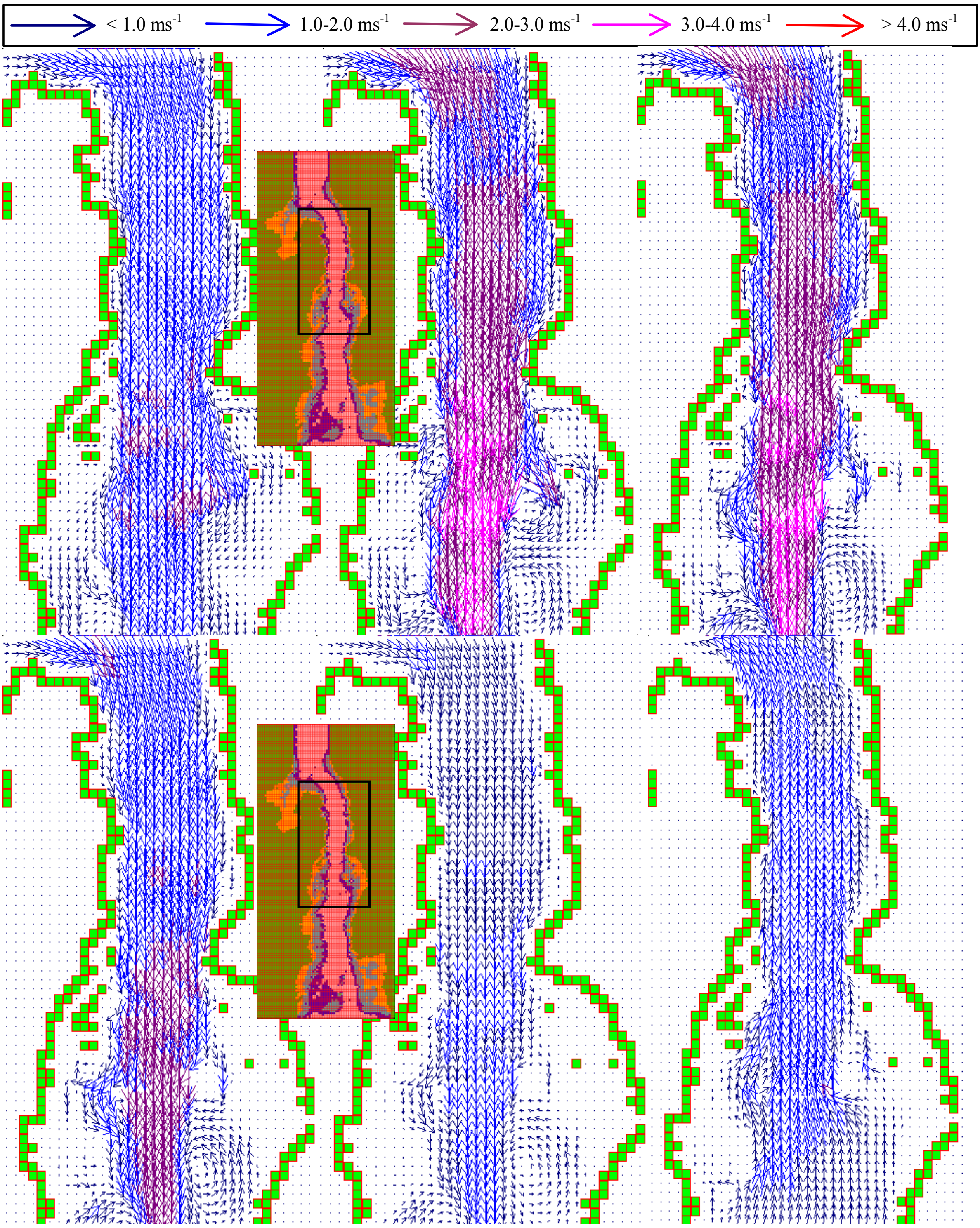

Figure 22 Instantaneous (hourly) snapshots of the flow development through the region of interest in Strangford Narrows (part 2). Inset indicates the zoomed area presented within the overall modelled region

Figure 23 indicates the variation in free surface elevation and stream-wise tidal current velocity averaged across the cross-section of interest. Very small scale variability of the result presented is due to shocks generated by flooding and drying (difficult to see at this resolution) and by the influence of eddies generated in the system. Given that within the cross-section of interest two of the twelve computational cells represent intertidal regions, the shocks observed are reassuringly very small. Considering the no extraction case in Figure 23, the local tidal range is observed to be of the order 3.2 metres, with peak flow velocity on the flood tide of 3.35 m/s and 2.45 m/s on the ebb tide (all values averaged across the cross-section). Peak values observed in the location deemed best representative of the position of the SeaGen turbine (from personal observation) are provided in Figure 24. This indicates that there is little difference in terms of free surface elevation (as would be expected), but that peak flow velocities on the flood and ebb tide are approximately 15% larger than the cross-sectional average. This again is not an unexpected finding, as the largest flow velocities in a cross-section would typically be in the centre of the channel with reducing velocities as the channel shelves to shallower regions and towards the no-slip boundaries. The impact of energy extraction indicated in both the overall response in the cross-section (Figure 23), and in the individual cell representative of the SeaGen location (Figure 24) is very similar. The free surface elevation response is minimal in terms of impact on tidal range, although there is a progressive phase shift with increasing levels of extraction. The flow velocity on the other hand exhibits a significant response in terms of the amplitude in the stream-wise direction with little alteration of phasing (the overall levels of energy extraction under consideration must be kept in mind when viewing the extreme response in terms of velocity reduction portrayed).

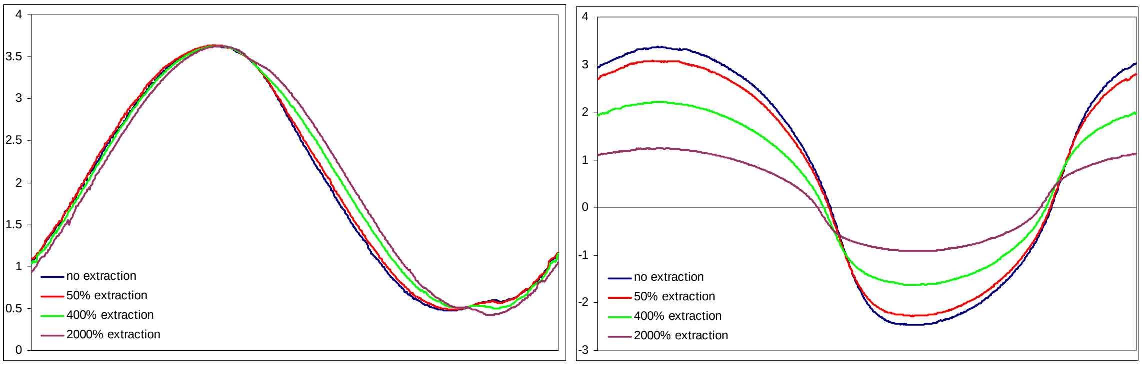

Figure 23 Variation of surface elevation and stream-wise component of velocity (averaged across the cross-section through point B)

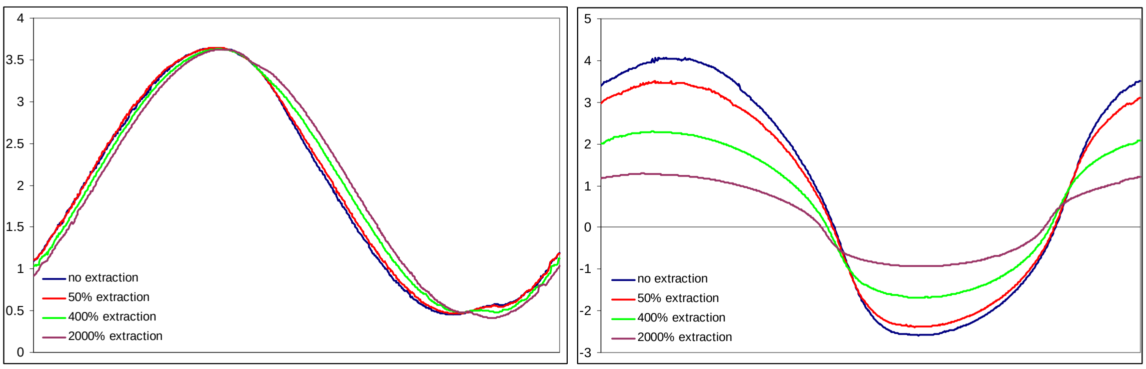

Figure 24 Variation of surface elevation and stream-wise component of velocity (at the assumed location of the SeaGen prototype)

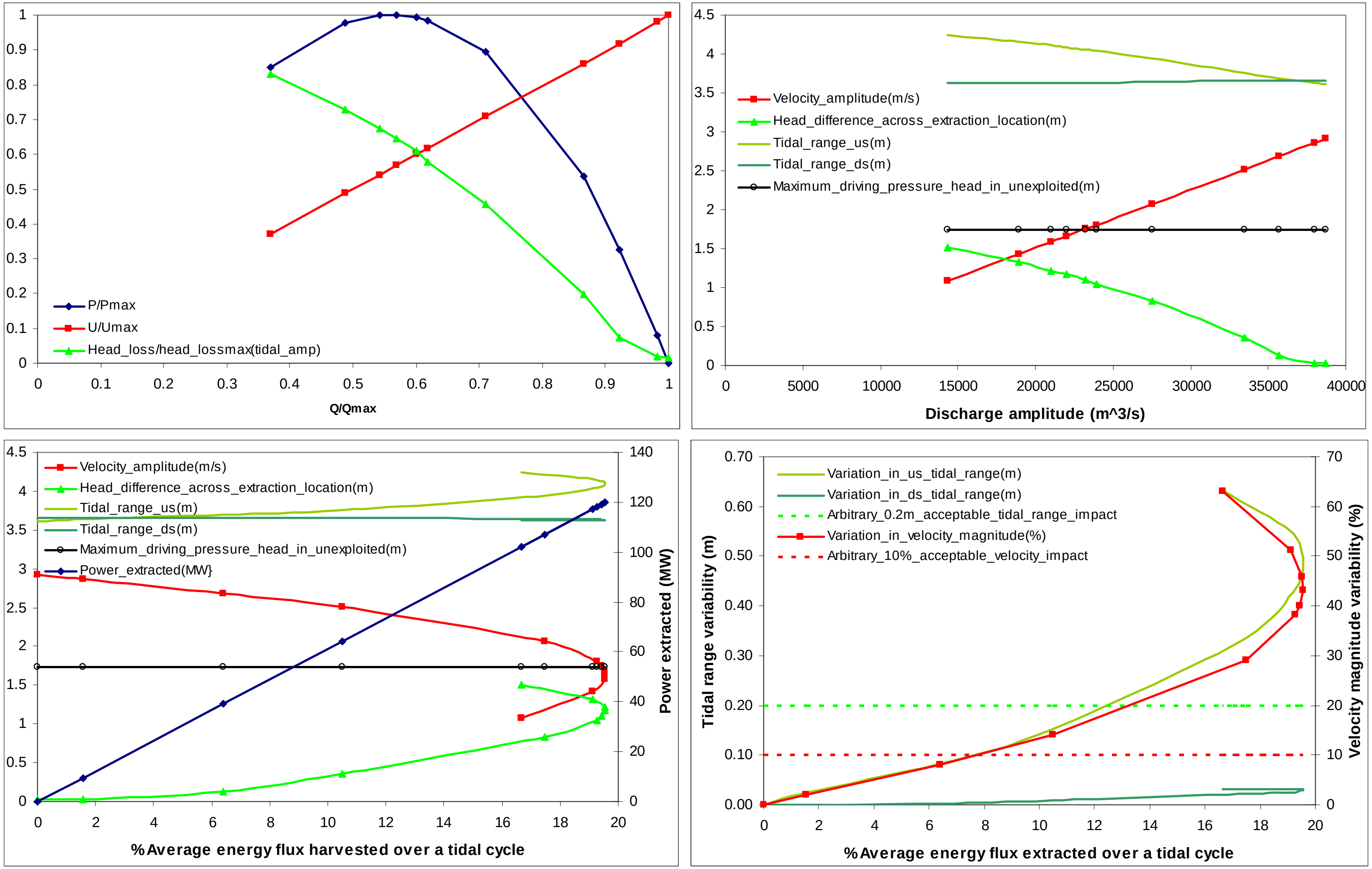

Figure 25 Impact of varying levels of energy extraction for Strangford Narrows: (i) Non-dimensional analysis, (ii) Discharge amplitude dependence, (iii) % average energy flux extracted dependence, and (iv) Variation with % average energy flux extracted and identification of constraints.

The 4-diagram summation of the response of the simulated regime to energy extraction is presented **Figure 25**. The first graph confirms the existence in this real world domain of an absolute theoretical limit on energy harvesting given the occurrence of Pmax as was indicated in all of the idealised regimes presented earlier. At Pmax, U and Q have been reduced to 56.8% of their respective maximum values (which occur in the no extraction case). At this stage, the head loss across the extraction location accounts for 64.5% of the overall maximum driving head available. The theoretical extraction limit as a function of % energy flux harvested across a tidal cycle in this case is 19.55% (graphs 3 and 4). The technical limit is imposed by concerns relating to potentially unacceptable reduction in velocity amplitude. This occurs at extraction levels representative of 40% of the theoretical limit (graph 4).

7.1.3 Interpretation

The simulation presented is representative of the flow development at Strangford Narrows and shows generally good agreement with the previously summarised numerical model simulation results presented in [24]. There is a similar slightly larger peak velocity observed on the flood tide, coupled with a shorter overall flood tide period than the ebb tide period. The difference between the peak flood and ebb tide velocities is heightened in the TFD-2d model results developed for this work. The occurrence of flood tide velocities of the order 4 m/s in the new simulations presented is supported by the ancillary evidence presented in [24, 25] which both indicate that tidal current velocity magnitudes of 8 knots (4.11 m/s) have been observed in the Narrows. This also resonates with statements made by Marine Current Turbines Ltd., the owner-operators of SeaGen who have recently reported tidal velocities of up to 10 miles per hour (4.47 m/s) observed acting on the device [23]. Similarly, the short snapshot of performance data provided in [23] is observed to reach a maximum tidal velocity of approximately 3.2 m/s. This is described as being data obtained “on a typical tide (roughly halfway between Neaps and Springs)” [23]. The data presented in Figure 18 and Figure 19 representing the previous modelling of the Narrows region are presented as Spring tide solutions. However the maximum velocity indicated in Figure 19 at point B reaches an absolute maximum (3.0 m/s) below the more recently in-situ observation of 3.2 m/s on a “typical” tide. Hence, we have a high level of confidence that the simulated velocities presented in this analysis are a good representation of the tidal current energy resource in the area of interest.

Strangford Narrows is a pre-dominantly hydraulic current regime in terms of generic classification. One difference between the results presented for this Strangford Narrows case and the generic hydraulic current cases presented earlier in section 6.1 is that the Strangford results refer to values averaged across the cross-section (as was necessary in the tidal streaming cases presented in section 6.3). The response of the system to energy harvesting presented in **Figure 25** indicates robust agreement with the trends observed in the generic hydraulic current cases. The responses of the flow regime in terms of Pmax, U and Q are in almost exact agreement with the generic case results. Head loss response is less than in the generic cases. Reasons for this could include the skewing of the head difference between the flood and ebb tidal cycle. Use of the amplitude of the available head difference as the maximum driving head available would then suggest that 80% of the head loss across the channel was occurring across the extraction plane at the theoretical extraction limit, Pmax. Further complications relating to the head difference occurring across the extraction plane can also be linked to flooding and drying at the extraction plane, and the local impact of tidal streaming occurring as the channel narrows. The response of tidal streaming to energy extraction was a much lower head difference across the extraction plane than observed in the hydraulic current case. Given the potential minor contribution of tidal streaming locally occurring in this narrow ‘neck’ region of the Narrows, a response some way in between the hydraulic current and tidal streaming cases for the head loss term is not a major concern. Taken together, and given the excellent agreement of the other parameter variables as presented in Figure 26, this provides high levels of confidence that the generic cases presented earlier are representative of more complex domain types.

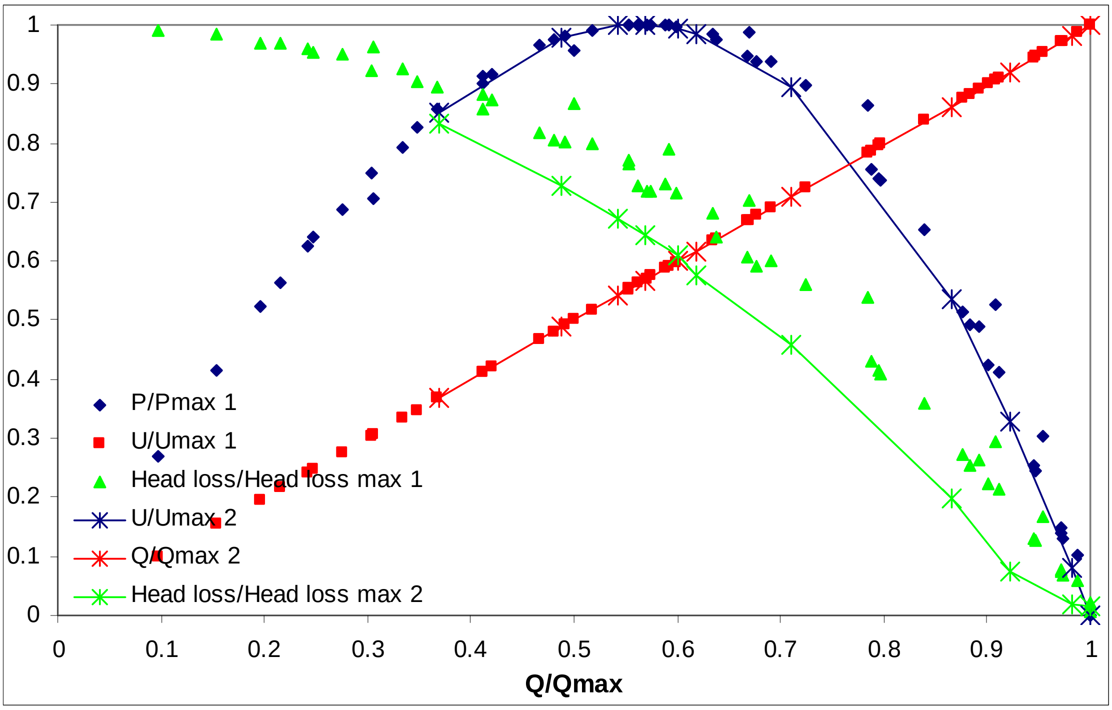

Figure 26 Comparison of variation of key non-dimensionalised parameters for hydraulic current cases 1-6 and the Strangford Narrows test case (indicated by the markers joined by lines)

As a further test of methods developed earlier using the output from the generic test cases, it is considered insightful to calculate the *theoretical* tidal current energy limit, and *technical* limit using Equation 11 and Equation 12 proposed in section 6.1.3. This will be compared with the figures for these variables output directly from the numerical model ($P_{Theoretical}$ = 119.92 MW, $P_{technical} \approx$ 47 MW). The observed amplitude of tidal velocity averaged across the cross-section at the extraction site is approximately 3.0 m/s (see Figure 23). The maximum driving head difference is known to be 1.74 m (see Figure 20). The width of the channel is 600 metres in this location, and average depth to mean sea level is 17 metres in the numerical grid derived from available Admiralty Chart data, hence the maximum flow discharge Q_{max} = 30,600 m^3/s.

Therefore

$$P_{Theoretical} = 0.2 \rho g Q_{\max} a_o = 0.2 \text{ x } 1025 \text{ x } 9.81 \text{ x } 30{,}600 \text{ x } 1.74 = 107 \text{ MW}$$

Equation 17

Considering the complexity of the domain, this is good agreement in assessing the *theoretical* extraction limit (119.92 MW vs. 107.08 MW) given that a simple parametric model formulation is being compared with the output of a numerical simulation that has conducted literally millions of complex calculations. The absolute error in this case is -10.1%. Additionally, considering that the flow across the cross-section is not uniform, the numerical model simulations will have the benefit of calculating the instantaneous energy harvested based on a formulation with a U^3 dependence. This would skew the results obtained towards a higher value than would be obtained if only the average value was operated on. Hence this is a satisfying overall result obtained for a complex flow domain using a simple parametric formula. Similarly for the *technical* resource quantification,

$$P_{Technical} = 0.086 \rho g Q_{\max} a_o = 0.086 \text{ x } 1025 \text{ x } 9.81 \text{ x } 30{,}600 \text{ x } 1.74 = 46 \text{ MW}$$

Equation 18

This is in excellent agreement with the value obtained in the numerical simulations (47 MW vs. 46 MW), indicating an absolute error of only -2%.

The purpose of the Strangford Narrows test case was to consider the relevance of the generic case examples presented in sections 6.1 to 6.3 to real world application given the potential limitations of the approach highlighted in section 6.5. This case presents good to excellent agreement between a detailed tidal hydrodynamic simulation and the simple parametric model derived from the generic cases presented in earlier sections. This provides reassurance that the parametric formulations are appropriate for application in national scale resource assessments. For the purposes of detailed project development, numerical model simulations significantly beyond the level of detail provided in section 7.1 would be desirable (e.g. extensive validation with various in-situ data sources, long-term simulations covering a minimum of a 15 day time period (preferably 30 days), grid convergence testing etc).

7.2 San Francisco Bay

The energy extraction approach described in Section 5.1.2 was applied to the UnTRIM San Francisco Bay-Delta model to provide a preliminary assessment of the potential impacts of hypothetical large-scale energy extraction scenarios on San Francisco Bay. This section presents an overview of the UnTRIM San Francisco Bay-Delta model, a description of the simulation period and the energy extraction scenarios simulated, and a summary of some of the potential hydrodynamic impacts on San Francisco Bay resulting from energy extraction near the Golden Gate. The main aim of this work was to assess whether the energy extraction approach proposed in Section 5.1.2 could be applied to a very sophisticated existing hydrodynamic model of a highly complex environment which has previously been extensively validated and used for a variety of other purposes (including an assessment of the natural resource's suitability for TEC deployment).

7.2.1 Description of the UnTRIM San Francisco Bay Delta model

The UnTRIM San Francisco Bay-Delta model (UnTRIM Bay-Delta model) is a three-dimensional hydrodynamic model of San Francisco Bay and the Sacramento-San Joaquin Delta. The UnTRIM Bay-Delta model applied in this project is the first three-dimensional hydrodynamic model extending from the Pacific Ocean through San Francisco Bay and the entire Sacramento-San Joaquin Delta. The model domain for the UnTRIM Bay-Delta model is shown in Figure 27.

The UnTRIM Bay-Delta model takes advantage of the grid flexibility allowed in an unstructured mesh by using gradually varying grid cell sizes, beginning with large grid cells in the Pacific Ocean and gradually transitioning to finer grid resolution in San Francisco Bay (Figure 28) and to the finest resolution in the smaller channels of the Sacramento-San Joaquin Delta (Figure 29). This approach offers significant advantages both in terms of numerical efficiency and accuracy, and allows for local grid refinement for detailed analysis of local hydrodynamics, while still incorporating the overall hydrodynamics of the larger estuary in a single model grid.

A full and detailed discussion of the UnTRIM model application to the San Francisco Bay-Delta is provided in [36] and [37], including a discussion of the model domain and grid, bathymetric data sources, and model boundary conditions, including inflows, wind, evaporation, agricultural diversions, and Delta barrier and gate operations. The model calibration for the UnTRIM Bay-Delta model has been well-documented (e.g. [36] and [37]), and is not reproduced here.

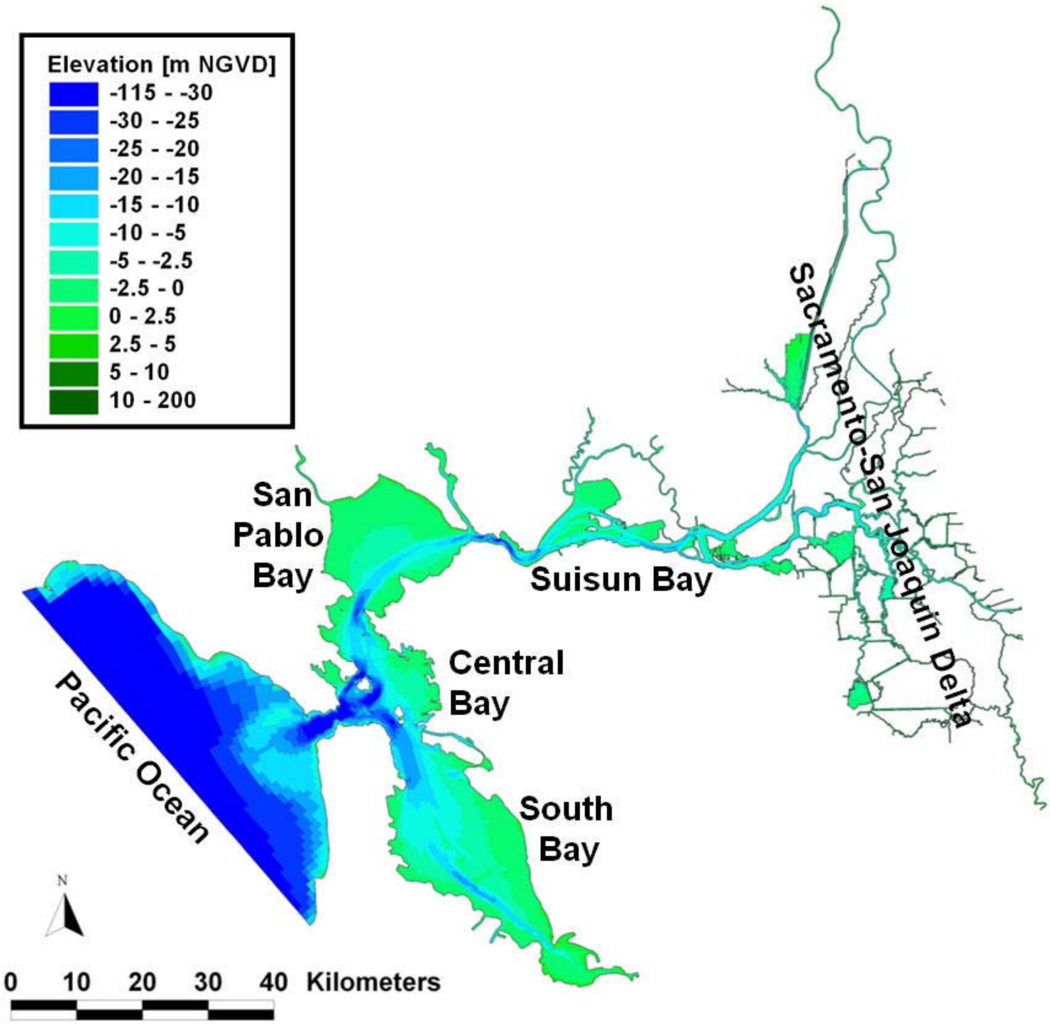

Figure 27 Model domain for the UnTRIM Bay-Delta model

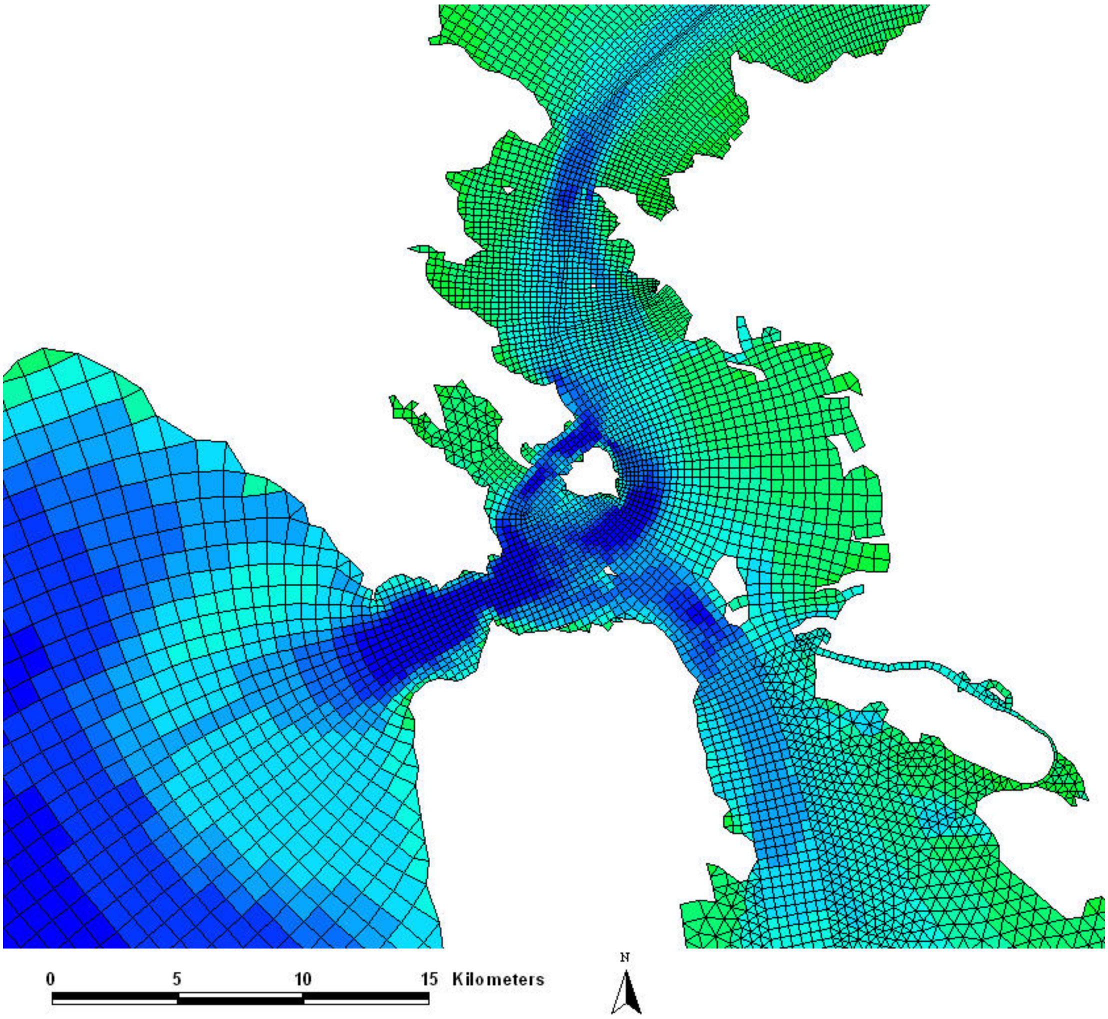

Figure 28 UnTRIM model grid in San Francisco Bay

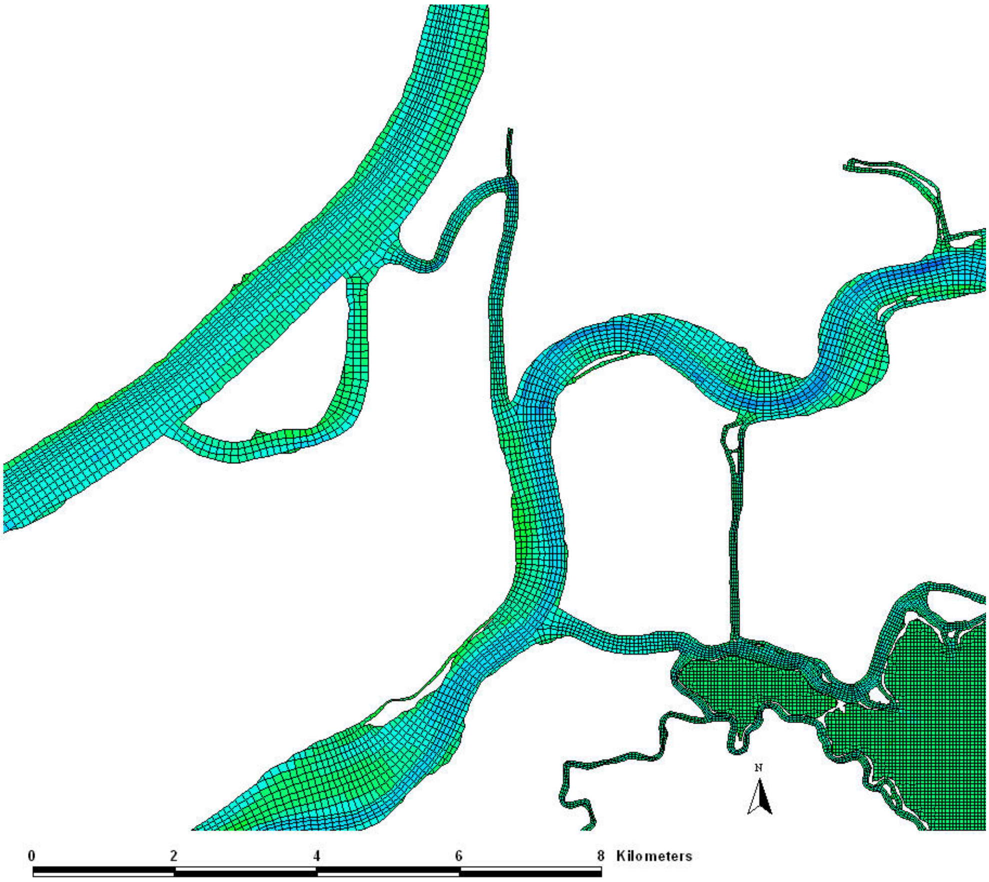

Figure 29 UnTRIM model grid in western portion of the Sacramento-San Joaquin Delta

7.2.2 Simulation period

The primary analysis of the potential impacts of energy extraction in San Francisco Bay focuses on a 29.5 day period spanning from December 1, 2007 at 00:00 PST through December 29 at 12:00 PST. This allows for two full days of hydrodynamic spin-up prior to the analysis period, providing adequate time for full hydrodynamic spin-up. A significantly longer spin-up period would be required to evaluate potential salinity impacts [37].

Figure 30 shows the predicted and observed water level at Fort Point for the analysis period spanning from December 1, 2007 at 00:00 PST through December 29 at 12:00 PST. The maximum tidal rage at Fort Point during this period occurs on December 23, when the maximum daily tidal range is 2.77 m. This day is used for an analysis of the potential impacts of energy extraction on tidal range in San Francisco Bay.

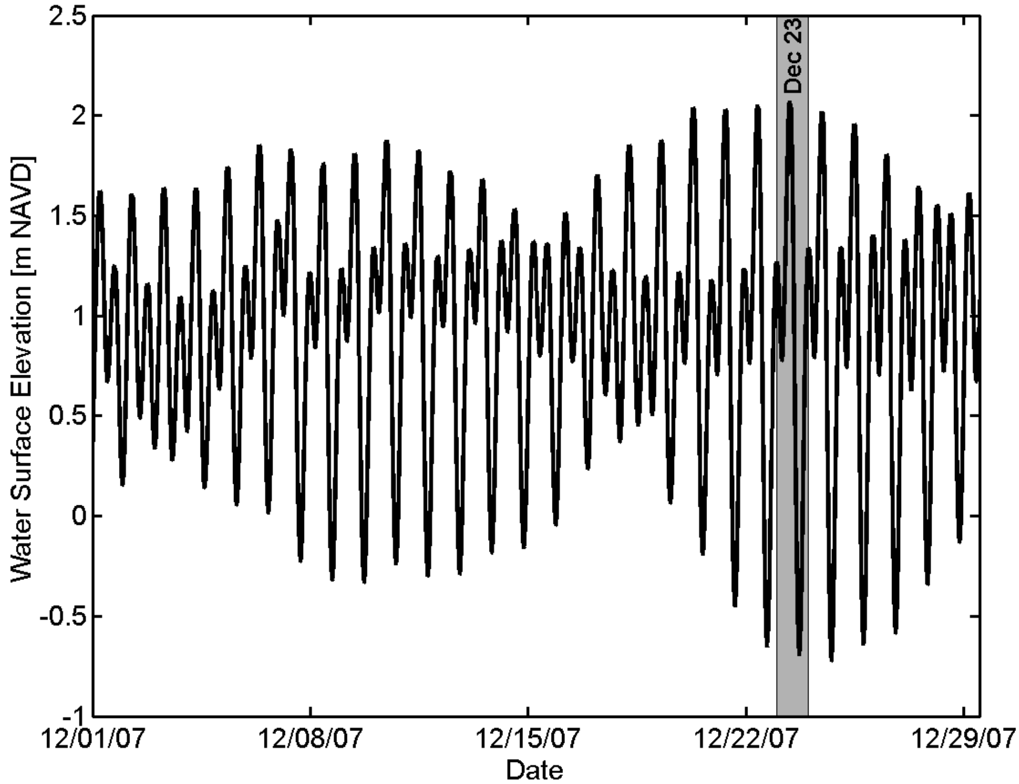

Figure 30 Observed water level at Fort Point for the analysis period spanning from December 1, 2007 at 00:00 PST through December 29 at 12:00 PST. The maximum observed tidal range at Fort Point during December 2007 occurs on December 23 (shaded grey)

7.2.3 San Francisco Bay energy extraction scenarios

The primary interest in the 3-D San Francisco Bay simulations is to understand the effects of large-scale energy extraction rather than the effects due to individual turbines. As a result, a cross-section extraction approach was used on San Francisco Bay, similar to that used in the test case presented in Section 5. A total of seven scenarios were simulated and are summarised in Table 4. The energy extraction took place in the vicinity of the Golden Gate as shown on Figure 31. The energy extraction transect can be considered to be an array of turbines installed along the transect which removes a specified percentage of the total available kinetic energy across the transect. As in previous cases, it is assumed that the turbines operate at the same extraction efficiency at all velocities, i.e. the cut-in velocity is zero and the rated velocity is the peak current velocity.

Scenario Name
Baseline
5% Extraction
10% Extraction
20% Extraction
50% Extraction
100% Extraction
200% Extraction

Table 4 Description of San Francisco Bay Energy Extraction Scenarios

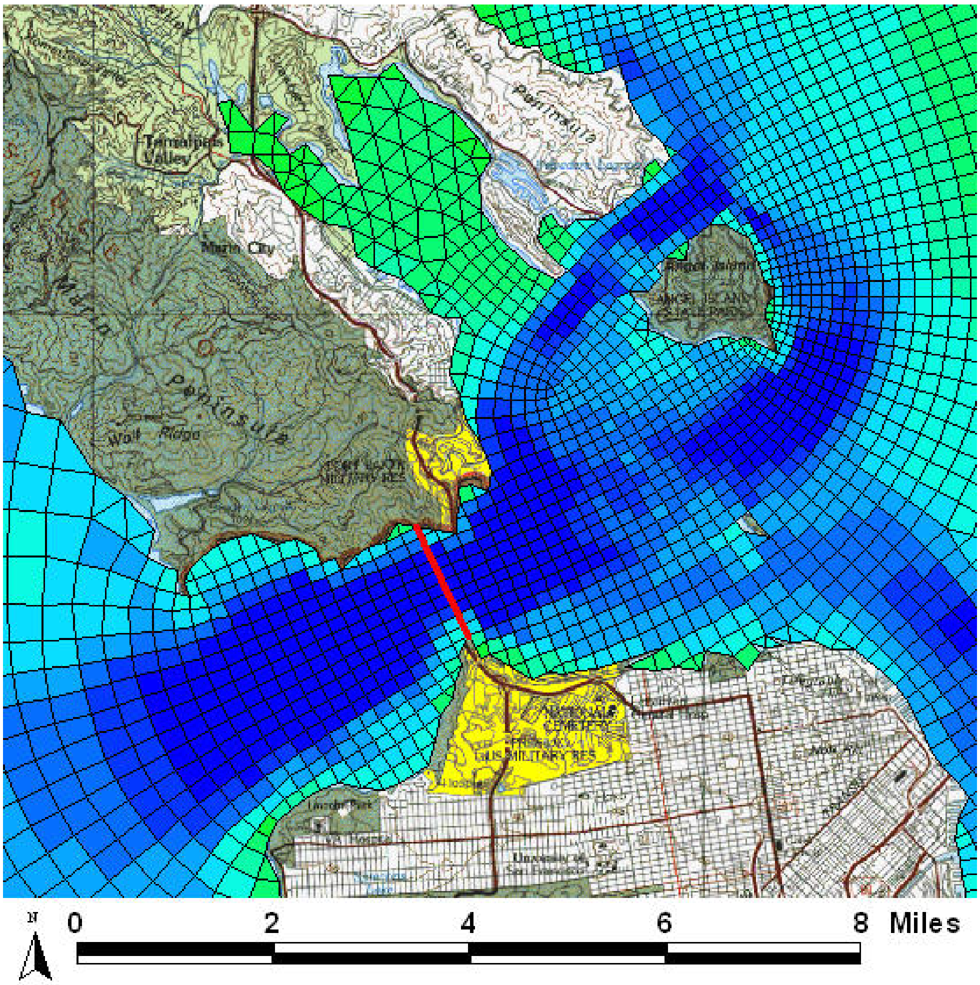

Figure 31 UnTRIM Bay-Delta model grid near the Golden Gate. Transect used for kinetic energy extraction scenarios is shown in red.

Figure 32 shows the instantaneous and daily-averaged energy extraction at the Golden Gate for each of the six energy extraction scenarios shown in Table 4. During the period simulated, the energy extraction was calculated as a fraction of the kinetic energy flux based on the percentages indicated on Table 4. Since the total kinetic energy flux through the Golden Gate decreases with increasing energy extraction (due to decreased tidal range and tidal prism in San Francisco Bay), the total amount of energy extracted for the 10% case is less than twice the total energy extracted for the 5% kinetic energy extraction case.

The instantaneous energy extraction ranges from 0 to almost 400 MW, and the daily averaged energy extraction ranges from less than 2 MW (for the 5% extraction scenario) to more than 90 MW (for the 200% extraction scenario). As seen in Figure 32, the amount of kinetic energy available for extraction varies significantly over the spring-neap cycle. Figure 33 shows the daily range of instantaneous energy extraction for a one week period from December 20 through December 27, 2007.

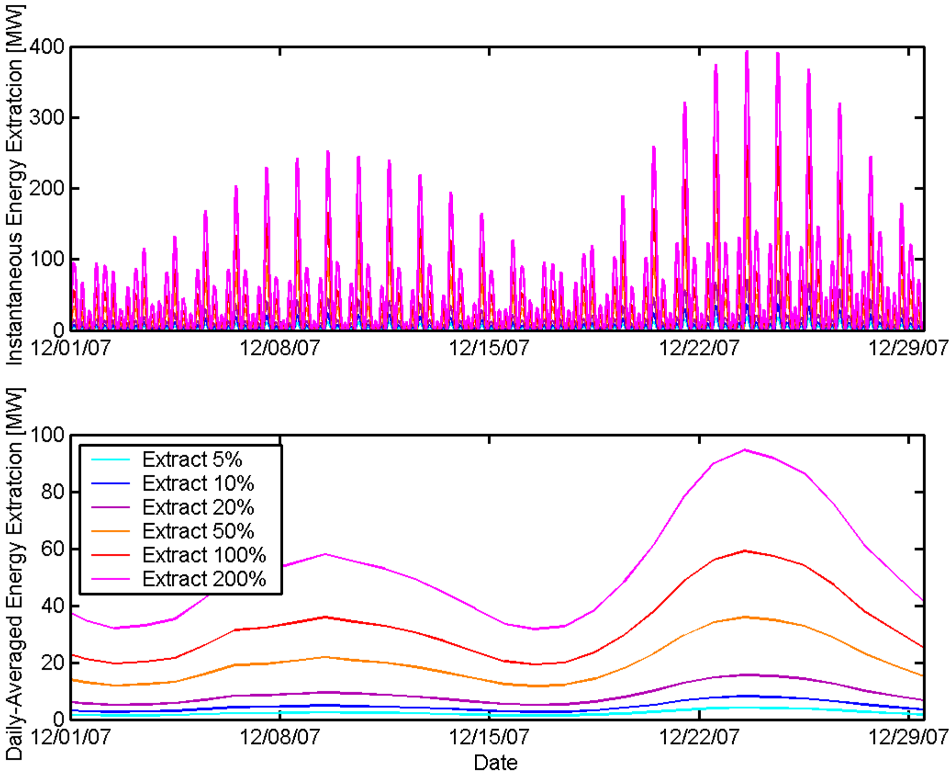

Figure 32 Instantaneous and daily-averaged energy extraction at the Golden Gate for six energy extraction scenarios for 29.5 day period beginning December 1, 2007.

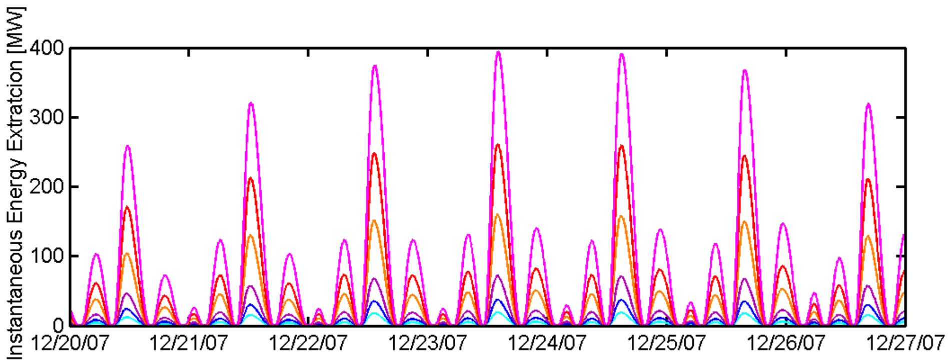

Figure 33 Instantaneous energy extraction at the Golden Gate for six energy extraction scenarios for a one week period beginning December 20, 2007.

7.2.4 Impacts of energy extraction in San Francisco Bay

Tidal range is expected to be a more important parameter for San Francisco Bay than velocity reduction, primarily as the areas of high velocity are relatively small in comparison to the area of the Bay and because of the waterfront nature of the local urban environment as well as the large areas of mudflats in various embayments (see below). Velocity reduction could also be important due to changes to tidal prism and consequent water quality impacts.

In order to analyse the effect of energy extraction on tidal range in San Francisco Bay and the Sacramento-San Joaquin Delta, the maximum tidal range at each grid cell within the domain was calculated for December 23, 2007. This day was selected because it has the maximum daily tidal range for the simulation period (see Figure 30), and also the maximum energy extraction for each of the extraction scenarios (see Figure 32 and Figure 33). Thus, the analysis of impacts to tidal range on this date should give an indication of the maximum impact for each of the scenarios presented in Table 4.

Figure 34 shows the maximum tidal range for December 23, 2007 in San Francisco Bay and the Sacramento-San Joaquin Delta (see Figure 27 for names of embayments referred to below). In the coastal Pacific Ocean, Central San Francisco Bay, and San Pablo Bay, the maximum tidal range is between 2.5 and 3 m. Due to amplification of tides in South San Francisco Bay, the maximum tidal range in the South Bay exceeds 3 m. In Suisun Bay and the Western Sacramento-San Joaquin Delta, predicted tidal range is between 1.5 and 2.5 m. In the central Delta and south Delta, predicted tidal range is between 1.0 and 1.5 m in most areas visible on Figure 34. Detailed calibration of water levels [36 and 37] have demonstrated that the UnTRIM Bay-Delta model accurately predicts tidal range in all of these regions of San Francisco Bay and the Sacramento-San Joaquin Delta.

In analysing Figure 34, it is evident that the tidal range along the margins of South San Francisco Bay and San Pablo Bay are noticeably less than in the center of the embayments. These results reflect the fact that these areas dry out at low water, thus they experience a lower tidal range than the channel areas which experience lower low waters. Similarly, in evaluating changes to tidal range, these areas show a lesser reduction in tidal range since they are generally not affected by changes to low water that occur below the mudflat elevations (since they are already dry within those low water level ranges).

By comparing the predicted tidal range on December 23, 2007 under each of the energy extraction scenarios to the baseline tidal range shown on Figure 34, the impact of energy extraction on tidal range within the estuary can be evaluated.

Figure 35 shows the predicted decrease in tidal range resulting from the 5% extraction scenario. For the 5% extraction scenario, the maximum tidal range in Central San Francisco Bay, San Pablo Bay, and South San Francisco Bay decreases by between 0.5 and 1 cm. The impact of the 5% extraction scenario on water levels in the coastal Pacific Ocean, Suisun Bay, and all of the Sacramento-San Joaquin Delta is predicted to be less than 0.5 cm.

Figure 36 shows the predicted decrease in tidal range resulting from the 10% extraction scenario. For the 10% extraction scenario, the maximum tidal range in Central San Francisco Bay, San Pablo Bay, and South San Francisco Bay decreases by between 1 and 2 cm, and the tidal range in Suisun Bay decreases by between 0.5 cm and 1 cm. The impact of the 10% extraction scenario on water levels in the coastal Pacific Ocean and all of the Sacramento-San Joaquin Delta is predicted to be less than 0.5 cm.

Figure 37 shows the predicted decrease in tidal range resulting from the 20% extraction scenario. For the 20% extraction scenario, the maximum tidal range in Central San Francisco Bay, San Pablo Bay, and South San Francisco Bay decreases by between 2 and 4 cm, and the tidal range in Suisun Bay decreases by between 1 cm and 2 cm. The predicted tidal range decreases by between 0.5 and 1 cm for many portions of the western and central Sacramento-San Joaquin Delta. The impact of the 20% extraction scenario on water levels in the coastal Pacific Ocean is predicted to be less than 0.5 cm.

Figure 38 shows the predicted decrease in tidal range resulting from the 50% extraction scenario. For the 50% extraction scenario, the maximum tidal range in Central San Francisco Bay and the northern part of South San Francisco Bay decreases by between 6 and 8 cm; in the southern portion of the South Bay tidal range decreases by between 8 cm and 10 cm for the 50 % extraction scenario. In San Pablo Bay, predicted tidal range decreases by between 4 and 6 cm, with a decrease in tidal range of between 2 and 4 cm in much of Suisun Bay. The predicted tidal range decreases by between 1 and 2 cm for many portions of the western Delta and by between 0.5 and 2 cm in portions of the central and northern Sacramento-San Joaquin Delta. The impact of the 50% extraction scenario on water levels in the most of coastal Pacific Ocean is predicted to be less than 0.5 cm; some reduction in tidal range of between 0.5 and 1 cm is evident west of the extraction sites.

Figure 39 shows the predicted decrease in tidal range resulting from the 100% extraction scenario. For the 100% extraction scenario, the maximum tidal range in Central San Francisco Bay and the northern part of South San Francisco Bay decreases by between 10 and 15 cm; in the southern portion of the South Bay near Calaveras Point the predicted tidal range decreases by between 15 cm and 20 cm for the 100 % extraction scenario. In San Pablo Bay, predicted tidal range decreases by between 8 and 10 cm, with a decrease in tidal range of between 6 and 8 cm through Carquinez Strait and between 4 and 6 cm in much of Suisun Bay. The predicted tidal range decreases by between 2 and 4 cm for many portions of the western Delta and by between 1 and 4 cm in portions of the central and northern Sacramento-San Joaquin Delta. The impact of the 100% extraction scenario on water levels in the most of coastal Pacific Ocean is predicted to be less than 0.5 cm; some reduction in tidal range of between 0.5 and 2 cm is evident west of the extraction sites.

Figure 40 shows the predicted decrease in tidal range resulting from the 200% extraction scenario. For the 200% extraction scenario, the maximum tidal range in Central San Francisco Bay and most of San Pablo Bay decreases by between 15 and 20 cm. In South San Francisco Bay, the maximum predicted tidal range decreases by more than 20 cm for the 200 % extraction scenario. Through Carquinez Strait, predicted tidal range decreases by between 10 and 15 cm, with a decrease in tidal range of between 6 and 10 cm in much of Suisun Bay. The predicted tidal range decreases by between 2 and 4 cm for many portions of the western Delta and by between 2 and 4 cm in many portions of the central and northern Sacramento-San Joaquin Delta. The impact of the 200% extraction scenario on water levels in the most of coastal Pacific Ocean is predicted to be less than 0.5 cm; some reduction in tidal range of between 0.5 and 4 cm is evident almost 15 km west of the extraction sites.

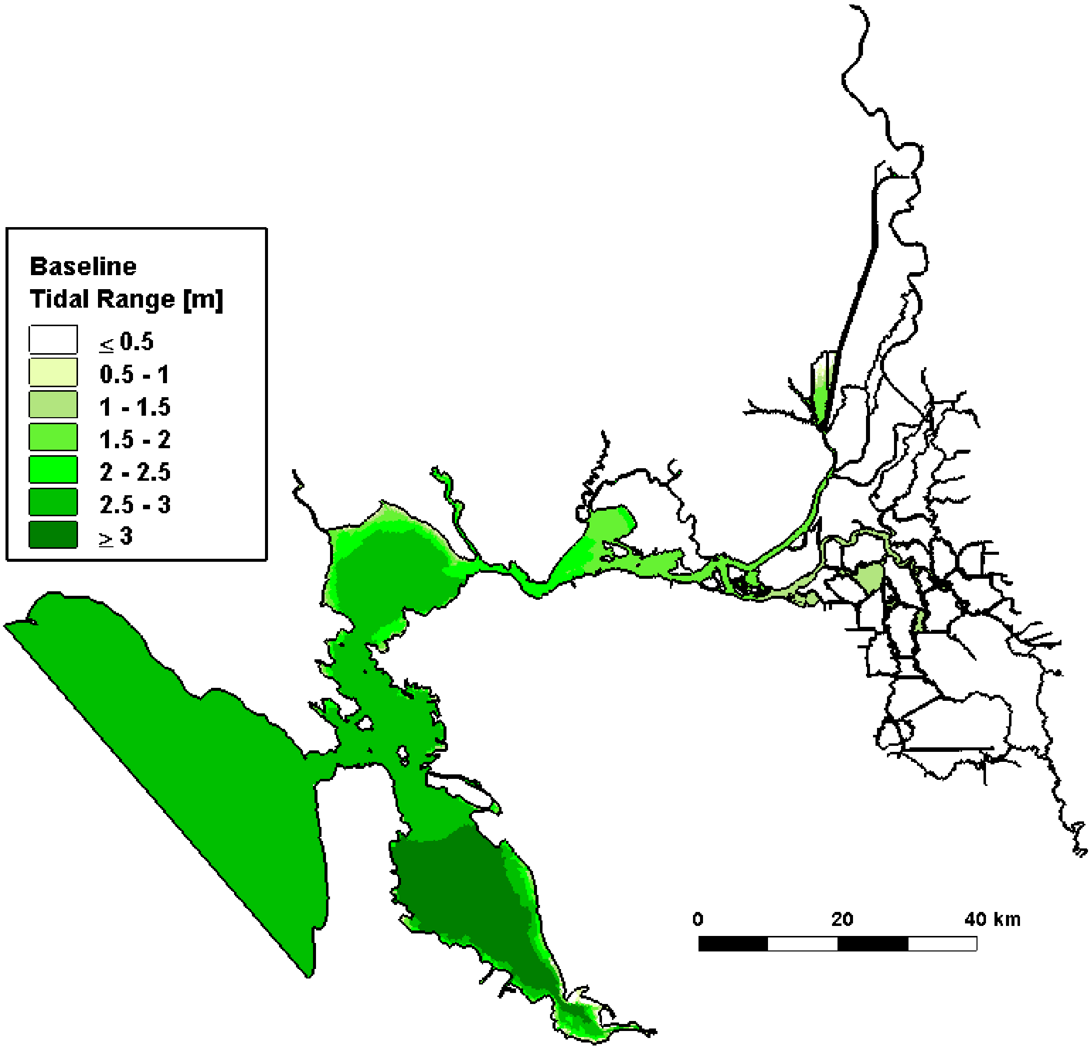

Figure 34 Maximum tidal range on December 23, 2007 in San Francisco Bay and the Sacramento-San Joaquin Delta.

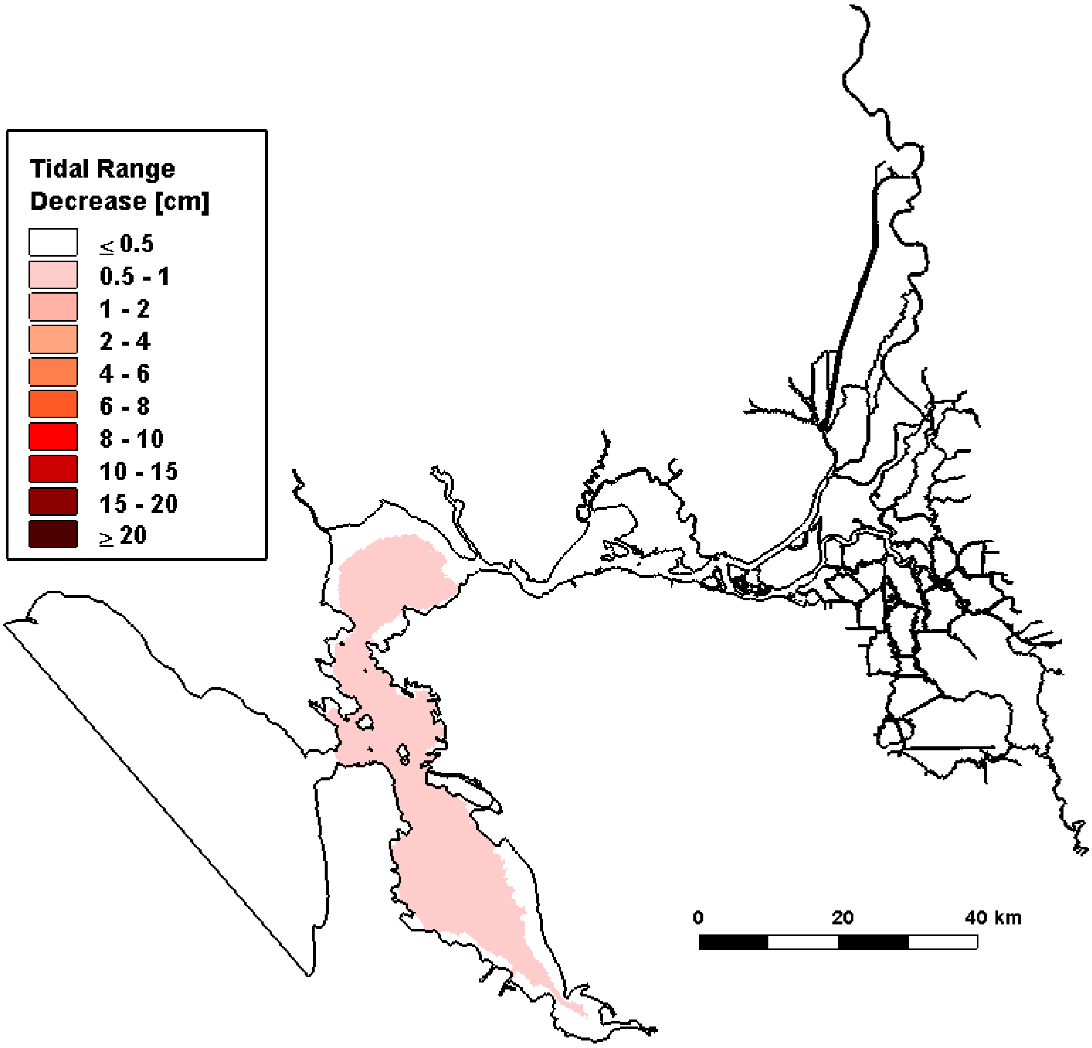

Figure 35 Decrease in maximum tidal range on December 23, 2007 resulting from 5% extraction scenario.

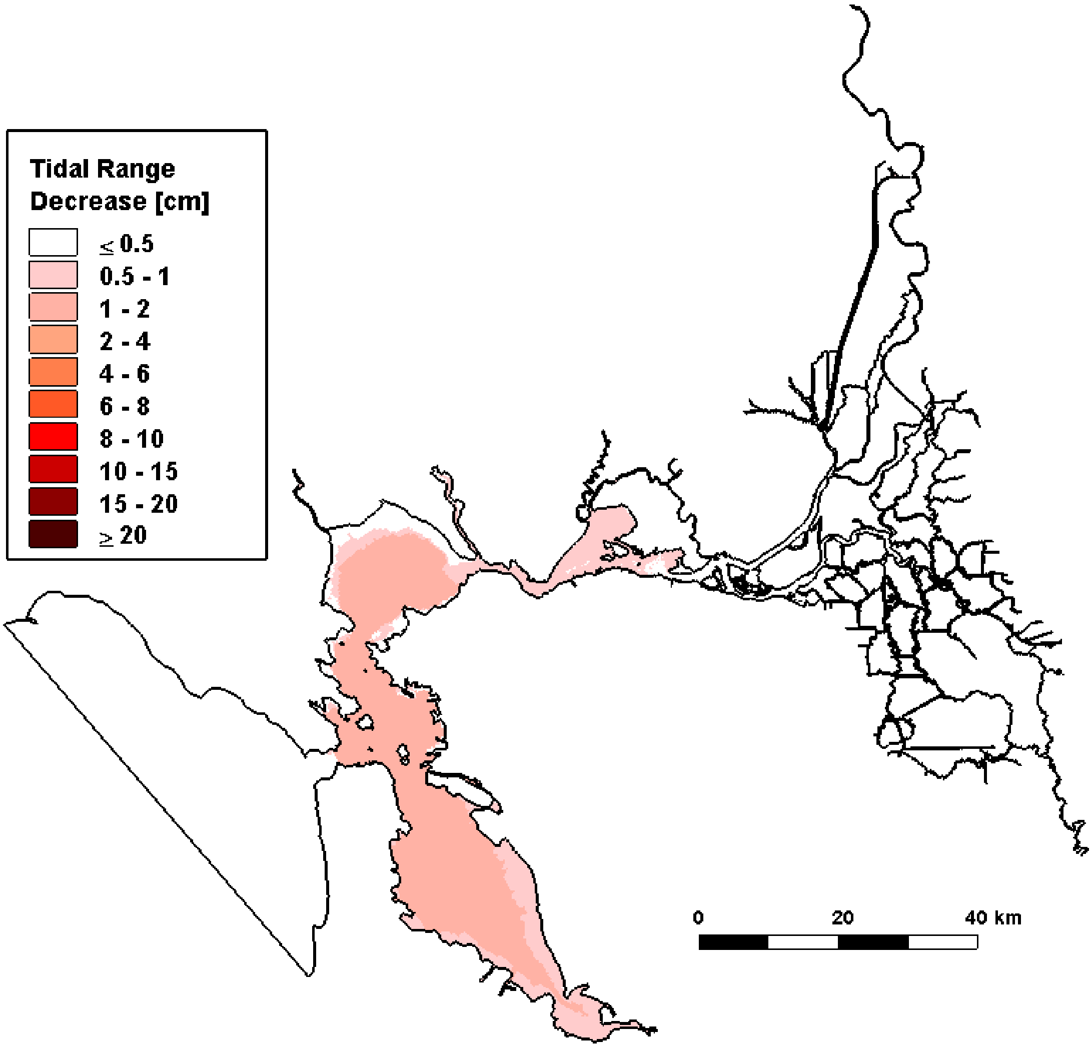

Figure 36 Decrease in maximum tidal range on December 23, 2007 resulting from 10% extraction scenario.

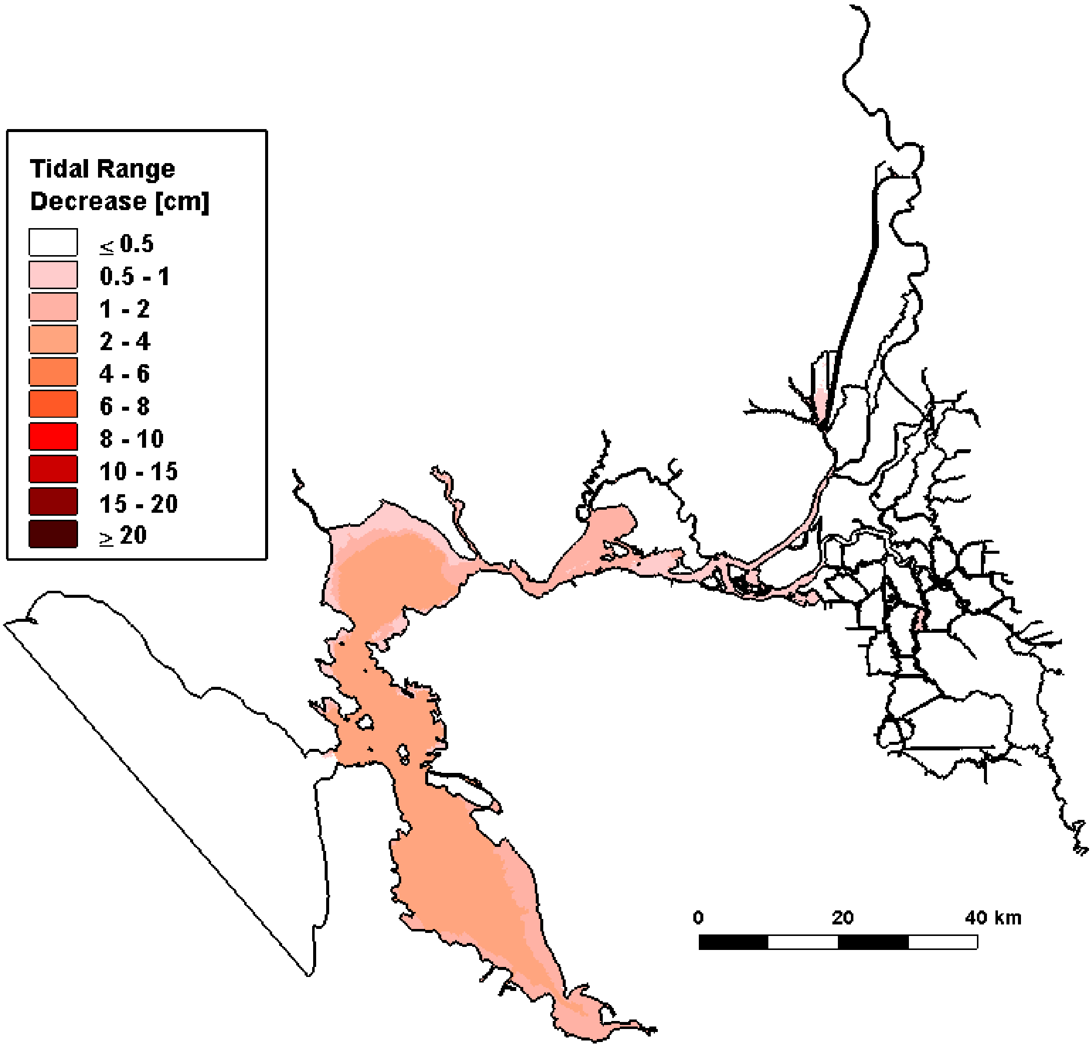

Figure 37 Decrease in maximum tidal range on December 23, 2007 resulting from 20% extraction scenario.

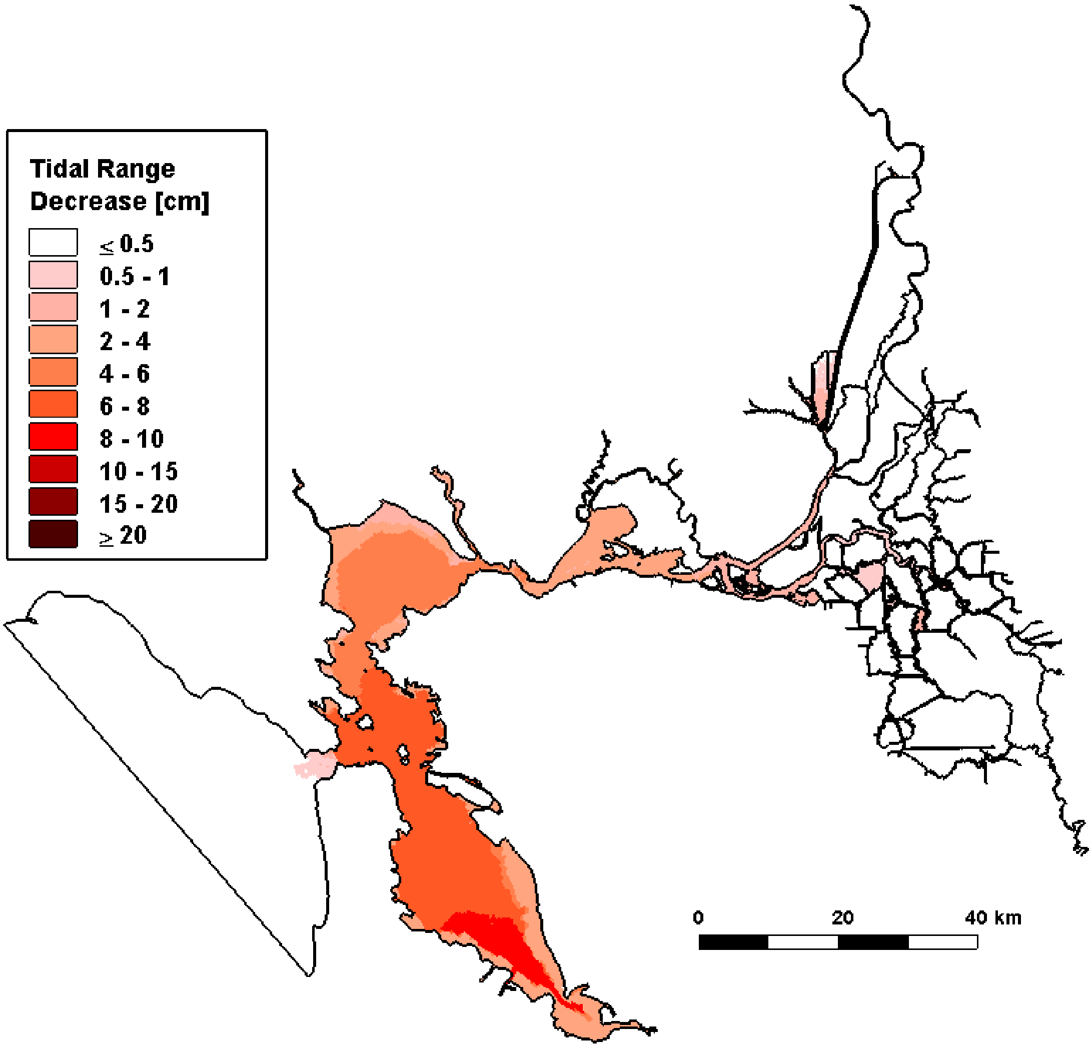

Figure 38 Decrease in maximum tidal range on December 23, 2007 resulting from 50% extraction scenario.

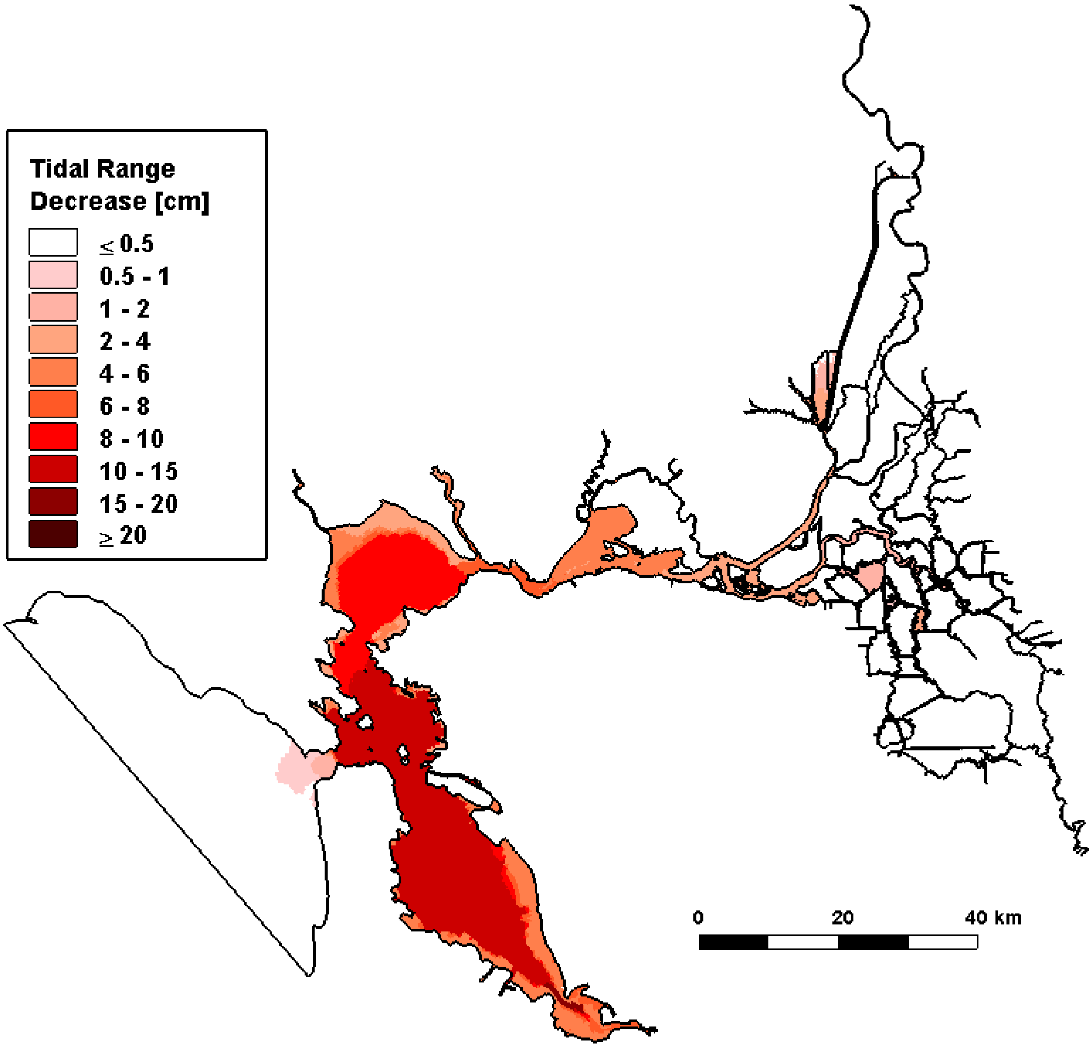

Figure 39 Decrease in maximum tidal range on December 23, 2007 resulting from 100% extraction scenario.

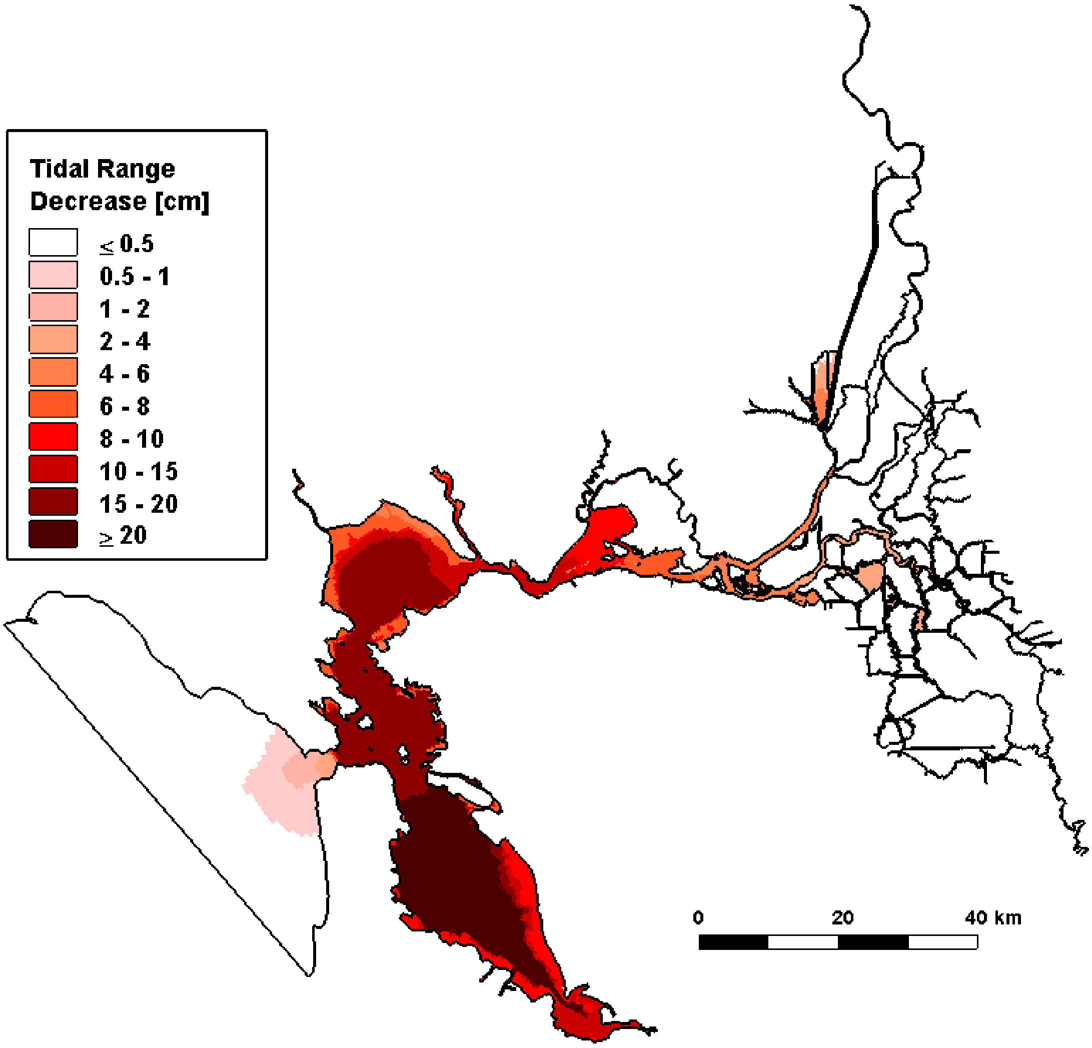

Figure 40 Decrease in maximum tidal range on December 23, 2007 resulting from 200% extraction scenario.

7.2.5 Interpretation of San Francisco Bay simulations

The analysis focuses on the effects of energy extraction on water levels inside San Francisco Bay. However, from this analysis it can also be seen that energy extraction also affecting the volume of water exchanged through the estuary (due to the reduction in tidal prism).

The six energy extraction scenarios presented in this section represent a wide spectrum of energy extraction ranging from a 29-day average energy extraction of 1.3 MW for the 5% extraction scenario to 53.5 MW for the 200% extraction scenario. In each scenario, the energy extraction was represented as a percentage of the available kinetic energy flux through one or more transects near the Golden Gate.

This approach does not take in to account the selection of the most appropriate sites for energy extraction or the technical, practical, or political feasibility of locating turbines at a particular location, nor the efficiency of the turbines at recovering the extracted energy. As such, the analysis is most suited as an assessment of the potential range of water level and tidal range impacts resulting from a range of energy extraction levels near the Golden Gate. It is expected that some differences may result depending on how and where individual turbines are placed, but the overall impacts on water levels and tidal range should be a reasonable estimate for a given level of energy extraction.

The approach used in San Francisco Bay also assumes that the water levels at the ocean boundary are not affected by the energy extraction. This assumption appears to be valid even for the largest extraction scenario, since the impact on water levels west of the extraction site is small (Figure 40).

In general, the effects of the energy extraction at the Golden Gate are similar to the generic energy extraction test case results. During flood tide, water levels are higher in the Pacific Ocean and propagate into San Francisco Bay. At the energy extraction transect(s) near the Golden Gate, the extraction results in a decrease in water level and an increase in velocity (due to the decrease in downstream cross-sectional area) across each transect where energy extraction is applied. This head loss results in lower water levels in San Francisco Bay near high water. During ebb tide, water levels are higher in San Francisco Bay and lower in the Pacific Ocean. The energy extraction across the Golden Gate transects during ebb, similarly result in a head loss across the Golden Gate, resulting in water levels remaining higher in San Francisco Bay near low water than in the no extraction case. The water levels at Fort Point, which is located just east of the extraction transects is a good indicator of the head loss which is predicted to occur across the energy extraction sites for each level of energy extraction.

Although it is not known what the acceptable limits to the reduction in tidal range in various areas of San Francisco Bay would be, we would expect that the acceptable limits would be within these scenarios, as they cover the arbitrarily prescribed limits for velocity reduction and tidal range.

It is noted that the tidal range in San Francisco Bay appears to be more sensitive to energy extraction than the generic idealised cases would suggest, with the arbitrarily prescribed limit for tidal range being reached at approximately the same energy extraction levels as the velocity limit for some areas. However, the figures above demonstrate how variable the tidal range impacts are across the different embayments.

If the technical resource for the day of the peak spring tide is calculated from the generic formula, using the same underlying methodology as for Strangford Narrows, and then compared to the modelled result, the answers are within 15-45% of each other, dependent on the exact locations used to determine the maximum driving tidal head difference, a_0. Given that San Francisco Bay is clearly a highly complex site with significant deviations from the ideal representations, this correlation is surprisingly good.

8 CONCLUSION AND SUGGESTIONS FOR FURTHER WORK

The main objective of this study was to undertake research to further the development of the flux approach to tidal current resource assessment which was first outlined in 2004 (based on leading-edge research of the time), so as to further understand the proportion of the tidal energy that one could extract using TECs from specific types of sites, and thus allow more accurate assessments of national and regional tidal current energy resources.

Three generic tidal regimes that give rise to kinetic power densities of interest for future economic deployment of TEC technology projects were identified and characterised; *hydraulic current* channels; *resonant basin* systems and regions of *tidal streaming*. The response to energy removal in each of the three key tidal regimes was investigated using a numerical modelling approach applied to idealised representations of each of the three generic tidal regimes, thus enabling the characterization of the generic response of each system to different levels of energy removal. In all three tidal regimes, an upper *theoretical* limit was identified beyond which attempts to extract more energy from the system actually reduces the overall energy that is harvested. In each of the individual tidal regimes, there was good agreement on the *theoretical* maximum energy removal limit – which can be quantified with reference to the flow discharge in the undisturbed (natural) simulation case (Q_{max}) and the available driving head difference (a_o). The flow discharge, flow velocities and tidal range were all reduced by energy harvesting, as expected, and these effects would at some point have impacts on the environment and the project economics that would be unacceptable, as outlined in 2004.

Consideration of arbitrarily prescribed 'environmentally and economically acceptable' impacts of energy removal on the overall tidal hydrodynamics of the system enables assessment of an 'acceptable' energy removal limit. Again, a common metric for determination of the *technical* energy removal limit has been identified in each of the three cases, again related to Q_{max} and a_o.

These findings, arrived at using idealised domain representations, are then tested by analysing the responses of real world hydraulic current locations. The Strangford Lough case presents good to excellent agreement between detailed tidal hydrodynamic simulations and the simple parametric model derived from the generic cases. The primary interest in the 3-D San Francisco Bay simulations was to understand whether the proposed energy extraction approach could be implemented within a sophisticated model of a high complex environment, and the likely effects of energy extraction in this highly sensitive area. The analysis suggests that highly complex sites such as San Francisco Bay, which are extensive departures from the idealised representations used in the generic cases, should be modelled to understand the different impacts even when only considering the technical resource.

Despite the lack of extensive testing, the combined numerical modelling analyses provide confidence in applying the key metrics identified for quantifying the *theoretical* resource equations in the final proposed parametric approach. There is also good confidence in the basis for the *technical* resource calculations, although the actual difference between the theoretical and technical resource is determined by the prescription of currently arbitrary (but reasonably informed) limits to the impacts. In a national or regional resource assessment, sensitivity testing of these arbitrarily prescribed limits is recommended, and different regions may well need to prescribe different 'base-line' limits due to different local environments. Clearly, consideration of the *practical* resource should consider acceptable limits to the impacts on a site-by-site basis, in conjunction with all the other aspects that would limit practical resource extraction.

Certain caveats as to the accuracy of the parametric approach are still necessary. Most sites will obviously not be fully representative of the idealised representations of the three generic regimes, and many sites will be significantly different, e.g. with all three regimes being present. In these cases, the parametric expressions will not be as accurate. The impact on power extraction levels if alternative flow pathways are available is one common example. In such scenarios, which are not uncommon, the derivation of the *theoretical* (and *technical, if ones assumes the imposed limits)* tidal current energy resource in the parametric methodology is an upper bound on the power available for extraction from the tidal current energy resource. Example cases include:

- Tidal systems where alternative flow channels are available [7]. Also see [10, 11].
- Channels where only a partial tidal fence is installed across the cross-section [6].
- The extreme case of a TEC device or small array in a theoretically unbounded (laterally) domain [6].

The other major issue requiring further consideration is the prescription of how much of the energy removal from the tidal hydrodynamic system can actually be ascribed to energy generation. Potential device efficiencies are of course fairly well understood, and best practice understanding of TEC device performance envelopes have been utilised in some of the key assumptions necessary in this analysis. What has not been considered in any detail in this analysis is the energy removal from the system that would have to be ascribed to the presence of the TEC device itself. Future focus to reduce this wasteful use of the resource by improved support structure design and streamlining has the potential to significantly reduce this loss of useful energy that would otherwise be available for harvesting.

REFERENCES

1. Black & Veatch Consulting Ltd. (2005); "Phase II UK tidal stream energy resource assessment". *Technical report 107799/D/2200/03, Carbon Trust, London*.
2. Boyle, G. (editor) (1996). "Renewable Energy: Power for a Sustainable Future". *Oxford University Press*. ISBN: 0-19-856451-1
3. Couch, S.J. & Bryden, I.G. (2004); "The impact of energy extraction on tidal flow development". *Proceedings of the 3rd International Conference on Marine Renewable Energy*
4. Garrett, C. & Cummins, P. (2004); "Generating power from tidal currents". *Journal of Waterway, Port, Coastal, and Ocean Engineering,* **130**, pp. 114-118.
5. Garrett, C. & Cummins, P. (2005); "The power potential of tidal currents in channels". *Proceedings of the Royal Society A*, **461**, pp.2563-2572.
6. Garrett, C. & Cummins, P. (2007). "The efficiency of a turbine in a tidal channel". *Journal of Fluid Mechanics*, **588**, pp. 243-251.
7. Sutherland, G., Foreman, M. & Garrett, C. (2007); "Tidal current energy assessment for Johnstone Strait, Vancouver Island". *Proceedings of the IMechE Part A: Journal of Power and& Energy,* **221**, pp. 147-157. doi:10.1243/09576509JPE338.
8. Blanchfield, J., Garrett, C., Rowe, A. & Wild, P. (2008). "The extractable power from a channel linking a bay to the open ocean". *Proceedings of the IMechE Part A: Journal of Power and Energy*, **222**, pp. 289-297. doi: 10.1243/09576509JPE524.
9. Garrett, C. & Cummins, P. (2008); "Limits to tidal current power". *Renewable Energy*, **33**, pp. 2485-2490. doi:10.1016/j.renene.2008.02.009,
10. Couch, S.J. & Bryden. I.G. (2005); "Numerical Modelling of Energy Extraction from Tidal Flows", *Proceedings of the World Renewable Energy Congress 2005 (WREC 2005).*
11. Polagye, B., Kawase, M & Malte, P. (2009); "In-stream tidal energy potential of Puget Sound, Washington". *Proceedings of the IMechE Part A: Journal of Power and Energy*, **223**, pp. 571-587. doi:10.1243/09576509JPE748.
12. Tarbotton, M. & Larson, M. (2006); "Canada Ocean Energy Atlas (Phase 1) Potential Tidal Current Energy Resources Analysis Report". *Report prepared for NRC-Canadian Hydraulics Centre*. Available online at http://web.me.com/michaeltarbotton1/Triton/download/TritonCanadaTidalPowerMay2006.pdf
13. Cornett, A. (2006); "Inventory of Canada's Marine Renewable Energy Resources". *NRC-CHC Technical Report CHC-TR-041*. Available online at http://oreg.ca/docs/Atlas/CHC-TR-041.pdf.
14. Polagye, B., Malte, P., Kawase, M. & Durran, D. (2008); "Effect of large-scale kinetic power extraction on time-dependent estuaries". *Proceedings of the IMechE Part A: Journal of Power and Energy*, **222**(5), pp. 471-484. **doi:** 10.1243/09576509JPE519.
15. Couch, S.J. & Bryden, I.G. (2006); "Tidal Current Energy Extraction: Hydrodynamic Resource Characteristics", *Proceedings of the IMechE, Part M: Engineering for the Maritime Environment*, **220**(4), pp. 185-194. doi:10.1243/14750902JEME50.
16. Bryden, I.G., Couch, S.J., Owen, A. & Melville, G. (2007); "Tidal current resource assessment". *Proceedings of the IMechE, Part A: Journal of Power and Energy,* **221**, pp. 125-135. doi:10.1243/0957609JPE238.
17. Neill, S.P., Litt, E.J., Couch, S.J. & Davies, A.G. (2009); "The impact of tidal stream turbines on large-scale sediment dynamics". *Renewable Energy*, **34**(12), pp. 2803-2812. doi:10.1016/j.renene.2009.06.015.
18. Couch, S.J. (2001); "Numerical Modelling of Tidal Flow Development around Headlands and Islands". *PhD Thesis (number T10342), Dept. Civil Engineering, University of Strathclyde, Glasgow, UK*.
19. Bryden, I.G. & Melville, G.T. (2004); "Choosing and evaluating sites for tidal current development". *Proceedings of the IMechE Part A: Journal of Power and Energy*, **218** pp. 567-577.

20. Stevens, C., Sutton, P., Smith M. & Dickson, R. (2008); “Tidal flows in Te Aumiti (French Pass), South Island, New Zealand”. *New Zealand Journal of Marine and Freshwater Research*, **42**, pp. 451-464.
21. El-Geziry, T.M., Bryden, I.G. & Couch, S.J. (2009); “Environmental Impact Assessment for tidal energy schemes: an exemplar case study of the Strait of Messina”. *Proc. IMarEST Part A: Journal of Marine Engineering and Technology*, **13**, pp. 39-48.
22. http://www.eorc.jaxa.jp/en/imgdata/topics/2006/tp060811.html
23. Marine Current Turbines Ltd. (2009); “Marine Current Turbines reveals details of SeaGen's Operating Performance”. *Press release*. Available online at http://www.marineturbines.com/3/news/article/26/marine_current_turbines_reveals_details_of_seagen_s_operating_performance/
24. Whittaker, T., Fraenkel, P.L., Bell, A. & Lugg, L. (2003); “The potential for the use of marine current energy in Northern Ireland”. *Report commissioned by the Department of Trade and Industry; Department of Enterprise, Trade and Investment and Northern Ireland Electricity.*50pp.
25. Brown, R. (1990); “Strangford Lough: The Wildlife of an Irish Sea Lough”. *The Institute of Irish Studies, The Queen's University of Belfast, Belfast*, ISBN 0 85389 356 X, 175pp.
26. George, K.J. & Stripling, S. (1995); “Improving the simulation of drying and wetting in a two-dimensional tidal numerical model”. *Applied Mathematical Modelling*, **19**(1), pp. 2-6.
27. IOC, IHO and BODC (2003); "Centenary Edition of the GEBCO Digital Atlas", *published on CD-ROM on behalf of the Intergovernmental Oceanographic Commission and the International Hydrographic Organization as part of the General Bathymetric Chart of the Oceans; British Oceanographic Data Centre, Liverpool.*
28. Iyer, A.S., Couch, S.J., Harrison, G.P. & Wallace, A.R. (2009); “Analysis and Comparison of Tidal Datasets”. *Proceedings of the 8th European Wave and Tidal Energy Conference EWTEC 2009, Uppsala, Sweden, 7-10 September 2009.*
29. Gooch, S., Thomson, J., Polagye, B. & Meggin, D. (2009); “Site Characterization for Tidal Power”. *Oceans 2009, Biloxi, MI, 26-29 October, 2009.*
30. Fraenkel, P. (2009) “The UK SeaGen Project: Marine Current Turbines’ experience”. *Presentation at the UK-Taiwan Workshop on Tidal Current Energy held at the Royal Society of Edinburgh 24 February 2009.*
31. ABPmer commissioned by npower Juice (2007), “Quantification of Exploitable Tidal Energy Resources in UK Waters”
32. Bryden I.G., Couch S.J. and Harrison, G., (2006); “Overview of the Issues Associated with Energy Extraction from Tidal Currents”. *World Renewable Energy Congress IX, Florence, Italy.*
33. Casulli, V. and Zanolli, P., (2002); “Semi-Implicit Numerical Modelling of Non-Hydrostatic Free-Surface Flows for Environmental Problems”. *Mathematical and Computer Modelling, 36: 1131 - 1149.*
34. Casulli, V. and Zanolli, P., (2005); “High Resolution Methods for Multidimensional Advection-Diffusion Problems in Free-Surface Hydrodynamics”. *Ocean Modelling, 2005, v. 10, 1-2, p. 137-151.*
35. http://www.ewea.org/index.php?id=203
36. MacWilliams, M.l., Salcedo, F.G., and E.S. Gross, (2008); “San Francisco Bay-Delta UnTRIM Model Calibration Report, POD 3-D Particle Tracking”. *Modelling Study Prepared for California Department of Water Resources.*
37. Mac Williams, M.L., Salcedo, F.G., and E.S. Gross, (2009), in review. “San Francisco Bay-Delta UnTRIM Model Calibration Report”, *Sacramento and Stockton Deep Eater Ship Channel 3-D Hydrodynamic and Salinity Modeling Study, Prepared for U.S. Army Corps of Engineers, San Francisco District, July 14, 2009, 574*
38. Department of Trade and Industry (2006); “The Energy Challenge Energy Review Report 2006” *The Stationary Office* ISBN 0-10-168872-5.

39. Salter, S.H. (2005); "Possible under-estimation of the UK tidal resource" *Submission for DTI Energy Review Question 2*. Available from http://www.berr.gov.uk/files/file31313.pdf.
40. Salter, S.H. & Taylor, J.R.M. (2007); "Vertical-axis tidal-current generators and the Pentland Firth". *Proceedings of the IMechE, Part A: Journal of Power and Energy.* **221**, pp. 181-199. doi: 10.1243/09576509JPE295.
41. Salter, S.H. (2009); "Correcting the Under-estimate of the Tidal-Stream Resource of the Pentland Firth". *Proceedings of the 8th European Wave and Tidal Energy Conference, Uppsala, Sweden*.
42. Salter, S.H., MacGregor, K., Jones, C. (2006); "Scottish Energy Review: Scotland's opportunity – Scotland's challenge". *Scottish National Party document*
43. Egbert, G.D. & Ray, R.D. (2000); "Significant dissipation of tidal energy in the deep ocean inferred from satellite altimeter data". *Nature*, **405**, pp. 775-778. doi: 10.1038/35015531.
44. Pugh, D.T. (1987); "Tides, surges and mean sea-level". *John Wiley & Sons*, ISBN 0 471 91505 X.
45. Howarth, M.J. & Souza, A.J. (2005); "Reynolds stress observations in continental shelf seas". *Deep-Sea Research II*, **52**, pp. 1075-1086. doi:10.1016/j.dsr2.2005.01.003.
46. MacKay, D.J.C. (2007); "Under-estimation of the UK tidal resource", *available from:* http://www.inference.phy.cam.ac.uk/sustainable/book/tex/TideEstimate.pdf.
47. MacKay, D.J.C. (2009); "Sustainable Energy — without the hot air". Web book, available from: http://www.withouthotair.com/.